

Discrete Dynamics in Nature and Society

Iterative Methods and Dynamics for Nonlinear Problems

Lead Guest Editor: Young I. Kim

Guest Editors: Alicia Cordero, Janak R. Sharma, Fazlollah Soleymani,
Juan R. Torregrosa, and Xiaofeng Wang





Iterative Methods and Dynamics for Nonlinear Problems


Discrete Dynamics in Nature and Society

Iterative Methods and Dynamics for Nonlinear Problems

Lead Guest Editor: Young I. Kim

Guest Editors: Alicia Cordero, Janak R. Sharma,

Fazlollah Soleymani, Juan R. Torregrosa, and Xiaofeng Wang



Copyright © 2017 Hindawi. All rights reserved.

This is a special issue published in “Discrete Dynamics in Nature and Society.” All articles are open access articles distributed under the Creative Commons Attribution License, which permits unrestricted use, distribution, and reproduction in any medium, provided the original work is properly cited.

Editorial Board

Douglas R. Anderson, USA
David Arroyo, Spain
Viktor Avrutin, Germany
Stefan Balint, Romania
Kamel Barkaoui, France
Gian I. Bischi, Italy
Gabriele Bonanno, Italy
Driss Boutat, France
Gabriella Bretti, Italy
Filippo Cacace, Italy
Pasquale Candito, Italy
Cengiz Çinar, Turkey
Carmen Coll, Spain
Alicia Cordero, Spain
Manuel De la Sen, Spain
Luisa Di Paola, Italy
Josef Diblík, Czech Republic
Xiaohua Ding, China
Elmetwally Elabbasy, Egypt
Hassan A. El-Morshedy, Egypt
Daniele Fournier-Prunaret, France
Genni Fragnelli, Italy
Ciprian G. Gal, USA
Gisèle R Goldstein, USA
Vladimir Gontar, Israel
Chris Goodrich, USA

Pilar R. Gordoá, Spain
Kannan Govindan, Denmark
Luca Guerrini, Italy
Antonio Iannizzotto, Italy
Giuseppe Izzo, Italy
Sarangapani Jagannathan, USA
Jun Ji, USA
Nikos I. Karachalios, Greece
Eric R. Kaufmann, USA
Victor S. Kozyakin, Russia
Mustafa R. S. Kulenovic, USA
Kousuke Kuto, Japan
Aihua Li, USA
Xiaohui Liu, UK
Miguel Ángel López, Spain
Ricardo López-Ruiz, Spain
Agustin Martin, Spain
Akio Matsumoto, Japan
Rigoberto Medina, Chile
Vicenç Méndez, Spain
Garyfalos Papashinopoulos, Greece
Juan Pavón, Spain
Allan C. Peterson, USA
Andrew Pickering, Spain
Chuanxi Qian, USA
Morteza Rafei, Netherlands

Mustapha A. Rami, Spain
Aura Reggiani, Italy
Pavel Rehak, Czech Republic
Paolo Renna, Italy
Marko Robnik, Slovenia
Yuriy Rogovchenko, Norway
Silvia Romanelli, Italy
Leonid Shaikhet, Israel
Seenith Sivasundaram, USA
Charalampos Skokos, South Africa
Piergiulio Tempesta, Spain
Tetsuji Tokihiro, Japan
J. R. Torregrosa, Spain
Delfim F. M. Torres, Portugal
Firdaus Udwardia, USA
Antonia Vecchio, Italy
Francisco R. Villatoro, Spain
Hubertus Von Bremen, USA
Abdul-Aziz Yakubu, USA
Bo Yang, USA
Guang Zhang, China
Zhengqiu Zhang, China
Lu Zhen, China
Yong Zhou, China
Zuonong Zhu, China

Contents

Iterative Methods and Dynamics for Nonlinear Problems

Y. I. Kim, A. Cordero, J. R. Sharma, F. Soleymani, J. R. Torregrosa, and X. Wang
Volume 2017, Article ID 8592140, 1 page

An Iteration Scheme for Contraction Mappings with an Application to Synchronization of Discrete Logistic Maps

Ke Ding, Jong Kyu Kim, Qiang Lu, and Bin Du
Volume 2017, Article ID 5156314, 7 pages

Multistep High-Order Methods for Nonlinear Equations Using Padé-Like Approximants

Alicia Cordero, José L. Hueso, Eulalia Martínez, and Juan R. Torregrosa
Volume 2017, Article ID 3204652, 6 pages

Recurrence Based Similarity Identification of Climate Data

Anita Bai, Swati Hira, and S. Deshpande Parag
Volume 2017, Article ID 7836720, 21 pages

Research on the Method of Traffic Organization and Optimization Based on Dynamic Traffic Flow Model

Shu-bin Li, Guang-min Wang, Tao Wang, and Hua-ling Ren
Volume 2017, Article ID 5292616, 9 pages

A Perspective of Evolution for Carbon Emissions Trading Market: The Dilemma between Market Scale and Government Regulation

Qi Zhu
Volume 2017, Article ID 1432052, 7 pages

Editorial

Iterative Methods and Dynamics for Nonlinear Problems

Y. I. Kim,¹ A. Cordero,² J. R. Sharma,³ F. Soleymani,⁴ J. R. Torregrosa,² and X. Wang⁵

¹*Dankook University, Cheonan, Republic of Korea*

²*Universitat Politècnica de València, Valencia, Spain*

³*Sant Longowal Institute of Engineering & Technology, Punjab, India*

⁴*Ferdowsi University of Mashhad, Mashhad, Iran*

⁵*Bohai University, Liaoning, China*

Correspondence should be addressed to Y. I. Kim; yikbell@yahoo.co.kr

Received 9 October 2017; Accepted 11 October 2017; Published 16 November 2017

Copyright © 2017 Y. I. Kim et al. This is an open access article distributed under the Creative Commons Attribution License, which permits unrestricted use, distribution, and reproduction in any medium, provided the original work is properly cited.

Since the advent of Kung-Traub's conjecture established in 1974 on optimal convergence of iterative memory-free methods, the development of iterative methods and their dynamics has been focused for several decades until present times to improve the order of convergence, initial condition behavior, and CPU time for effectively solving nonlinear equations encountered in many fields of sciences such as applied mathematics, computational physics, engineering mathematics, and nonlinear discrete dynamics and chaos. Real-life nonlinear problems including weather forecast, satellite-orbit tracing, image processing via discrete data, and locating objects through global positioning systems can be solved by efficient iterative methods with the aid of high-precision modern computers.

The primary aim of this special issue is for authors from diversified scientific disciplines to accomplish their high-quality research goals that seek recent developments and innovational techniques on iterative methods and their dynamics for nonlinear problems under consideration. The areas to be covered in this issue are root-finding iterative methods for nonlinear equations, nonlinear recurrence relations, fixed point theory, initial-boundary value problems, stability analysis and dynamics of iteration functions, and computational complexity of iterative techniques.

In total, 34 papers were initially submitted in this special issue, covering various aspects of iterative or dynamical approaches to resolve their governing equations of the system. After thorough inspections and microscopic strict reviews on these papers, it is our regret to be able to select

only five papers for their publication in the current issue, even though many of them were of very good quality. Those selected five papers describe very important topics dealing with iterative maps from functional analysis, root-finding Padé-like approximants, recurrence relations from climate data, recursive optimization on modern traffic control systems, and dynamical analysis from partial differential equations reducing carbon emission based on strict government regulations.

Acknowledgments

Our special gratitude must be expressed to enthusiastic participants in preparation of their manuscripts as well as to contributing reviewers of these manuscripts from the international community.

*Y. I. Kim
A. Cordero
J. R. Sharma
F. Soleymani
J. R. Torregrosa
X. Wang*

Research Article

An Iteration Scheme for Contraction Mappings with an Application to Synchronization of Discrete Logistic Maps

Ke Ding,^{1,2} Jong Kyu Kim,³ Qiang Lu,¹ and Bin Du⁴

¹School of Automation, Hangzhou Dianzi University, Zhejiang 310018, China

²Jiangxi E-Commerce High Level Engineering Technology Research Centre, Jiangxi University of Finance and Economics, Nanchang 330013, China

³Department of Mathematics Education, Kyungnam University, Changwon, Gyeongnam 631-701, Republic of Korea

⁴School of Information Technology, Jiangxi University of Finance and Economics, Nanchang 330013, China

Correspondence should be addressed to Ke Ding; k.ding78@hotmail.com

Received 29 June 2017; Accepted 27 September 2017; Published 9 November 2017

Academic Editor: Pasquale Candito

Copyright © 2017 Ke Ding et al. This is an open access article distributed under the Creative Commons Attribution License, which permits unrestricted use, distribution, and reproduction in any medium, provided the original work is properly cited.

This paper deals with designing a new iteration scheme associated with a given scheme for contraction mappings. This new scheme has a similar structure to that of the given scheme, in which those two iterative schemes converge to the same fixed point of the given contraction mapping. The positive influence of feedback parameters on the convergence rate of this new scheme is investigated. Moreover, the derived convergence and comparison results can be extended to nonexpansive mappings. As an application, the derived results are utilized to study the synchronization of logistic maps. Two illustrated examples are used to reveal the effectiveness of our results.

1. Introduction

Fixed point theory has achieved great progress since the last two decades. Various schemes have been constructed to approximate the fixed point of a contraction mapping (see, e.g., [1–30]).

For a contraction mapping, we can define an iteration scheme which converges to the fixed point of that mapping. Here is a question whether we can design another iteration scheme with a similar structure to that of given scheme to approximate the fixed point. Motivated by this question, we design a new iteration scheme which is associated with the given iteration scheme.

This new scheme has a similar structure to that of the given scheme. Those two schemes converge to the same fixed point of the given contraction mapping. The convergence rate of this new scheme can be accelerated by the increase of the feedback parameters. Those convergence and comparison criteria can be applied to nonexpansive mappings. Moreover, the derived results are utilized to study the synchronization of logistics maps. Two examples are used to reveal the effectiveness of our results.

2. Preliminaries

Let C be a nonempty convex subset of a normed linear space E . Let T be a contraction mapping of C into itself with the contraction constant μ ; that is,

$$\|Tx - Ty\| \leq \mu \|x - y\|, \quad 0 < \mu < 1, \quad (1)$$

for any $x, y \in C$. The set of fixed points of T is denoted by $F(T) = \{x \in C : Tx = x\}$. The set of natural numbers is denoted by \mathbb{N} . $\{\alpha_n\}$ and $\{\beta_n\}$ are two sequences of real numbers such that $0 \leq \alpha_n$ and $0 \leq \beta_n$ for all $n \in \mathbb{N}$. Consider the following scheme:

$$\begin{aligned} x_1 &\in C, \\ x_{n+1} &= \alpha_n x_n + \beta_n T x_n, \quad n \in \mathbb{N}. \end{aligned} \quad (2)$$

Remark 1. It should be pointed out that scheme (2) is a general framework which includes the following well-known schemes as special cases.

- (i) If $\alpha_n = 0$ and $\beta_n = 1$, scheme (2) reduces to Picard iteration.

- (ii) If $0 < \alpha_n < 1$ and $\beta_n = 1 - \alpha_n$, scheme (2) reduces to Mann iteration.
- (iii) If $0 < \alpha_n < 1$, $\beta_n = 1 - \alpha_n$, and $Tx_n = \tilde{T}((1 - \gamma_n)x_n + \gamma_n \tilde{T}x_n)$, where \tilde{T} is a contraction mapping of C into itself and $0 < \gamma_n < 1$, scheme (2) reduces to Ishikawa iteration.

For the fixed point scheme described by (2), a question naturally arises whether we can design another iteration scheme with a similar structure to scheme (2) to approximate the fixed point. Moreover, this new scheme has a similar structure to that of the given scheme. Those two schemes converge to the same fixed point of the given contraction mapping.

Motivated by this question, we define the following scheme associated with scheme (2):

$$\begin{aligned} y_1 &\in C, \\ y_{n+1} &= \alpha_n y_n + \beta_n T y_n + k_n (x_n - y_n), \quad n \in \mathbb{N}, \end{aligned} \quad (3)$$

where $\{k_n\}$ is a scheme of feedback parameters which can be determined later. Let $e_n = x_n - y_n$ for $n \in \mathbb{N}$. Then we can construct the following scheme from schemes (2) and (3):

$$\begin{aligned} e_1 &= x_1 - y_1 \in C, \\ e_{n+1} &= (\alpha_n - k_n) e_n + \beta_n (Tx_n - Ty_n), \quad n \in \mathbb{N}. \end{aligned} \quad (4)$$

From [4, 31, 32], the fact $\lim_{n \rightarrow \infty} \|e_n\| = 0$ will ensure $\lim_{n \rightarrow \infty} \|x_n - y_n\| = 0$. The main purpose of this paper is to find the conditions to guarantee $\lim_{n \rightarrow \infty} \|e_n\| = 0$, which means that scheme (3) has a similar structure to scheme (2). Schemes (2) and (3) converge to the same fixed point of the given contraction mapping T .

3. Main Results

3.1. Convergence Results. Now, we give some convergence results for iteration (3).

Theorem 2. *Let C be a nonempty convex subset of a normed linear space E . Let T be a contraction mapping of C into itself and $F(T) \neq \emptyset$. If*

$$\bar{\alpha} + \bar{\beta}\mu - 1 < \underline{k} \leq k_i \leq \bar{k} \leq \underline{\alpha}, \quad (5)$$

where $\bar{\alpha} = \max\{\alpha_i\}$, $\underline{\alpha} = \min\{\alpha_i\}$, $\bar{\beta} = \max\{\beta_i\}$, $\bar{k} = \max\{k_i\}$, and $\underline{k} = \min\{k_i\}$, $i = 1, 2, \dots, n$, then $\lim_{n \rightarrow \infty} \|x_{n+1} - y_{n+1}\| = 0$, which also implies that scheme (3) and scheme (2) converge to the same fixed point of T .

Proof. From (5), we have

$$\begin{aligned} 0 &< \alpha_i - k_i, \\ 0 &< \alpha_i - k_i + \beta_i \mu \end{aligned} \quad (6)$$

for $i = 1, 2, \dots, n$. Then,

$$\begin{aligned} \|e_{n+1}\| &= \|(\alpha_n - k_n) e_n + \beta_n (Tx_n - Ty_n)\| \\ &\leq (\alpha_n - k_n) \|e_n\| + \beta_n \|Tx_n - Ty_n\| \\ &\leq (\alpha_n - k_n) \|e_n\| + \beta_n \mu \|x_n - y_n\| \\ &\leq (\alpha_n - k_n + \beta_n \mu) \|e_n\| \\ &\vdots \\ &\leq \prod_{i=1}^n (\alpha_i - k_i + \beta_i \mu) \|e_1\|. \end{aligned} \quad (7)$$

It follows from (5) that $0 < \bar{\alpha} + \bar{\beta}\mu - \underline{k} < 1$, where $\bar{\alpha} = \max\{\alpha_i\}$, $\bar{\beta} = \max\{\beta_i\}$, and $\underline{k} = \min\{k_i\}$, $i = 1, 2, \dots, n$. Thus,

$$\|e_{n+1}\| \leq \prod_{i=1}^n (\alpha_i - k_i + \beta_i \mu) \|e_1\| \leq (\bar{\alpha} + \bar{\beta}\mu - \underline{k})^n \|e_1\|. \quad (8)$$

It is easy to see that $\|e_{n+1}\| \rightarrow 0$, as $n \rightarrow \infty$; that is, $\lim_{n \rightarrow \infty} \|x_{n+1} - y_{n+1}\| = 0$. This completes the proof. \square

Remark 3. It follows from Theorem 2 that $|k_i| < 1$ for $i = 1, 2, \dots, n$.

Theorem 2 can be applied to approximating the fixed point of a nonexpansive mapping where the contraction constant $\mu = 1$. If $\mu = 1$, Theorem 2 reduces to the following result.

Corollary 4. *Let C be a nonempty convex subset of a normed linear space E . Let T be a nonexpansive mapping of C into itself and $F(T) \neq \emptyset$. If*

$$\bar{\alpha} + \bar{\beta} - 1 < \underline{k} \leq k_i \leq \bar{k} \leq \underline{\alpha}, \quad (9)$$

where $\bar{\alpha} = \max\{\alpha_i\}$, $\underline{\alpha} = \min\{\alpha_i\}$, $\bar{\beta} = \max\{\beta_i\}$, $\bar{k} = \max\{k_i\}$, and $\underline{k} = \min\{k_i\}$, $i = 1, 2, \dots, n$, then $\lim_{n \rightarrow \infty} \|x_{n+1} - y_{n+1}\| = 0$.

3.2. Three Special Cases. Now, we use Theorem 2 to construct the associated schemes for Picard iteration scheme, Mann iteration scheme, and Ishikawa iteration scheme for contraction mappings and derive the convergence theorems for those schemes, respectively. First, we consider the Picard iteration scheme. The Picard iteration scheme is defined by

$$\begin{aligned} \hat{x}_1 &\in C, \\ \hat{x}_{n+1} &= T\hat{x}_n, \quad n \in \mathbb{N}. \end{aligned} \quad (10)$$

We define the iteration scheme associated with Picard iteration scheme (10):

$$\begin{aligned} \hat{y}_1 &\in C, \\ \hat{y}_{n+1} &= T\hat{y}_n + k_n (\hat{x}_n - \hat{y}_n), \quad n \in \mathbb{N}. \end{aligned} \quad (11)$$

Let $\hat{e}_n = \hat{x}_n - \hat{y}_n$ for $n \in \mathbb{N}$. Schemes (2) and (3) give the following scheme:

$$\begin{aligned} \hat{e}_1 &= \hat{x}_1 - \hat{y}_1 \in C, \\ \hat{e}_{n+1} &= -k_n \hat{e}_n + (T\hat{x}_n - T\hat{y}_n), \quad n \in \mathbb{N}. \end{aligned} \tag{12}$$

Then, by the similar proof of Theorem 2, we have the following convergence theorem.

Theorem 5. *Let C be a nonempty convex subset of a normed linear space E . Let T be a contraction mapping of C into itself and $F(T) \neq \phi$. If $\max\{|k_i|\} + \mu < 1$, $i = 1, 2, \dots, n$, then $\lim_{n \rightarrow \infty} \|\hat{x}_{n+1} - \hat{y}_{n+1}\| = 0$.*

Second, we consider the Mann iteration scheme. The Mann iteration scheme is defined by

$$\begin{aligned} \check{x}_1 &\in C, \\ \check{x}_{n+1} &= (1 - \beta_n) \check{x}_n + \beta_n T\check{x}_n, \quad n \in \mathbb{N}. \end{aligned} \tag{13}$$

We construct the following iteration scheme associated with Mann iteration scheme (13):

$$\begin{aligned} \check{y}_1 &\in C, \\ \check{y}_{n+1} &= (1 - \beta_n) \check{y}_n + \beta_n T\check{y}_n + k_n (\check{x}_n - \check{y}_n), \quad n \in \mathbb{N}. \end{aligned} \tag{14}$$

By defining an error variable $\check{e}_i = \check{x}_i - \check{y}_i$ for $i = 1, 2, \dots, n$, we obtain the following iteration scheme:

$$\begin{aligned} \check{e}_1 &= \check{x}_1 - \check{y}_1 \in C, \\ \check{e}_{n+1} &= (1 - \beta_n - k_n) \check{e}_n + \beta_n (T\check{x}_n - T\check{y}_n), \quad n \in \mathbb{N}. \end{aligned} \tag{15}$$

Then, from the similar proof for Theorem 2, we derive the following convergence result.

Theorem 6. *Let C be a nonempty convex subset of a normed linear space E . Let T be a contraction mapping of C into itself and $F(T) \neq \phi$. If $\bar{\beta}\mu - \underline{\beta} < \underline{k}_i \leq k_i \leq \bar{k} < 1 - \bar{\beta}$, where $\underline{\beta} = \min\{\beta_i\}$, $\bar{\beta} = \max\{\beta_i\}$, $\bar{k} = \max\{k_i\}$, and $\underline{k} = \min\{k_i\}$, $i = 1, 2, \dots, n$, then $\lim_{n \rightarrow \infty} \|\check{x}_{n+1} - \check{y}_{n+1}\| = 0$.*

Third, we consider the Ishikawa iteration scheme. The Ishikawa iteration scheme is defined by

$$\begin{aligned} \tilde{x}_1 &\in C, \\ \tilde{x}_{n+1} &= (1 - \beta_n) \tilde{x}_n + \beta_n \tilde{T} \left((1 - \gamma_n) \tilde{x}_n + \gamma_n \tilde{T} \tilde{x}_n \right), \end{aligned} \tag{16}$$

$n \in \mathbb{N}$,

where \tilde{T} is a contraction mapping of C into itself with the contraction constant μ . We generate the following iteration scheme associated with Ishikawa iteration scheme (16):

$$\begin{aligned} \tilde{y}_1 &\in C, \\ \tilde{y}_{n+1} &= (1 - \beta_n) \tilde{y}_n + \beta_n \tilde{T} \left((1 - \gamma_n) \tilde{y}_n + \gamma_n \tilde{T} \tilde{y}_n \right) \\ &\quad + k_n (\tilde{x}_n - \tilde{y}_n), \quad n \in \mathbb{N}. \end{aligned} \tag{17}$$

After defining an error variable $\tilde{e}_i = \tilde{x}_i - \tilde{y}_i$ for $i = 1, 2, \dots, n$, we obtain the error scheme:

$$\begin{aligned} \tilde{e}_1 &= \tilde{x}_1 - \tilde{y}_1 \in C, \\ \tilde{e}_{n+1} &= (1 - \beta_n - k_n) \tilde{e}_n + \beta_n \left(\tilde{T} \left((1 - \gamma_n) \tilde{x}_n + \gamma_n \tilde{T} \tilde{x}_n \right) \right. \\ &\quad \left. - \tilde{T} \left((1 - \gamma_n) \tilde{y}_n + \gamma_n \tilde{T} \tilde{y}_n \right) \right), \quad n \in \mathbb{N}. \end{aligned} \tag{18}$$

Then, from the similar proof for Theorem 2, we achieve the following convergence theorem.

Theorem 7. *Let C be a nonempty convex subset of a normed linear space E . Let T be a contraction mapping of C into itself and $F(T) \neq \phi$. If $\bar{\beta}\mu(1 - \underline{\gamma} + \bar{\gamma}\mu) - \underline{\beta} < \underline{k} \leq k_i \leq \bar{k} < 1 - \bar{\beta}$, where $\underline{\beta} = \min\{\beta_i\}$, $\bar{\beta} = \max\{\beta_i\}$, $\underline{\gamma} = \min\{\gamma_i\}$, $\bar{\gamma} = \max\{\gamma_i\}$, $\bar{k} = \max\{k_i\}$, and $\underline{k} = \min\{k_i\}$, $i = 1, 2, \dots, n$, then $\lim_{n \rightarrow \infty} \|\tilde{x}_{n+1} - \tilde{y}_{n+1}\| = 0$.*

3.3. Impact of k_i to the Convergent Rate. Next, we analyze the influence of size k_i to the convergence rate of (3). We first give another iteration scheme associated with iteration scheme (2):

$$\begin{aligned} z_1 &\in C, \\ z_{n+1} &= \alpha_n z_n + \beta_n Tz_n + \check{k}_n (x_n - z_n), \quad n \in \mathbb{N}, \end{aligned} \tag{19}$$

where $\check{k}_n > k_n$. In order to compare the convergence rate of (3) with that of (19), we give the following definitions for the convergent rates of two different iteration schemes.

Definition 8 (see [4]). Let $\{a_n\}$ and $\{b_n\}$ be two sequences of real numbers which converges to a and b , respectively. We say that the sequence $\{a_n\}$ converges faster than $\{b_n\}$ if $\lim_{n \rightarrow \infty} (|a_n - a|/|b_n - b|) = 0$.

Definition 9. Let $\{x_n\}$, $\{y_n\}$, $\{z_n\}$ be three iterative schemes which satisfy $z_n \rightarrow x_n, y_n \rightarrow x_n$ as $n \rightarrow \infty$. Let $\{a_n\}$ and $\{b_n\}$ be two sequences of real numbers which converge to 0. We say that the scheme $\{z_n\}$ converges faster than $\{y_n\}$ to $\{x_n\}$, if

$$\begin{aligned} \|z_n - x_n\| &\leq a_n, \quad \text{for all } n \in \mathbb{N}, \\ \|y_n - x_n\| &\leq b_n, \quad \text{for all } n \in \mathbb{N}, \end{aligned} \tag{20}$$

and $\{a_n\}$ converges faster than $\{b_n\}$.

By the similar method for Theorem 2, we have

$$\|z_{n+1} - x_{n+1}\| \leq (\bar{\alpha} + \bar{\beta}\mu - \check{k})^n \|z_1 - x_1\|, \tag{21}$$

where $\check{k} = \min\{\check{k}_i\}$, $i = 1, 2, \dots, n$, and $0 < \bar{\alpha} + \bar{\beta}\mu - \check{k} < 1$. It follows from $\underline{k} < \check{k}$ that $0 < \bar{\alpha} + \bar{\beta}\mu - \check{k} < \bar{\alpha} + \bar{\beta}\mu - \underline{k} < 1$, which implies

$$\begin{aligned} \lim_{n \rightarrow \infty} \frac{\|z_{n+1} - x_{n+1}\|}{\|y_{n+1} - x_{n+1}\|} &= \lim_{n \rightarrow \infty} \left(\frac{\bar{\alpha} + \bar{\beta}\mu - \check{k}}{\bar{\alpha} + \bar{\beta}\mu - \underline{k}} \right)^n \frac{\|z_1 - x_1\|}{\|y_1 - x_1\|} \\ &= 0. \end{aligned} \tag{22}$$

Hence, from the above mentions, we have the following comparison result for the convergence rate according to the size k_i .

Theorem 10. *The iteration scheme defined by (19) converges faster than the iteration scheme defined by (3).*

Remark 11. The convergence rate of iteration scheme defined by (3) increases as k_i increases which means that the convergence rate of iteration scheme defined by (3) can be controlled by the adjustment of size k_i .

Remark 12. If T is a nonexpansive mapping, i.e., $\mu = 1$, limitation (22) reduces to

$$\lim_{n \rightarrow \infty} \frac{\|z_{n+1} - x_{n+1}\|}{\|y_{n+1} - x_{n+1}\|} = \lim_{n \rightarrow \infty} \left(\frac{\bar{\alpha} + \bar{\beta} - \check{k}}{\bar{\alpha} + \bar{\beta} - \underline{k}} \right)^n \frac{\|z_1 - x_1\|}{\|y_1 - x_1\|} \quad (23)$$

$$= 0,$$

which means that Theorem 10 is still valid for the nonexpansive mapping.

4. An Application to Synchronization of Logistic Maps

Logistic maps are classical discrete systems which can generate bifurcation and chaos. Synchronization of two logistic maps, which means the state variable of one logistic map is eventually equal to the counterpart of another logistic map, has been widely used in secure communication, image encryption, and signal transmission [22, 31]. Our results can be applied to studying the synchronization of logistic maps.

If $Tx_n = -\beta_n x_n^2$ and $\alpha_n = \beta_n = r$, then scheme (2) reduces to the following logistic map

$$x_{n+1} = rx_n - rx_n^2, \quad n \in \mathbb{N}, \quad (24)$$

where $x_1 \in C$. If $0 < r < 0.5$ and $0 < x_1 < 1$, then we can derive $0 < x_n < 1$, which implies that

$$\begin{aligned} |Tx_n - Ty_n| &= r |x_n^2 - y_n^2| = r |x_n + y_n| |x_n - y_n| \\ &< |x_n - y_n| \end{aligned} \quad (25)$$

for any $0 < x_n, y_n < 1$.

Here, we consider another logistic map

$$y_{n+1} = ry_n - ry_n^2, \quad n \in \mathbb{N}, \quad (26)$$

where $y_1 \in C$. Defining $e_n = x_n - y_n$, we can have the following scheme:

$$e_{n+1} = r(1 - (x_n + y_n))e_n, \quad n \in \mathbb{N}, \quad (27)$$

where $e_1 = x_1 - y_1 \in C$.

Definition 13. If $\lim_{n \rightarrow \infty} |x_n - y_n| = 0$, the logistic map described by (24) is said to achieve the global synchronization with the logistic map described by (26).

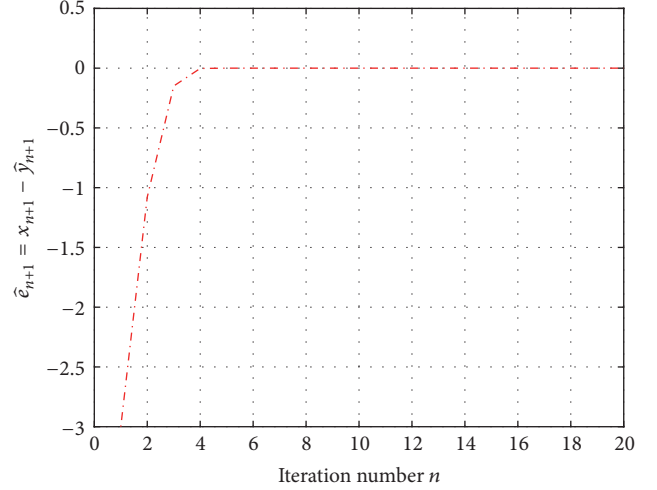


FIGURE 1: The trajectory of \hat{e}_{n+1} with $\mu = 0.78$ and $k_i = 0.21$.

By using the similar proof method of Theorem 2 with $k_i = 0$ and $|r(1 - (x_n + y_n))| < 0.5$, we can derive the following result.

Theorem 14. *If $0 < r < 0.5$ and $0 < x_1, y_1 < 1$, the logistic map described by (24) achieves the global synchronization with the logistic map described by (26).*

5. Two Illustrated Examples

Example 15. Now we give an example for the main theorems with numerical analysis.

Consider $Tx = \sqrt{x^2 - 8x + 40}$ on $[4.1, 10]$ with the contraction constant $\mu = 0.78$. The fixed point of T is $x = 5$. We first construct the iteration scheme (11) associated with Picard iteration (10). From Theorem 5, we know that $\max\{|k_i|\} + \mu < 1$, $i = 1, 2, \dots, n$, which implies $|k_i| < 0.22$ for $i = 1, 2, \dots, n$. We choose $k_i = 0.21$, for $i = 1, 2, \dots, n$, and $x_1 = 6$ and $\hat{y}_1 = 8$. Figure 1 gives a demonstration of trajectory of \hat{e}_{n+1} of (11). From Figure 1, we can see that $\lim_{n \rightarrow \infty} \|\hat{e}_{n+1}\| = 0$; that is, $\lim_{n \rightarrow \infty} \|x_{n+1} - \hat{y}_{n+1}\| = 0$, which indicates the effectiveness of Theorem 5.

Then, we construct the iteration scheme (14) associated with Mann iteration (13) with $\beta_i = 0.75$ for $i = 1, 2, \dots, n$. From Theorem 6, we can get $\bar{\beta}\mu - \beta < \underline{k} \leq k_i \leq \bar{k} < 1 - \bar{\beta}$, which indicates $-0.165 < k_i < 0.25$ for $i = 1, 2, \dots, n$. We choose $k_i = 0.24$, for $i = 1, 2, \dots, n$, and $x_1 = 6$ and $\hat{y}_1 = 8$. Figure 2 provides the trajectory of \check{e}_{n+1} of (14). From Figure 2, we can observe that $\lim_{n \rightarrow \infty} \|\check{e}_{n+1}\| = 0$; that is, $\lim_{n \rightarrow \infty} \|x_{n+1} - \check{y}_{n+1}\| = 0$, which indicates the effectiveness of Theorem 6.

Now, we construct the iteration scheme (17) associated with Ishikawa iteration (16) with $\beta_i = 0.5$ and $\gamma_i = 0.75$ for $i = 1, 2, \dots, n$. From Theorem 7, we can have $\bar{\beta}\mu(1 - \gamma + \bar{\gamma}\mu) - \beta < \underline{k} \leq k_i \leq \bar{k} < 1 - \bar{\beta}$, which implies $-0.1744 < k_i < 0.5$ for $i = 1, 2, \dots, n$. We choose $k_i = 0.49$, for $i = 1, 2, \dots, n$, and $x_1 = 6$ and $\hat{y}_1 = 8$. Figure 3 reveals the trajectory of \tilde{e}_{n+1} of (17). It follows from Figure 3 that $\lim_{n \rightarrow \infty} \|\tilde{e}_{n+1}\| = 0$; that is,

TABLE 1: Comparison for convergent rates of iteration scheme (3) with different k_i .

	$n = 1$	$n = 2$	$n = 3$...	$n = 17$	$n = 18$	$n = 19$	$n = 20$
y_n as $k_i = 0.39$	9.00	6.63	5.58	...	5.00	5.00	5.00	5.00
y_n as $k_i = 0.01$	9.00	7.77	6.80	...	5.02	5.01	5.01	5.00
y_n as $k_i = -0.1$	9.00	8.10	7.30	...	5.05	5.03	5.02	5.01

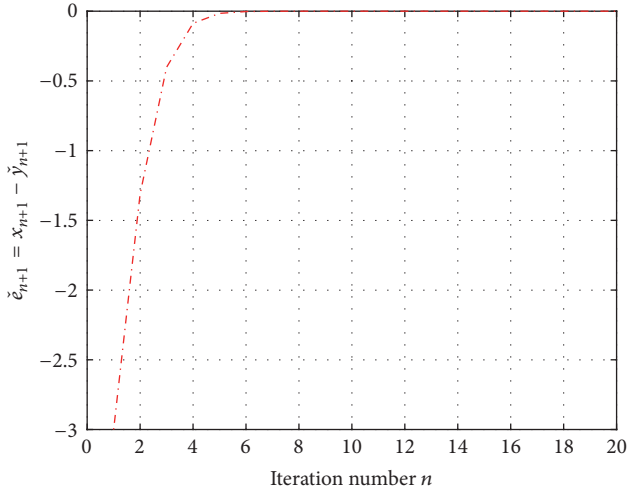


FIGURE 2: The trajectory of \tilde{e}_{n+1} with $\mu = 0.78$ and $k_i = 0.24$.

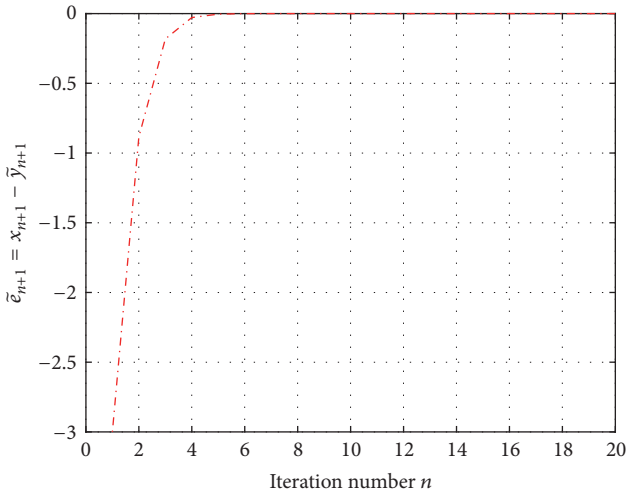


FIGURE 3: The trajectory of \tilde{e}_{n+1} with $\mu = 0.78$ and $k_i = 0.49$.

$\lim_{n \rightarrow \infty} \|x_{n+1} - \tilde{y}_{n+1}\| = 0$, which indicates the effectiveness of Theorem 7.

Finally, we compare the convergence rates of (3) with different k_i . We choose scheme (14) with $\beta_i = 0.6$. From Theorem 6, we can have $-0.132 < k_i < 0.4$ for $i = 1, 2, \dots, n$. Let $x_1 = 6$ and $y_1 = z_1 = 9$. We choose k_i as 0.39, 0.01, and -0.1 to approximate the fixed point, respectively. Table 1 shows that the convergence rate of (3) increases as k_i increases, which also illustrates the effectiveness of Theorem 10.

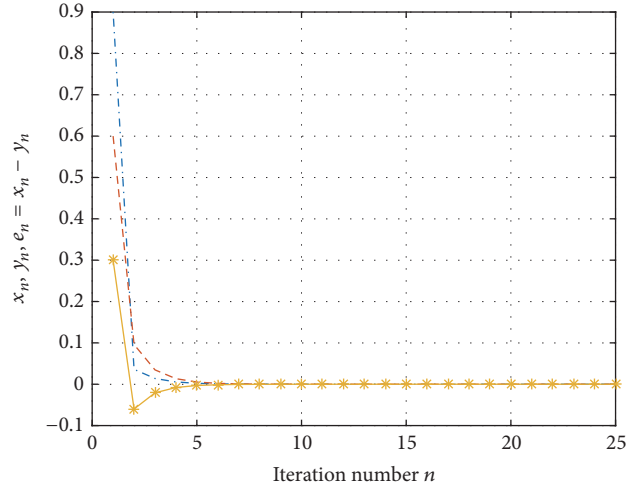


FIGURE 4: The trajectories of x_n, y_n, e_n .

FIGURE 4: The trajectories of x_n, y_n, e_n .

Example 16. Consider the logistic maps described by (24) and (26) with $r = 0.4$ and $x_1 = 0.9$ and $y_1 = 0.6$. Figure 4 reveals the global synchronization of the logistic maps described by (24) and (26) which illustrates the effectiveness of Theorem 14.

6. Conclusions and Future Works

For a given convergent scheme to approximate the fixed point of a contraction mapping, we have provided an associated scheme which had a similar structure to that of the given scheme. We have derived conditions to ensure this new scheme and the given scheme to converge to the same fixed point. We have used our derived results to construct the associated schemes for Picard, Mann, and Ishikawa iterative schemes for contraction mappings and derived the convergence theorems for those schemes, respectively. Moreover, we can accelerate the convergence rate of this new scheme by controlling the feedback parameter. We have extended those convergence and comparison results to nonexpansive mappings. In addition, we have utilized those derived results to investigate the synchronization of logistic maps. We have used two examples to illustrate the effectiveness of our derived results. In this paper, we only consider the linear feedback in the scheme. Our future research focus is to design a faster scheme by using the nonlinear feedback.

Conflicts of Interest

The authors declare that there are no conflicts of interest regarding the publication of this paper.

Acknowledgments

The authors are most grateful to the suggestions of colleagues of Zhejiang Open Foundation of the Most Important Subjects for this paper. This paper is partially supported by the National Natural Science Foundation of China under Grants 61561023 and 71461011, the Zhejiang Open Foundation of the Most Important Subjects, the Key Project of Youth Science Fund of Jiangxi China under Grant 20133ACB21009, the project of Science and Technology Fund of Jiangxi Education Department of China under Grant GJJ160429, the project of Jiangxi E-Commerce High Level Engineering Technology Research Centre, and the Basic Science Research Program through the National Research Foundation (NRF) grant funded by Ministry of Education of the Republic of Korea (2015R1D1A1A09058177).

References

- [1] A. A. Abdou, Y. J. Cho, and R. Saadati, "Distance type and common fixed point theorems in Menger probabilistic metric type spaces," *Applied Mathematics and Computation*, vol. 265, Article ID 21173, pp. 1145–1154, 2015.
- [2] I. K. Argyros, Y. J. Cho, and S. K. Khattri, "On the convergence of Broyden's method in Hilbert spaces," *Applied Mathematics and Computation*, vol. 242, pp. 945–951, 2014.
- [3] Q. H. Ansari, J. Balooee, and J.-C. Yao, "Iterative algorithms for systems of extended regularized nonconvex variational inequalities and fixed point problems," *Applicable Analysis: An International Journal*, vol. 93, no. 5, pp. 972–993, 2014.
- [4] V. Berinde, *Iterative Approximation of Fixed Points*, Springer, Berlin, Germany, 2007.
- [5] Y. J. Cho, S. Hirunworakit, and N. Petrot, "Set-valued fixed-point theorems for generalized contractive mappings without the Hausdorff metric," *Applied Mathematics Letters*, vol. 24, no. 11, pp. 1959–1967, 2011.
- [6] Y. J. Cho, R. Saadati, and Y.-O. Yang, "Approximation of homomorphisms and derivations on Lie C^* -algebras via fixed point method," *Journal of Inequalities and Applications*, vol. 2013, article no. 415, 2013.
- [7] J. M. Epstein and R. A. Hammond, "Non-explanatory equilibria: an extremely simple game with (mostly) unattainable fixed points," *Complexity*, vol. 7, no. 4, pp. 18–22, 2002.
- [8] E. Karapinar, " α - ψ -Geraghty contraction type mappings and some related fixed point results," *Filomat*, vol. 28, no. 1, pp. 37–48, 2014.
- [9] M. A. Khamsi and W. M. Kozłowski, "On asymptotic pointwise nonexpansive mappings in modular function spaces," *Journal of Mathematical Analysis and Applications*, vol. 380, no. 2, pp. 697–708, 2011.
- [10] A. T. Lau and Y. Zhang, "Fixed point properties for semigroups of nonlinear mappings on unbounded sets," *Journal of Mathematical Analysis and Applications*, vol. 433, no. 2, Article ID 19741, pp. 1204–1219, 2016.
- [11] L.-J. Lin and W. Takahashi, "Attractive point theorems for generalized nonspreading mappings in Banach spaces," *Journal of Convex Analysis*, vol. 20, no. 1, pp. 265–284, 2013.
- [12] X. Qin and R. P. Agarwal, "Shrinking projection methods for a pair of asymptotically quasi-f-nonexpansive mappings," *Numerical Functional Analysis and Optimization*, vol. 31, no. 7-9, pp. 1072–1089, 2010.
- [13] X. Qin, S. Y. Cho, T. Wang, and S. M. Kang, "Convergence of an implicit iterative process for asymptotically pseudocontractive nonself-mappings," *Nonlinear Analysis. Theory, Methods & Applications*, vol. 74, no. 17, pp. 5851–5862, 2011.
- [14] X. Qin, S. Y. Cho, and S. M. Kang, "An extragradient-type method for generalized equilibrium problems involving strictly pseudocontractive mappings," *Journal of Global Optimization*, vol. 49, no. 4, pp. 679–693, 2011.
- [15] S. Reich and S. Sabach, "A projection method for solving nonlinear problems in reflexive Banach spaces," *Journal of Fixed Point Theory and Applications*, vol. 9, no. 1, pp. 101–116, 2011.
- [16] S. Reich and A. J. Zaslavski, "Approximate fixed points of nonexpansive mappings in unbounded sets," *Journal of Fixed Point Theory and Applications*, vol. 13, no. 2, pp. 627–632, 2013.
- [17] S. Reich and R. Zalas, "A modular string averaging procedure for solving the common fixed point problem for quasi-nonexpansive mappings in Hilbert space," *Numerical Algorithms*, vol. 72, no. 2, pp. 297–323, 2016.
- [18] S. Saejung, "Two remarks on the modified Halpern iterations in CAT(0) spaces," *Fixed Point Theory*, vol. 15, no. 2, pp. 595–602, 2014.
- [19] D. R. Sahu, Q. H. Ansari, and J. C. Yao, "The prox-Tikhonov-like forward-backward method and applications," *Taiwanese Journal of Mathematics*, vol. 19, no. 2, pp. 481–503, 2015.
- [20] P. Saipara, P. Chaipunya, Y. J. Cho, and P. Kumam, "n strong and Δ -convergence of modified S-iteration for uniformly continuous total asymptotically nonexpansive mappings in CAT(k) spaces," *Journal of Nonlinear Sciences and Applications*, vol. 8, no. 6, pp. 965–975, 2015.
- [21] T. Suzuki, "Subrahmanyam's fixed point theorem," *Nonlinear Analysis: Theory, Methods and Applications*, vol. 71, no. 5-6, pp. 1678–1683, 2009.
- [22] U. Tirnakli and C. Tsallis, "Noisy coupled logistic maps in the vicinity of chaos threshold," *Chaos: An Interdisciplinary Journal of Nonlinear Science*, vol. 26, no. 4, Article ID 043114, 2016.
- [23] H.-K. Xu, "Averaged mappings and the gradient-projection algorithm," *Journal of Optimization Theory and Applications*, vol. 150, no. 2, pp. 360–378, 2011.
- [24] X. Chen and L. Ren, "Bifurcation Analysis and Chaos Control in a Discrete-Time Parasite-Host Model," *Discrete Dynamics in Nature and Society*, vol. 2017, Article ID 9275474, 2017.
- [25] A. Petrușel and G. Petrușel, "Nonlinear dynamics, Fixed points and coupled fixed points in generalized gauge spaces with applications to a system of integral equations," *Discrete Dynamics in Nature and Society*, vol. 2015, Article ID 143510, 2015.
- [26] Y. I. Kim, R. Behl, and S. S. Motsa, "An optimal family of eighth-order iterative methods with an inverse interpolatory rational function error corrector for nonlinear equations," *Mathematical Modelling and Analysis*, vol. 22, no. 3, pp. 321–336, 2017.
- [27] A. Cordero and J. R. Torregrosa, "A sixth-order iterative method for approximating the polar decomposition of an arbitrary matrix," *Journal of Computational and Applied Mathematics*, vol. 318, pp. 591–598, 2017.

- [28] F. Soleymani, T. Lotfi, and P. Bakhtiari, "A multi-step class of iterative methods for nonlinear systems," *Optimization Letters*, vol. 8, no. 3, pp. 1001–1015, 2014.
- [29] J. R. Sharma and P. Gupta, "An efficient fifth order method for solving systems of nonlinear equations," *Computers & Mathematics with Applications*, vol. 67, no. 3, pp. 591–601, 2014.
- [30] X. Wang, T. Zhang, and Y. Qin, "Efficient two-step derivative-free iterative methods with memory and their dynamics," *International Journal of Computer Mathematics*, vol. 93, no. 8, pp. 1423–1446, 2016.
- [31] L. Liu and S. Miao, "The complexity of binary sequences using logistic chaotic maps," *Complexity*, vol. 21, no. 6, pp. 121–129, 2016.
- [32] R. Luo, H. Su, and Y. Zeng, "Chaos control and synchronization via switched output control strategy," *Complexity*, Art. ID 6125102, 11 pages, 2017.

Research Article

Multistep High-Order Methods for Nonlinear Equations Using Padé-Like Approximants

Alicia Cordero, José L. Hueso, Eulalia Martínez, and Juan R. Torregrosa

Instituto de Matemática Multidisciplinar, Universitat Politècnica de València, Camino de Vera, s/n, 46022 Valencia, Spain

Correspondence should be addressed to Juan R. Torregrosa; jrtorre@mat.upv.es

Received 23 May 2017; Accepted 29 August 2017; Published 3 October 2017

Academic Editor: Chuanxi Qian

Copyright © 2017 Alicia Cordero et al. This is an open access article distributed under the Creative Commons Attribution License, which permits unrestricted use, distribution, and reproduction in any medium, provided the original work is properly cited.

We present new high-order optimal iterative methods for solving a nonlinear equation, $f(x) = 0$, by using Padé-like approximants. We compose optimal methods of order 4 with Newton's step and substitute the derivative by using an appropriate rational approximant, getting optimal methods of order 8. In the same way, increasing the degree of the approximant, we obtain optimal methods of order 16. We also perform different numerical tests that confirm the theoretical results.

1. Introduction

Many applied problems in different fields of science and technology require to find the solution of a nonlinear equation. Iterative methods are used to approximate its solutions. The performance of an iterative method can be measured by the efficiency index introduced by Ostrowski in [1]. In this sense, Kung and Traub conjectured in [2] that a multistep method without memory performing $n + 1$ functional evaluations per iteration can have at most convergence order 2^n , in which case it is said to be optimal.

Recently, different optimal eighth-order methods, with 4 functional evaluations per step, have been published. A very interesting survey can be found in [3]. Some of them are a generalization of the well-known Ostrowski's optimal method of order four [4–7]. In [8] the authors start from a third-order method due to Potra-Pták, combine this scheme with Newton's method using “frozen” derivative, and estimate the new functional evaluation. The procedure designed in [9] uses weight-functions and “frozen” derivative for the development of the schemes. As far as we know, beyond the family described by Kung and Traub in [2], only in [10] a general technique to obtain new optimal methods has been presented; the authors use inverse interpolation and methods of sixteenth order have also been obtained.

While computational engineering has achieved significant maturity, computational costs can be extremely large

when high accuracy simulations are required. The development of a practical high-order solution method could diminish this problem by significantly decreasing the computational time required to achieve an acceptable error level (see, e.g., [11]).

The existence of an extensive literature on higher order methods (see, e.g., [3, 12] and the references therein) reveals that they are only limited by the nature of the problem to be solved: in particular, the numerical solutions of nonlinear equations and systems are needed in the study of dynamical models of chemical reactors [13], or in radioactive transfer [14]. Moreover, many of numerical applications use high precision in their computations; in [15], high-precision calculations are used to solve interpolation problems in Astronomy; in [16] the authors describe the use of arbitrary precision computations to improve the results obtained in climate simulations; the results of these numerical experiments show that the high-order methods associated with a multiprecision arithmetic floating point are very useful, because it yields a clear reduction in iterations. A motivation for an arbitrary precision in interval methods can be found in [17], in particular for the calculation of zeros of nonlinear functions.

The objective of this paper is to present a general procedure to obtain optimal order methods for $n = 3, 4$ starting from optimal order methods for $n = 2$. The procedure consists in composing optimal methods of order 4 that use

two evaluations of the function and one of the derivative, with Newton's step and approximating the derivative in this last step by using an adequate rational function which allows duplicating the convergence order, introducing only one new functional evaluation per iteration.

In Section 2, we describe the process to generate the new eighth-order methods and establish their convergence order. In Section 3, the same procedure is used to obtain sixteenth-order methods by increasing the approximant degree. Finally, in Section 4, we collect several optimal methods of order 4 that are the starting point for our new methods and present numerical experiments that confirm the theoretical results.

2. Optimal Methods of Order 8

In this section, we describe a procedure that allows us to obtain new optimal methods of order 8, starting from optimal schemes of order 4. Let us denote by Ψ_{2^m} the set of iteration functions corresponding to optimal methods of order 2^m .

Consider the three-step method given by

$$\begin{aligned}\phi_1(x_k) &= x_k - \frac{f(x_k)}{f'(x_k)}, \\ \phi_2(x_k) &= \psi_f(x_k), \\ \phi_3(x_k) &= \phi_2(x_k) - \frac{f(\phi_2(x_k))}{f'(\phi_2(x_k))},\end{aligned}\quad (1)$$

where $\psi_f \in \Psi_4$.

In order to simplify the notation, we will omit the argument x_k in the iterative process, so that we will write $\phi_i(x_k)$ as ϕ_i , $i = 1, 2, 3$ and $\phi_0 = x_k$.

Obviously, this three-step method has order 8, being a composition of schemes of orders 4 and 2, respectively (see [2], Th. 2.4), but the method is not optimal because it introduces two new functional evaluations in the last step.

Thus, to maintain the optimality, we substitute $f'(\phi_2(x_k))$ with the derivative $h'_2(\phi_2(x_k))$ of the second-degree approximant

$$h_2(t) = \frac{a_0^{(2)} + a_1^{(2)}(t - \phi_0) + a_2^{(2)}(t - \phi_0)^2}{1 + b_1^{(2)}(t - \phi_0)}, \quad (2)$$

verifying the conditions

$$h_2(\phi_0) = f(\phi_0), \quad (3)$$

$$h'_2(\phi_0) = f'(\phi_0), \quad (4)$$

$$h_2(\phi_1) = f(\phi_1), \quad (5)$$

$$h_2(\phi_2) = f(\phi_2). \quad (6)$$

From the first condition one has $a_0^{(2)} = f(\phi_0)$. Substituting in (4)–(6) we obtain the following linear system:

$$a_1^{(2)} - b_1^{(2)} f(\phi_0) = f'(\phi_0)$$

$$a_1^{(2)} + a_2^{(2)}(\phi_1 - \phi_0) - b_1^{(2)} f(\phi_1) = f[\phi_0, \phi_1] \quad (7)$$

$$a_1^{(2)} + a_2^{(2)}(\phi_2 - \phi_0) - b_1^{(2)} f(\phi_2) = f[\phi_0, \phi_2],$$

where, as usual, $f[x, y]$ denotes the divided difference of order 1, $(f(y) - f(x))/(y - x)$. Applying Gaussian elimination the following reduced system is obtained

$$\begin{aligned}a_1^{(2)} - b_1^{(2)} f(\phi_0) &= f'(\phi_0) \\ a_2^{(2)} - b_1^{(2)} f[\phi_0, \phi_1] &= f[\phi_0, \phi_0, \phi_1] \\ -b_1^{(2)} f[\phi_0, \phi_1, \phi_2] &= f[\phi_0, \phi_0, \phi_1, \phi_2].\end{aligned}\quad (8)$$

In the divided differences with a repeated argument, one places the derivative instead of an undetermined quotient. The coefficients of the approximant are obtained by backward substitution. Then, the derivative of the approximant in ϕ_2 is

$$\begin{aligned}h'_2(\phi_2) &= \frac{a_1^{(2)} - a_0^{(2)}b_1^{(2)} + 2a_2^{(2)}(\phi_2 - \phi_0) + a_2^{(2)}b_1^{(2)}(\phi_2 - \phi_0)^2}{(1 + b_1^{(2)}(\phi_2 - \phi_0))^2}.\end{aligned}\quad (9)$$

Substituting $f'(\phi_2)$ by this value, we obtain an iterative method, M_3 , defined by

$$x_{k+1} = \phi_3(x_k), \quad (10)$$

where

$$\phi_1(x_k) = x_k - \frac{f(x_k)}{f'(x_k)}, \quad (11)$$

$$\phi_2(x_k) = \psi_f(x_k), \quad (12)$$

$$\phi_3(x_k) = \phi_2(x_k) - \frac{f(\phi_2(x_k))}{h'_2(\phi_2(x_k))}. \quad (13)$$

This method only uses 4 functional evaluations per iteration. Showing that it is of order 8 we will prove that it is optimal in Kung-Traub's sense.

Theorem 1. *Let $\alpha \in I$ be a simple root of a function $f : I \subseteq \mathbb{R} \rightarrow \mathbb{R}$ sufficiently differentiable in an open interval I . For an x_0 close enough to α , the method defined by (11)–(13) has optimal convergence order 2^3 .*

Proof. Let $\epsilon_{m,k}$ be the error of $\phi_m(x_k)$; that is, $\epsilon_{m,k} = \phi_m(x_k) - \alpha$, $m = 0, 1, 2, 3$, for $k = 0, 1, \dots$. Then, by the definition of each step of the iterative method, we have

$$\epsilon_{0,k} = \epsilon_k = x_k - \alpha, \quad (14)$$

$$\epsilon_{1,k} = \phi_1(x_k) - \alpha = O(\epsilon_k^2), \quad (15)$$

$$\epsilon_{2,k} = \phi_2(x_k) - \alpha = O(\epsilon_k^4), \quad (\text{since } \psi_f \in \Psi_4). \quad (16)$$

Consider the expansion of $f(\phi_0)$ around α

$$\begin{aligned}f(\phi_0) &= c_1\epsilon_k + c_2\epsilon_k^2 + c_3\epsilon_k^3 + c_4\epsilon_k^4 + c_5\epsilon_k^5 + c_6\epsilon_k^6 + c_7\epsilon_k^7 \\ &\quad + c_8\epsilon_k^8 + O(\epsilon_k^9),\end{aligned}\quad (17)$$

where $c_j = f^{(j)}(\alpha)/j!$, for $j = 1, 2, \dots$; then,

$$f'(\phi_0) = c_1 + 2c_2\epsilon_k + 3c_3\epsilon_k^2 + 4c_4\epsilon_k^3 + 5c_5\epsilon_k^4 + 6c_6\epsilon_k^5 + 7c_7\epsilon_k^6 + 8c_8\epsilon_k^7 + O(\epsilon_k^8), \quad (18)$$

so that using (11) and (14)

$$\begin{aligned} \epsilon_{1,k} &= \epsilon_k - \frac{f(x_k)}{f'(x_k)} \\ &= \frac{c_2}{c_1}\epsilon_k^2 + \frac{2(-c_2^2 + c_1c_3)}{c_1^2}\epsilon_k^3 \\ &\quad + \frac{4c_2^3 - 7c_1c_2c_3 + 3c_1^2c_4}{c_1^3}\epsilon_k^4 + \dots \end{aligned} \quad (19)$$

Substituting (19) in the expansion of $f(\phi_1)$ around α we get

$$\begin{aligned} f(\phi_1) &= c_2\epsilon_k^2 + \left(-\frac{2c_2^2}{c_1} + 2c_3\right)\epsilon_k^3 \\ &\quad + \left(\frac{5c_2^3}{c_1^2} - \frac{7c_2c_3}{c_1} + 3c_4\right)\epsilon_k^4 + \dots \end{aligned} \quad (20)$$

Using in (15) that $\psi_f \in \Psi_4$, we write

$$\epsilon_{2,k} = i_4\epsilon_k^4 + i_5\epsilon_k^5 + i_6\epsilon_k^6 + i_7\epsilon_k^7 + i_8\epsilon_k^8 + O(\epsilon_k^9), \quad (21)$$

for some i_j constants, $j = 4, 5, \dots$. Substituting (21) in Taylor's expansion of $f(\phi_2)$, we obtain

$$\begin{aligned} f(\phi_2) &= c_1i_4\epsilon_k^4 + c_1i_5\epsilon_k^5 + c_1i_6\epsilon_k^6 + c_1i_7\epsilon_k^7 \\ &\quad + (c_2i_4^2 + c_1i_8)\epsilon_k^8 + O(\epsilon_k^9). \end{aligned} \quad (22)$$

Using (17), (18), (20), and (22) in the determination of the coefficients of the rational approximant and in the expression of its derivative (9) gives

$$\begin{aligned} h_2'(\phi_2) &= c_1 + \frac{-c_2^2 + c_2(c_4 + 2c_1i_4)}{c_1}\epsilon_k^4 + \dots \\ &= f'(\alpha) + O(\epsilon_k^4). \end{aligned} \quad (23)$$

Now, Taylor's expansion of $f'(\phi_2)$ in $x = \alpha$ gives

$$f'(\phi_2) = f'(\alpha) + f''(\alpha)(\phi_2 - \alpha) + O(\phi_2 - \alpha)^2, \quad (24)$$

and the fact that $\phi_2(x)$ is of fourth order allows us to establish

$$f'(\phi_2) = f'(\alpha) + O(\epsilon_k^4). \quad (25)$$

Using this expression and (23) one can write

$$f'(\phi_2) = h_2'(\phi_2)(1 + O(\epsilon_k^4)). \quad (26)$$

The order of the method M_3 is obtained by computing

$$\epsilon_{3,k} = \phi_3(x_k) - \alpha = \phi_2(x_k) - \alpha - \frac{f(\phi_2(x_k))}{h_2'(\phi_2(x_k))}. \quad (27)$$

Using (26) we have

$$\begin{aligned} \epsilon_{3,k} &= \phi_3(x_k) - \alpha \\ &= \phi_2(x_k) - \alpha - \frac{f(\phi_2(x_k))(1 + O(\epsilon_k^4))}{f'(\phi_2(x_k))} \\ &= \phi_2(x_k) - \alpha - \frac{f(\phi_2(x_k))}{f'(\phi_2(x_k))} \\ &\quad - \frac{f(\phi_2(x_k))}{f'(\phi_2(x_k))}O(\epsilon_k^4). \end{aligned} \quad (28)$$

From (19) it can be deduced that

$$\frac{f(x_k)}{f'(x_k)} = \epsilon_k - \epsilon_{1,k} = (x_k - \alpha) - \frac{c_2}{c_1}(x_k - \alpha)^2 - \dots \quad (29)$$

So, it is clear that

$$\begin{aligned} \frac{f(\phi_2(x_k))}{f'(\phi_2(x_k))} &= (\phi_2(x_k) - \alpha) - \frac{c_2}{c_1}(\phi_2(x_k) - \alpha)^2 \\ &\quad - \dots \end{aligned} \quad (30)$$

By substituting (30) in (28) and using that $\psi_f \in \Psi_4$ one has

$$\begin{aligned} \epsilon_{3,k} &= \frac{c_2}{c_1}(\phi_2(x_k) - \alpha)^2 + \dots + (\phi_2(x_k) - \alpha)O(\epsilon_k^4) \\ &\quad + \dots = O(\epsilon_k^8), \end{aligned} \quad (31)$$

which proves that method M_3 has optimal order 2^3 . \square

3. Optimal Methods of Order 16

The idea of this section is to extend the former process performing a new step to obtain optimal methods of order 2^n starting from optimal methods of order 2^{n-1} . For $n = 4$ the method M_4 can be defined as follows:

$$x_{k+1} = \phi_4(x_k), \quad k = 0, 1, \dots \quad (32)$$

with

$$\begin{aligned} \phi_1(x) &= x - \frac{f(x)}{f'(x)}, \\ \phi_2(x) &= \psi_f(x), \\ \phi_3(x) &= \varphi_f(x), \end{aligned} \quad (33)$$

$$\phi_4(x) = \phi_3(x) - \frac{f(\phi_3(x))}{h_3'(\phi_3(x))},$$

where $\psi_f \in \Psi_4$ and $\varphi_f \in \Psi_8$. (See [2, 5, 6, 8, 14, 16, 18] for some optimal eighth-order methods.)

Then, we start from a method that, in its first three steps, performs 4 functional evaluations and another additional evaluation in the last step $f(\phi_3(x))$ that allows us to construct the following rational approximant:

$$h_3(t) = \frac{a_0^{(3)} + a_1^{(3)}(t - \phi_0) + a_2^{(3)}(t - \phi_0)^2 + a_3^{(3)}(t - \phi_0)^3}{1 + b_1^{(3)}(t - \phi_0)}. \quad (34)$$

The coefficients are determined by imposing the following conditions:

$$h_3(\phi_0) = f(\phi_0), \quad (35)$$

$$h_3'(\phi_0) = f'(\phi_0), \quad (36)$$

$$h_3(\phi_1) = f(\phi_1), \quad (37)$$

$$h_3(\phi_2) = f(\phi_2), \quad (38)$$

$$h_3(\phi_3) = f(\phi_3). \quad (39)$$

Similarly to the former case, $a_0^{(3)} = f(\phi_0)$. Substituting in (36)–(39) we obtain the linear system

$$\begin{aligned} a_1^{(3)} - b_1^{(3)} f(\phi_0) &= f'(\phi_0) \\ a_1^{(3)} + a_2^{(3)}(\phi_1 - \phi_0) + a_2^{(3)}(\phi_1 - \phi_0)^2 - b_1^{(3)} f(\phi_1) &= f[\phi_0, \phi_1] \\ a_1^{(3)} + a_2^{(3)}(\phi_2 - \phi_0) + a_2^{(3)}(\phi_2 - \phi_0)^2 - b_1^{(3)} f(\phi_2) &= f[\phi_0, \phi_2] \\ a_1^{(3)} + a_2^{(3)}(\phi_3 - \phi_0) + a_2^{(3)}(\phi_3 - \phi_0)^2 - b_1^{(3)} f(\phi_3) &= f[\phi_0, \phi_3]. \end{aligned} \quad (40)$$

The remaining coefficients are obtained by reducing the system to triangular form and solving it by backward substitution

$$\begin{aligned} a_1^{(3)} - b_1^{(3)} f(\phi_0) &= f'(\phi_0) \\ a_2^{(3)} + a_3^{(3)}(\phi_1 - \phi_0) - b_1^{(3)} f[\phi_0, \phi_1] &= f[\phi_0, \phi_0, \phi_1] \\ a_3^{(3)} - b_1^{(3)} f[\phi_0, \phi_0, \phi_2] &= f[\phi_0, \phi_0, \phi_1, \phi_2] \\ -b_1^{(3)} f[\phi_0, \phi_0, \phi_2, \phi_3] &= f[\phi_0, \phi_0, \phi_1, \phi_2, \phi_3]. \end{aligned} \quad (41)$$

The derivative of the rational approximant in ϕ_3 is

$$\begin{aligned} h_3'(\phi_3) &= \frac{a_1^{(3)} - a_0^{(3)}b_1^{(3)} + 2a_2^{(3)}(\phi_3 - \phi_0)}{(1 + b_1^{(3)}(\phi_3 - \phi_0))^2} \\ &+ \frac{(3a_3^{(3)} + a_2^{(3)}b_1^{(3)})(\phi_3 - \phi_0)^2 + 2a_3^{(3)}b_1^{(3)}(\phi_3 - \phi_0)^3}{(1 + b_1^{(3)}(\phi_3 - \phi_0))^2}. \end{aligned} \quad (42)$$

As in the previous case, this expression allows us to establish that

$$h_3'(\phi_3) = f'(\alpha) + O(\epsilon_k^8), \quad (43)$$

and taking into account the fact that

$$f'(\phi_3) = f'(\alpha) + O(\epsilon_k^8), \quad (44)$$

we get

$$f'(\phi_3) = h_3'(\phi_3)(1 + O(\epsilon_k^8)). \quad (45)$$

Similarly to the eighth-order case, from this expression it results that M_4 has optimal convergence order 2^4 .

4. Numerical Experiments

First of all, we consider some optimal four-order methods that we have used for developing high-order methods with the procedure described; all of them use Newton's step as a predictor and another evaluation of function f .

$$y_k = x_k - \frac{f(x_k)}{f'(x_k)}. \quad (46)$$

(1) Ostrowski's method (see [1])

$$x_{k+1} = y_k - \frac{f(y_k)(x_k - y_k)}{f(x_k) - 2f(y_k)}. \quad (47)$$

(2) The family of King's method (see [18])

$$x_{k+1} = y_k - \frac{f(y_k)}{f'(x_k)} \frac{f(x_k) + bf(y_k)}{f(x_k) + (b-2)f(y_k)}. \quad (48)$$

(3) An optimal variant of Potra-Pták's method (see [8])

$$\begin{aligned} x_{k+1} &= x_k - \frac{f(x_k) + f(y_k)}{f'(x_k)} \\ &- \frac{f(y_k)^2(2f(x_k) + f(y_k))}{f(x_k)^2 f'(x_k)}. \end{aligned} \quad (49)$$

(4) Maheshwari method (see [19])

$$x_{k+1} = x_k - \frac{f(x_k)}{f'(x_k)} \left(\frac{f(y_k)^2}{f(x_k)^2} - \frac{f(x_k)}{f(y_k) - f(x_k)} \right). \quad (50)$$

Now we check the performance of the methods M_3 and M_4 generated by (5) and (32), taking the different methods $\psi_f \in \Psi_4$ described above.

We have chosen the following examples:

(a) $f(x) = (x-2)(x^{10} + x + 1)e^{-x-1}$, $\alpha = 2$.

(b) $f(x) = e^x \sin(5x) - 2$, $\alpha \approx 1.36397318$.

TABLE 1: Numerical results for $f(x) = (x-2)(x^{10}+x+1)e^{-x-1}$; $\alpha = 2$, with $x_0 = 2.1$.

M_3 with ψ_f	$ x_1 - \alpha $	$ x_2 - \alpha $	$ x_3 - \alpha $	p
Ostrowski	9.5688(-6)	3.1934(-37)	4.9152(-289)	8
King $_{\beta=-1}$	7.25(-5)	2.62(-29)	7.68(-225)	8
King $_{\beta=1}$	7.34(-5)	8.65(-29)	3.23(-220)	8
Opt. Potra	3.17(-5)	3.48(-33)	7.34(-257)	7.99
Maheshwari	1.03(-4)	2.56(-27)	3.72(-208)	8

TABLE 2: Numerical results for $f(x) = (x-2)(x^{10}+x+1)e^{-x-1}$; $\alpha = 2$, with $x_0 = 2.1$.

M_4 with ψ_f	$ x_1 - \alpha $	$ x_2 - \alpha $	$ x_3 - \alpha $	p
Ostrowski	3.76(-10)	1.34(-143)	9.25(-2279)	15.8399
King $_{\beta=-1}$	2.08(-8)	5.55(-114)	3.83(-1803)	15.7977
King $_{\beta=1}$	2.17(-8)	1.02(-112)	5.72(-1782)	15.6564
Opt. Potra	3.94(-9)	1.56(-127)	5.93(-2022)	15.9907
Maheshwari	4.28(-8)	2.03(-107)	1.29(-1696)	15.5962

TABLE 3: Numerical results for $f(x) = e^x \sin(5x) - 2$; $\alpha \approx 1.36397318 \dots$, with $x_0 = 1.2$.

M_3 with ψ_f	$ x_1 - x_0 $	$ x_2 - x_1 $	$ x_3 - x_2 $	ρ
Ostrowski	0.00363	3.13(-17)	2.43(-128)	8
King $_{\beta=-1}$	0.00228	4.44(-18)	4.81(-135)	8
King $_{\beta=1}$	-0.00544	1.72(-16)	1.64(-122)	8
Opt. Potra	0.00669	4.15(-16)	1.74(-119)	7.99
Maheshwari	0.00305	1.5(-17)	7.5(-131)	7.99

We have performed the computations in MATLAB in variable precision arithmetic with 1000 digits of mantissa.

Tables 1 and 2 show the distance $|x_k - \alpha|$ for the first three iterations of the new order 8 and 16 methods, respectively. The last column, when we know the exact solution α , that is, for example, (a), depicts the computational convergence order p (see [20])

$$p = \frac{\ln(|x_{k+1} - \alpha| / |x_k - \alpha|)}{\ln(|x_k - \alpha| / |x_{k-1} - \alpha|)}, \quad (51)$$

and for example (b), we compute the approximated computational convergence order ρ (see [21])

$$\rho = \frac{\ln(|x_{k+1} - x_k| / |x_k - x_{k-1}|)}{\ln(|x_k - x_{k-1}| / |x_{k-1} - x_{k-2}|)}. \quad (52)$$

The results from Tables 3 and 4 correspond to an equation without exact solution, so that $|x_{k+1} - x_k|$ is computed, instead of the actual error. In both cases, the numerical results support the optimality of the new methods, according to the proven theoretical results.

5. Conclusions

In this paper, we develop high-order iterative methods to solve nonlinear equations. The procedure to obtain the iteration functions is rigorously deduced and can be generalized.

TABLE 4: Numerical results for $f(x) = e^x \sin(5x) - 2$; $\alpha \approx 1.36397318 \dots$, with $x_0 = 1.2$.

M_4 with ψ_f	$ x_1 - x_0 $	$ x_2 - x_1 $	$ x_3 - x_2 $	ρ
Ostrowski	6.45(-5)	7.08(-75)	5.13(-1188)	16.0342
King $_{\beta=-1}$	4.02(-5)	-2.65(-78)	7.38(-1243)	15.9919
King $_{\beta=1}$	9.73(-5)	-5.81(-72)	2.3(-1141)	16.0731
Opt. Potra	5.41(-5)	3.43(-76)	4.58(-1209)	16.0182
Maheshwari	1.2(-4)	2.11(-70)	2.25(-1116)	16.0957

There are numerous applications where these schemes are needed because it is necessary to use high precision in their computations, as occurs in dynamical models of chemical reactors and in radioactive transfer and also high-precision calculations are used to solve interpolation problems in Astronomy and so forth. Moreover, the methods presented are optimal in terms of efficiency; this fact makes them very competitive.

Conflicts of Interest

The authors declare that there are no conflicts of interest regarding the publication of this paper.

Acknowledgments

This work has been supported by Ministerio de Ciencia e Innovación de España MTM2014-52016-C2-02-P and Generalitat Valenciana PROMETEO/2016/089.

References

- [1] A. M. Ostrowski, *Solution of Equations and Systems of Equations*, Academic Press, London, UK, 1966.
- [2] H. T. Kung and J. F. Traub, "Optimal order of one-point and multipoint iteration," *Journal of the Association for Computing Machinery*, vol. 21, pp. 643–651, 1974.
- [3] M. S. Petković, B. Neta, L. D. Petković, and J. Džunić, *Multipoint Methods for Solving Nonlinear Equations*, Academic Press, Amsterdam, The Netherlands, 2013.
- [4] W. Bi, H. Ren, and Q. Wu, "Three-step iterative methods with eighth-order convergence for solving nonlinear equations," *Journal of Computational and Applied Mathematics*, vol. 225, no. 1, pp. 105–112, 2009.
- [5] A. Cordero, J. R. Torregrosa, and M. a. Vassileva, "Three-step iterative methods with optimal eighth-order convergence," *Journal of Computational and Applied Mathematics*, vol. 235, no. 10, pp. 3189–3194, 2011.
- [6] L. Liu and X. Wang, "Eighth-order methods with high efficiency index for solving nonlinear equations," *Applied Mathematics and Computation*, vol. 215, no. 9, pp. 3449–3454, 2010.
- [7] J. R. Sharma and R. Sharma, "A new family of modified Ostrowski's methods with accelerated eighth order convergence," *Numerical Algorithms*, vol. 54, no. 4, pp. 445–458, 2010.
- [8] A. Cordero, J. L. Hueso, E. Martínez, and J. R. Torregrosa, "New modifications of Potra-Pták's method with optimal fourth and eighth orders of convergence," *Journal of Computational and Applied Mathematics*, vol. 234, no. 10, pp. 2969–2976, 2010.

- [9] X. Wang and L. Liu, "New eighth-order iterative methods for solving nonlinear equations," *Journal of Computational and Applied Mathematics*, vol. 234, no. 5, pp. 1611–1620, 2010.
- [10] B. Neta and M. S. Petković, "Construction of optimal order nonlinear solvers using inverse interpolation," *Applied Mathematics and Computation*, vol. 217, no. 6, pp. 2448–2455, 2010.
- [11] K. J. Fidkowski, T. A. Oliver, J. Lu, and D. L. Darmofal, "p-Multigrid solution of high-order discontinuous Galerkin discretizations of the compressible Navier-Stokes equations," *Journal of Computational Physics*, vol. 207, no. 1, pp. 92–113, 2005.
- [12] S. Amat and S. Busquier, *Advances in Iterative Methods for Nonlinear Equations*, vol. 10, Springer, Berlin, Germany, 2016.
- [13] D. D. Bruns and J. E. Bailey, "Nonlinear feedback control for operating a nonisothermal CSTR near an unstable steady state," *Chemical Engineering Science*, vol. 32, no. 3, pp. 257–264, 1977.
- [14] J. A. Ezquerro, J. M. Gutiérrez, M. A. Hernández, and M. A. Salanova, "Chebyshev-like methods and quadratic equations," *Revue d'Analyse Numérique et de Théorie de l'Approximation*, vol. 28, no. 1, pp. 23–35, 1999.
- [15] Y. Zhang and P. Huang, "High-precision Time-interval Measurement Techniques and Methods," *Progress in Astronomy*, vol. 24, no. 1, pp. 1–15, 2006.
- [16] Y. He and C. Ding, "Using accurate arithmetics to improve numerical reproducibility and stability in parallel applications," *The Journal of Supercomputing*, vol. 18, no. 3, pp. 259–277, 2001.
- [17] N. Revol and F. Rouillier, "Motivations for an arbitrary precision interval arithmetic and the MPFI library," *Reliable Computing*, vol. 11, no. 4, pp. 275–290, 2005.
- [18] R. F. King, "A family of fourth order methods for nonlinear equations," *SIAM Journal on Numerical Analysis*, vol. 10, pp. 876–879, 1973.
- [19] A. K. Maheshwari, "A fourth order iterative method for solving nonlinear equations," *Applied Mathematics and Computation*, vol. 211, no. 2, pp. 383–391, 2009.
- [20] S. Weerakoon and T. G. Fernando, "A variant of Newton's method with accelerated third-order convergence," *Applied Mathematics Letters. An International Journal of Rapid Publication*, vol. 13, no. 8, pp. 87–93, 2000.
- [21] A. Cordero and J. R. Torregrosa, "Variants of Newton's method using fifth-order quadrature formulas," *Applied Mathematics and Computation*, vol. 190, no. 1, pp. 686–698, 2007.

Research Article

Recurrence Based Similarity Identification of Climate Data

Anita Bai,¹ Swati Hira,² and S. Deshpande Parag¹

¹Department of Computer Science & Engineering, VNIT, Nagpur, India

²Department of Computer Science & Engineering, RCOEM, Nagpur, India

Correspondence should be addressed to Swati Hira; hiras@rknec.edu

Received 2 December 2016; Revised 23 April 2017; Accepted 15 May 2017; Published 19 July 2017

Academic Editor: Alicia Cordero

Copyright © 2017 Anita Bai et al. This is an open access article distributed under the Creative Commons Attribution License, which permits unrestricted use, distribution, and reproduction in any medium, provided the original work is properly cited.

Climate change has become a challenging and emerging research problem in many research related areas. One of the key parameters in analyzing climate change is to analyze temperature variations in different regions. The temperature variation in a region is periodic within the interval. Temperature variations, though periodic in nature, may vary from one region to another and such variations are mainly dependent on the location and altitude of the region and also on other factors like the nearness of sea and vegetation. In this paper, we analyze such periodic variations using recurrence plot (RP), cross recurrence plot (CRP), recurrence rate (RR), and correlation of probability of recurrence (CPR) methods to find similarities of periodic variations between and within climatic regions and to identify their connectivity trend. First, we test the correctness of our method by applying it on voice and heart rate data and then experimentation is performed on synthetic climate data of nine regions in the United States and eight regions in China. Finally, the accuracy of our approach is validated on both real and synthetic datasets and demonstrated using ANOVA, Kruskal–Wallis, and z -statistics significance tests.

1. Introduction

No location on the earth will have exactly the same climate as another; many do have very similar climatic characteristics, which depend on various factors such as latitude and longitude of the region, temperature, humidity, air pressure, wind, cloudiness, and nearness of sea and vegetation. Temperature is one of the important factors in climate change. The temperature of a region affects humans and biological and physical systems in all continents [1]. Currently, temperature is rising all over the world because greenhouse gases are trapping more heat in the earth's atmosphere. Effective and urgent solutions are needed to identify its impact on agriculture, energy, water supplies, health, plants, animals, ecosystems, forests, recreation, and so forth. Decisions about temperature change are complex and costly and have long-term implications. It is therefore vital that such decisions are based on the best available evidence. We need to understand the quality and provenance of that evidence and to find whether any assumptions have been made in generating it. Understanding temperature change patterns and their periodic variations across time (such as yearly, monthly, and

daily changes) and their changes across environmental space is of great significance.

Climate change adjustment refers to dealing with the present or future expected impacts of climate change. There are various ongoing research efforts on the collection of climate data, the analysis of climate changes, and the modeling of climate processes. Finding correlations or similarities among climate data is one of the central themes of many scientific analyses. A good example is climate data analysis to understand temperature changes over wide ranges of time. It has many applications to agriculture [2, 3], fisheries, ecosystems, water resources, energy infrastructure, business [2, 4], food industry [2, 5, 6], and disaster planning. In addition, climate impacts have also been assessed in potato [7], maize [8], coffee [9], rice [10], sugar [11], wine grape production [12], and so forth. For example, climate change eventually increases the additional price for the agricultural crops such as rice, wheat, maize, and soya beans, which tends to cause a higher substantial fall in cereals consumption.

To identify such climate change pattern, we proposed a recurrence based approach to analyze temperature variations

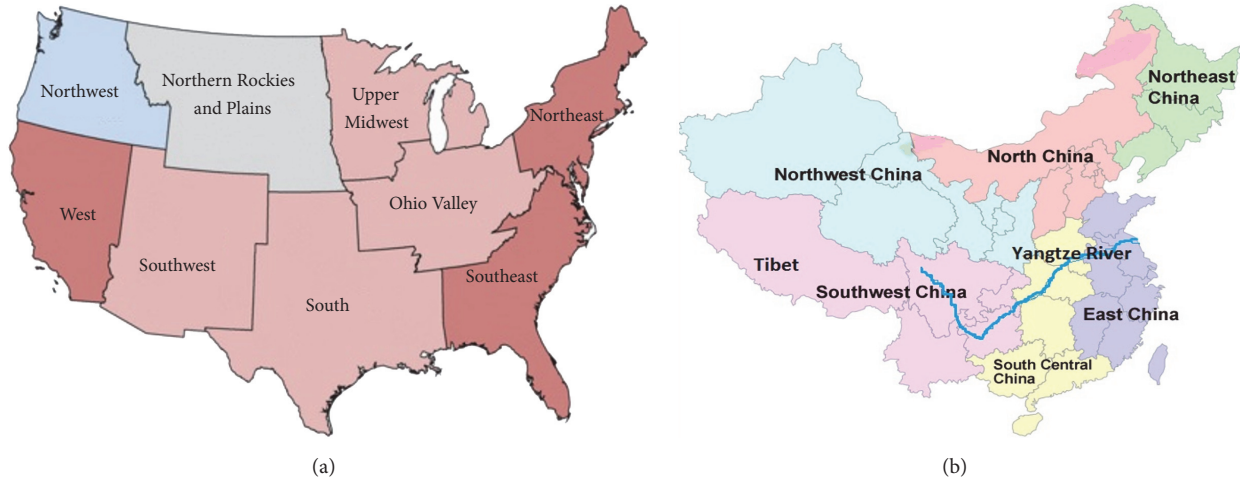


FIGURE 1: (a) Regions in the United States. (b) Regions in China.

in various climatic regions. The major contributions of our approach are summarized as follows:

- (1) Identify the periodic variations of temperature by analyzing trends using recurrence plot (RP) for time series data.
- (2) Discover the climate differences or similarities of the periodic variations existing between two regions using cross recurrence plot (CRP), for example, nine regions in the United States (Ohio Valley, Upper Midwest, Northeast, Northwest, South, Southeast, Southwest, West, and Northern Rockies and Plains) and eight regions in China (South China, the middle and lower reaches of the Yangtze River, North China, Northeast China, the east of Northwest China, the west of Northwest China, Tibet, and Southwest China), shown in Figures 1(a) and 1(b).
- (3) Extract similarities among regions by using techniques such as recurrence rate (RR), RP, CRP, and correlation of probability of recurrence (CPR) on temperature data.
- (4) Calculate the number of connections in each bin over time by binning CPR into three categories of relatedness (weak, moderate, and strong).

We have demonstrated the potentials of this approach for nine regions in the US, eight regions in China, and synthetic, voice, and heart rate data. In this paper, we analyzed nine connected regions in the US using monthly temperature data spread over 120 years. Using RP, we proved the periodic behavior of the variations. Using CRP, we provided the method to test whether two regions have similar variations. RR and CPR are used to show the correlation of probability of occurrence of temperature points between time series of two regions. Substantial experiments indicate that the proposed approach successfully provides useful interpretation of similar or dissimilar patterns between and within regions related to climate change.

2. Literature Review

Climate data (temperature) are usually multidimensional arrays of floating-point numbers. These arrays typically have one temporal dimension and two or three spatial dimensions, which describes the evolution of climate parameters in a time span. The volume of climate data is expanding exponentially day by day and it brings about some challenges for climate data archiving, sharing, and analyzing. A lot of research has been done to analyze financial, stock, economic, and other time series data using recurrence plots, but very few analyses are available for climate data based on recurrence analysis [13–15]. Climate data is analyzed using several other techniques. We are explaining some of them.

Sukharev et al. [16] presented a correlation analysis for time varying multivariate climate datasets. They used k -means clustering method and graph partitioning algorithm to find patterns and connections. The correlation of a single or a couple of variables is also analyzed using pointwise correlation coefficients and canonical correlation analysis. Liu et al. [17] proposed a lossless compression algorithm for the time-spatial climate floating-point arrays. They used adaptive prediction, XOR differencing, and multiway compression to eliminate more data redundancy efficiently and also tried to exploit the correlations among the multidimensions to remove more data redundancy. Sap and Awan [18] used kernel methods for unsupervised partitioning of data to find spatiotemporal patterns in complex and nonlinearly separable climate data. Hendrix et al. [19] described a methodology for capturing and identifying the estimation of a climate network. They performed this by splitting the climate data into a set of overlying decadal time intervals and creating a network for each of these datasets representing the complex interdependencies in the climate system over a particular decade.

RPs and RQA have been successfully used in a large number of scientific disciplines [20] and are particularly used for modeling financial and economic time series. In recent years, several researchers concentrated on RPs and RQA techniques to study deterministic dependencies in financial data. These

techniques are used in various fields such as stock market [21], exchange rates [22], electricity prices [23], and heart beat interval [24]. Furthermore, synchronicity and convergence are also examined among member nations of the Euro region for GDP using cross recurrence analysis [25]. Silva et al. [26] gave an overview of recurrence plots as a representation domain for time series classification, in which Campana-Keogh (CK-1) and Kolmogorov complexity based distances are used to measure the closeness between recurrence plots and to estimate image similarity, respectively.

From the above literature we observed that various analyses are performed using recurrence plots to find hidden data relationships in a sequence of time series datasets, such as stocks, exchange rates, financial data, heart rates, voice, and electricity processes, but very little research has been done to find and visualize the interrelationship in temperature periodic trends for climate data using RP, CRP, and CPR. At the same time, we also observed that no significant research has been done to indicate the difference between and within the temperatures of various climatic regions. So, we decided to use recurrence based methods RR, CRP, and CPR to identify the differences in climate on the basis of temperature for nine US and eight Chinese regions and also the probabilistic correlations between time series. The accuracy of the recurrence based approach is validated on real and synthetic datasets and analyzed using ANOVA, Kruskal–Wallis, and z -statistical significance tests [27, 28].

The rest of the paper is organized as follows. In Section 3, we discuss the brief introduction of terms used in our approach. Section 4 represents the proposed approach. Section 5 shows the experimentation results on various datasets and the validation of the proposed method by applying the significance test. Section 6 concludes the work done in this paper.

3. Materials and Methods

3.1. Recurrence Plots (RPs). Recurrence plots are used to analyze periodic data by visualizing the recurrent behavior of dynamical systems which does not stay constant and changes periodically. It is also applicable to analyze the behavior of nonlinear dynamical and nonstationary systems, for example, temperature. It is used for the study of difference or similarity within a process on time series data. A recurrence plot (RP) is a visual tool that shows the recurrence patterns of a dynamical system [29]. Recurrence is defined as return of the trajectory of a system to a previous state. Recurrence occurs when the system returns to the neighborhood of an earlier point in the phase space. The distributions of recurrence points and diagonal lines along the main diagonal provide an evaluation of the similarity of the phase space trajectories of both dynamical systems.

A cross recurrence plot (CRP) is a tool for nonlinear data analysis, which can be used for the study of differences between dynamical systems. The basic idea of this approach is to compare the phase space trajectories of two tasks in the similar phase space. CRP can be used in order to study the similarity of two different phase space trajectories. On the other hand, the CRP discloses all possible times when the

phase space trajectory of the first system visits approximately a similar area in the phase space trajectory of the second system. The data length of both systems can differ in the CRP matrix which leads to a nonsquare matrix.

We use an extension of the method of recurrence plot to the method of cross recurrence plot, which compares the time dependent behavior of two processes, which are recorded in a time series. Here, we have two time series, each one represented by trajectories X_i and Y_j in the phase space. The test for equality of each point of trajectory X_i with each point of trajectory Y_j by taking the embedding dimension m and delay time τ results in an $N_X * N_Y$ array.

$$CR_{i,j} = \Theta(\varepsilon_i - \|X_i - Y_j\|), \quad X_i, Y_j \in R^m, \quad (1)$$

where $X_i = \{x_i, x_{i+\tau}, \dots, x_{i+(m-1)\tau}\}$ and $Y_j = \{y_j, y_{j+\tau}, \dots, y_{j+(m-1)\tau}\}$. i is $1 \dots N_X$, j is $1 \dots N_Y$, N is the number of points, ε is threshold distance, $\Theta(\cdot)$ is the Heaviside function (i.e., $\Theta(a) = 0$ if $a < 0$ and 1 if $a \geq 0$), and $\|\cdot\|$ is a norm. CR is a matrix of $\{0s, 1s\}$ and an RP is a visual representation of CR obtained by marking a black and white dot for every 1 and 0. Embedding dimension m and delay time τ can be obtained by correlation dimension and autocorrelation function. In this paper, we select the fixed embedding dimension $m = 2$ and delay time $\tau = 4$.

Next, we give some measures to analyze RP and CRP using the sine wave. In order to present the idea of RP and CRP, some figures of the sine wave are presented to guide the description. The sine wave is a geometrical waveform which oscillates (moves up or down) periodically (i.e., the same pattern occurs after a particular time interval). The functionality of the sine is used to build models for processes that repeat in cycles or involve oscillations. Examples that present oscillations include the monthly and seasonal cycles of temperature, heart beats, voice, music, population cycles, and tides.

So, we can say that the sine wave follows the periodic pattern and distinct patterns emerge in its RP. If the data is collected from systems having periodic variations, then a distinct pattern can be seen in its RP; for example, data of climate, voice, and heart rate show a distinct pattern in RP. Also, the distance between diagonals indicates the signal periodicity. Therefore, we can visualize and study the motion of the dynamical system and infer some characteristics that generated the time series. To show the periodic variations clearly, first we explain the RP and CRP on the sine wave, based on which further other datasets are considered. Figure 2 shows the plot of different sine waves and their RPs. We have generated different sine waves in MATLAB using the $\sin()$ function. In Figure 2, we can visualize that the same pattern emerges in RP if series are periodic in nature.

If two time series are periodic and exhibit similarity, then the same pattern emerges in CRP also. CRP of sine waves is shown in Figure 3. CRP discovers all possible points when one sine wave (simple sine wave) visits approximately a similar area of the other sine wave (phase shift). We can see that, in Figure 3(a), clearer patterns emerged because both sine waves are almost the same (i.e., same frequency cycle, but differing by 0.8 phase shift). Even in Figure 3(b),

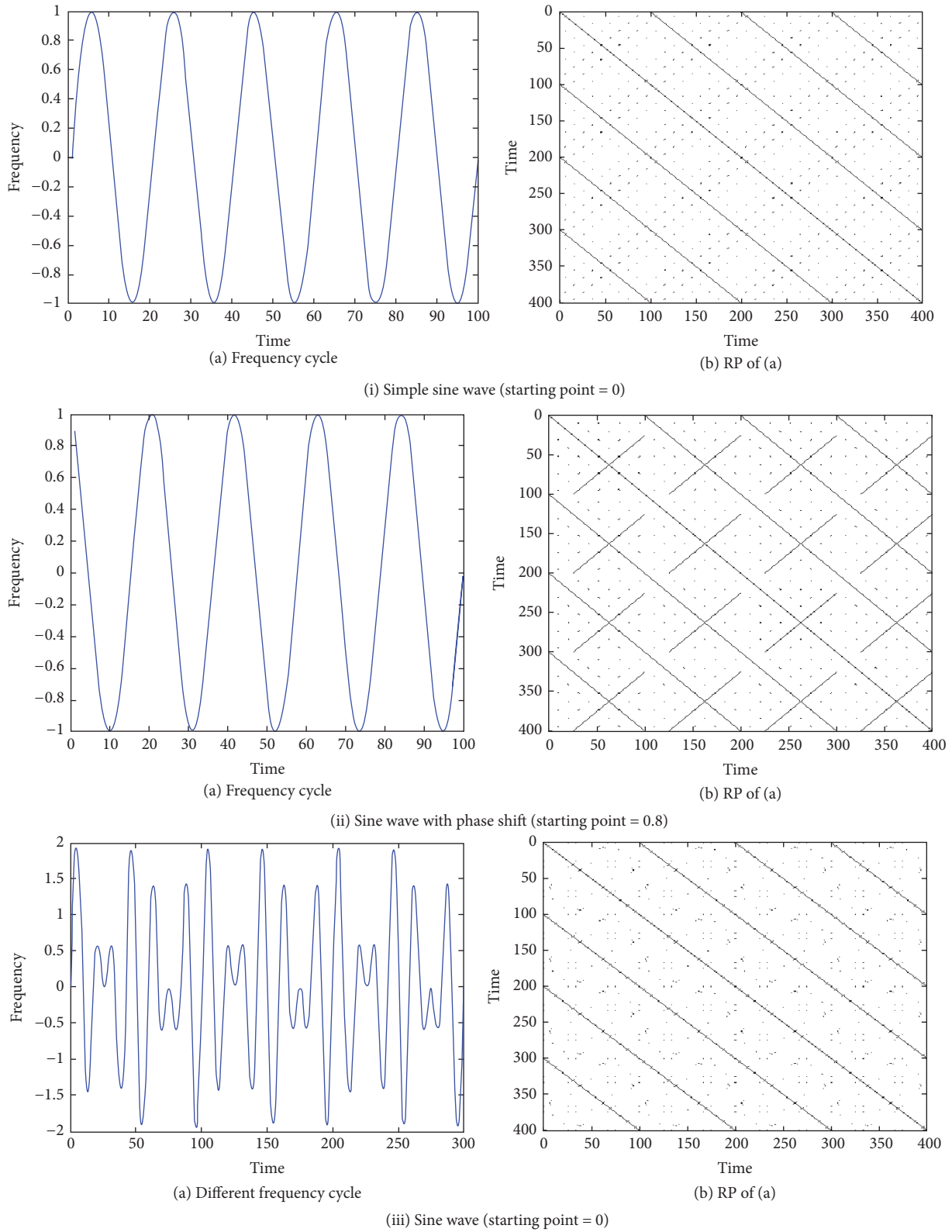


FIGURE 2: Recurrence plots for sine waves.

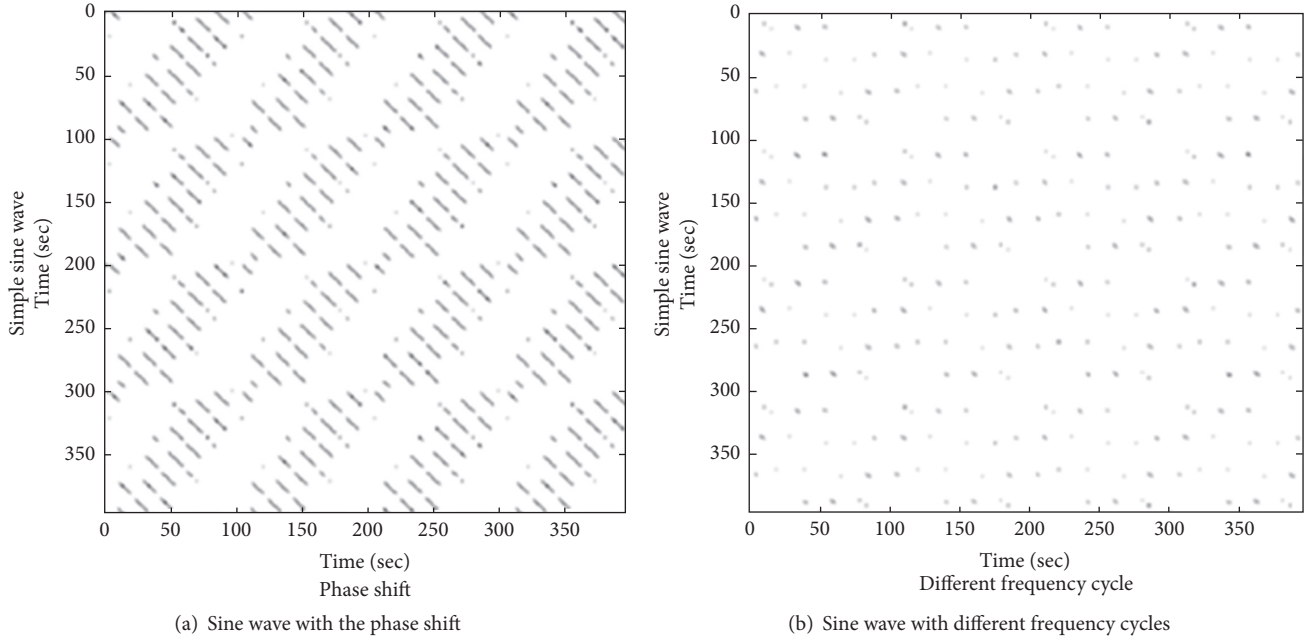


FIGURE 3: CRP for sine wave.

fewer patterns emerged because of their different frequency cycles. So, we can conclude that individual series can follow recurrent behavior, but when they are plotted together, that recurring pattern will not necessarily be followed. Figure 4 shows recurrence rate (RR) graph, described in the next section for all three sine waves shown in Figure 2.

3.2. Probability of Recurrence (τ -Recurrence Rate). The probability of recurrence $p(\tau)$ is the recurrence rate of a diagonal line situated at τ steps from the main diagonal, that is, $CR_{i,j+\tau} \forall i, j = 1, \dots, N - \tau$. This evaluation gives the probability of a $(j + \tau)$ th point falling in the ε -neighborhood of the i th point.

$$RR = p(\tau) = \frac{1}{N - \tau} \sum_{i,j=1}^{N-\tau} CR_{i,j+\tau}. \quad (2)$$

Figure 5(a) represents RP for northeast climate time series and shows a similar probability of occurrence to a prior state for all values of τ in Figure 5(b).

3.3. Correlation of Probability of Recurrence (CPR). CPR is based on RPs and was originally devised to quantify phase synchronization between two systems or stationary time series. It represents the probability of recurrence of the first system and second system. CPR describes the cross-correlation coefficient between the probabilities of recurrence of two trajectories \vec{x} and \vec{y} [20, 30]:

$$CPR = \langle \bar{p}_{\vec{x}}(\tau) \bar{p}_{\vec{y}}(\tau) \rangle, \quad (3)$$

where $\langle \cdot \rangle$ represents the expectation value. All the $p(\tau)$ curves in Figure 5(b) start from $p(0) = 1$, because the calculated recurrence rate always occurs 1 at $\tau = 0$, the main

diagonal. $CPR \approx 1$ implies that two time series variations are periodically synchronized. To predict CPR correctly, we consider an appropriate $p(\tau)$ value where τ is greater than autocorrelation time of the system because mostly a high CPR value is predicted for all trajectories having a similar initial portion of the $p(\tau)$ curve.

$$CPR = \langle \bar{p}_{\vec{x}}(\tau > \tau_s) \bar{p}_{\vec{y}}(\tau > \tau_s) \rangle, \quad (4)$$

where

$$\tau_s = \max(\tau_s(\vec{x}), \tau_s(\vec{y})). \quad (5)$$

Figure 6 illustrates the process involved in evaluating the CPR. The CPR between Ohio Valley and Southeast is calculated using (4) and (5), which is 0.785. In this study, this indicates that two climate time series (Ohio Valley and Southeast) with a high CPR tend to recur at similar times, suggesting some similarity (strong connectivity; refer to Figure 15(a)) in their trends.

3.4. ANOVA. Analysis of variance [28] is used to analyze differences among the group mean values and can identify the significant difference between group means if it exists. ANOVA's F -statistic is calculated as follows.

(i) The variation between the groups is calculated as

$$\begin{aligned} &\text{Between sum of squares (BS)} \\ &= m1 (\bar{Z}_1 - \bar{Z})^2 + m2 (\bar{Z}_2 - \bar{Z})^2 + \dots \\ &\quad + mi (\bar{Z}_i - \bar{Z})^2, \end{aligned} \quad (6)$$

$$\text{Between mean squares (BM)} = \frac{\text{BS}}{\text{degree of freedom}}.$$

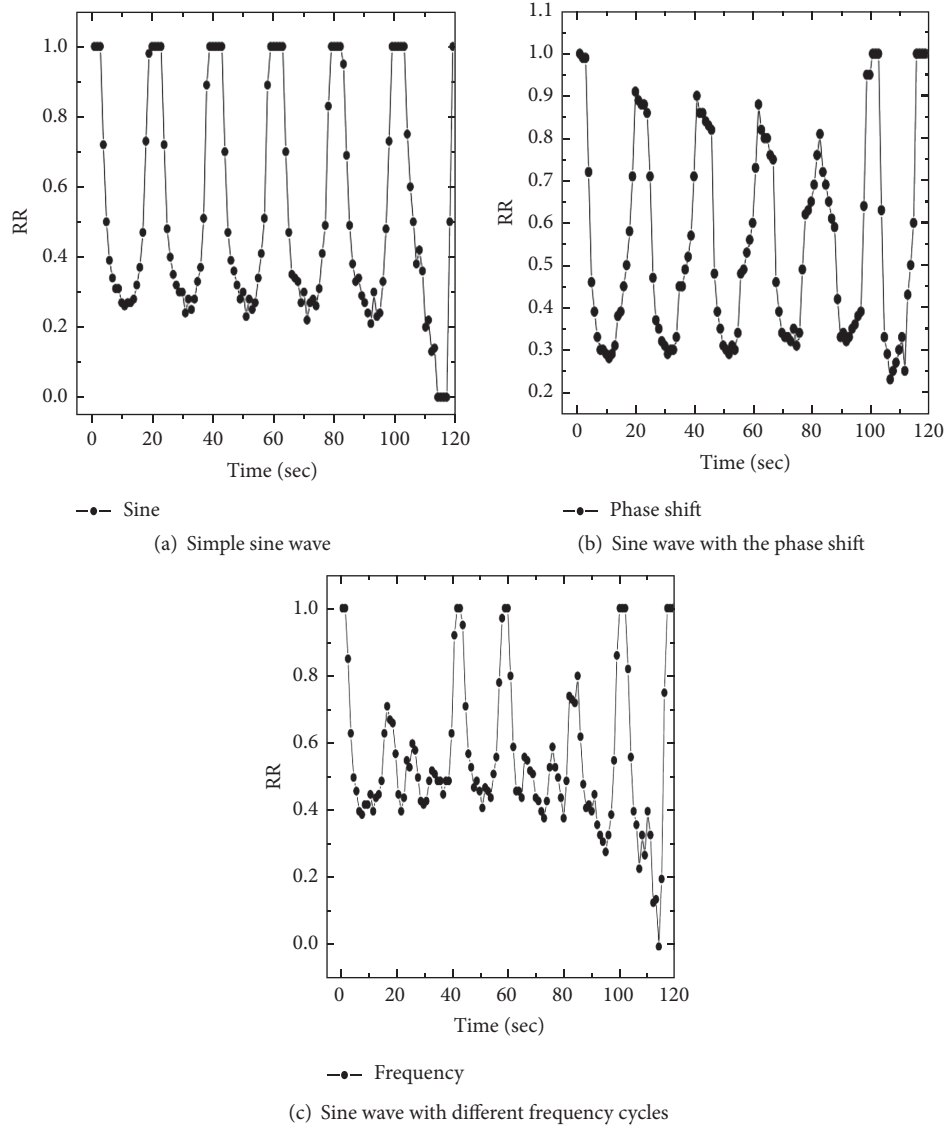


FIGURE 4: Recurrence rate (RR) or $p(\tau)$ curve for sine wave.

(ii) The variation within the groups is calculated as

Within sum of squares (WS)

$$= (m_1 - 1)\sigma_1^2 + (m_2 - 1)\sigma_2^2 + \cdots + (m_i - 1)\sigma_i^2, \quad (7)$$

Within mean squares (WM) = $\frac{WS}{(M - i)}$,

where σ is the standard deviation, M is the number of samples, i is the number of groups, and m_i is the number of samples in group i .

(iii) F -test statistic is calculated as

$$F = \frac{BM}{WM}. \quad (8)$$

3.5. *Kruskal–Wallis Test*. The Kruskal–Wallis test [28] is a rank-based nonparametric test used to determine the

statistically significant differences between two or more groups of an independent variable on a continuous or ordinal dependent variable. It is used when (1) the data are ordinal and do not meet the precision of interval data, (2) there are serious concerns about extreme deviation from normal distribution, and (3) there is considerable difference in the number of subjects for each comparative group. K -statistics can be calculated as follows:

Computing the K statistic, K

$$= \frac{12}{n(n+1)} \sum \frac{R_j^2}{n_j} - 3(n+1), \quad (9)$$

where n_j is the number of items in sample j , R_j is the sum of the ranks of all items in sample j , and $n = n_1 + n_2 + \cdots + n_k$, the total number of observations in all samples.

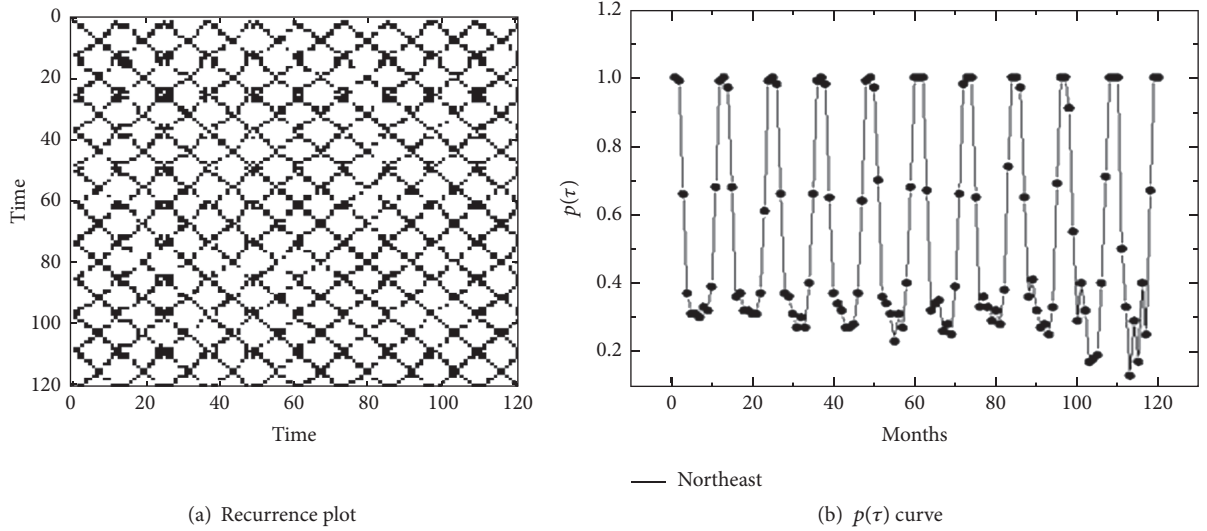


FIGURE 5: Plots for Northeast temperature data.

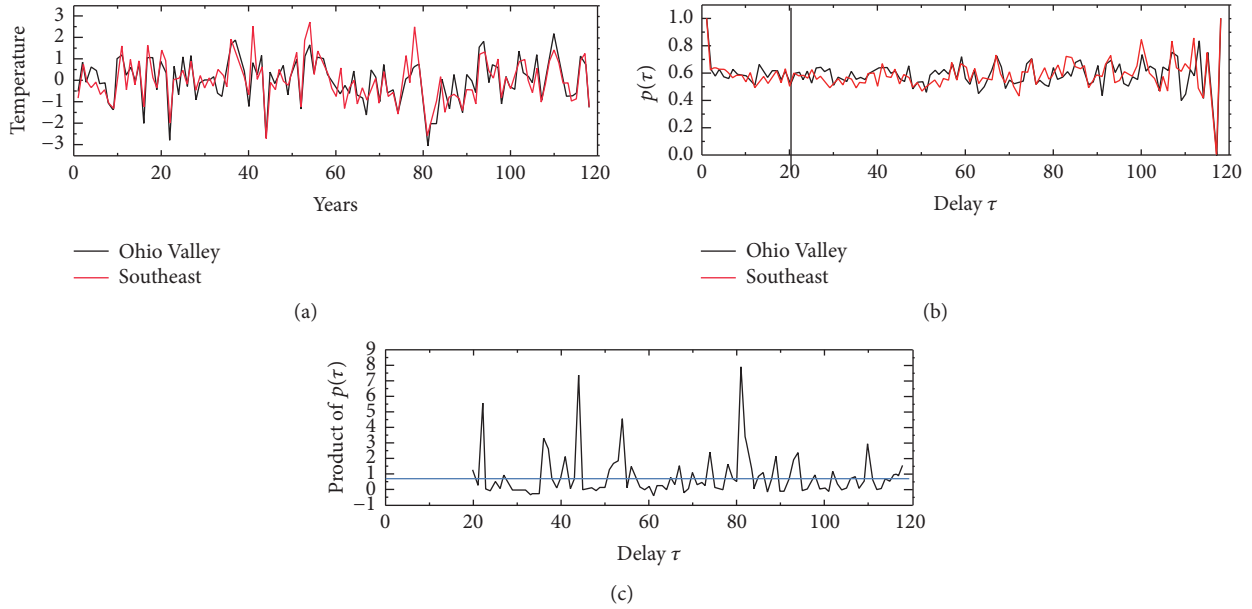


FIGURE 6: Evaluation of CPR from $p(\tau)$. (a) Normalized yearly data for 120 years. (b) $p(\tau)$ curves for these time series with $\tau_s = 20$ are shown with a vertical line. (c) The product of Ohio Valley and Southeast in (b). The horizontal line is the mean of this series, which is the CPR.

4. The Proposed Method

In this section, first we have shown the proposed method in an algorithmic form and then explained each step in detail. The detailed processing of recurrence based similarity identification approach is explained using nine US regions. Experiments are performed on other datasets also.

4.1. Recurrence Based Similarity Identification Algorithm. This section presents a high level summary of the proposed approach, shown in Algorithm 1.

Algorithmic steps involved in the proposed method are explained as follows.

4.2. Data Preparation. In our approach, we used monthly average temperature data for analysis. Since daily data fluctuates more and suffers from estimation error, it is difficult to analyze and compute for 120 years (43800 days). Instead of daily data, monthly data is used because it is approximately normally distributed, fast to compute, and easier to model and it is easier to identify changes in trends and it helps in better strategic decisions.

Sometimes the data collected from available repositories contains missing values, special characters, noise, and outliers. So, first, we clean the data by replacing missing values and special characters, determining presented noise, and removing outliers and then further steps are performed on clean data.

TABLE 1: Monthly average temperature data.

US regions	1895/01	1895/02	1895/03	1895/04	1895/05	1895/06	1895/07	1895/08	...	2014/12
R ₁	18.8	15.6	27.6	43.5	57.1	67.2	65.7	66.7	...	31.6
R ₂	9.5	13.8	28.2	47.3	51.9	58.1	65.6	65.1	...	24.3
R ₃	24.4	29.8	34.3	44.3	49.4	56.1	62.2	62.6	...	33.3
R ₄	24.6	21.9	40.2	55	63	73.5	73.2	74.5	...	37.1
R ₅	39.2	34.8	53.1	63.4	69.2	77	79.3	80	...	46.9
R ₆	43.7	37.3	53.1	61.1	68.3	76.8	77.8	78.5	...	50.5
R ₇	30.3	30.3	40.8	51	58.4	65.1	70.4	70.6	...	36
R ₈	6.9	9.7	26	47.8	56.8	65.8	67.3	67.2	...	24.8
R ₉	35	40.1	44	51.1	58.8	66.2	71.7	71.8	...	31.6

TABLE 2: Normalized temperature values.

US regions	1895/01	1895/02	1895/03	1895/04	1895/05	1895/06	1895/07	1895/08	...	2014/12
R ₁	0.13	0.08	0.27	0.53	0.75	0.91	0.88	0.13	...	0.34
R ₂	0.13	0.19	0.37	0.62	0.68	0.76	0.85	0.13	...	0.32
R ₃	0.22	0.31	0.39	0.56	0.65	0.76	0.87	0.22	...	0.37
R ₄	0.15	0.11	0.38	0.61	0.73	0.89	0.88	0.15	...	0.34
R ₅	0.16	0.08	0.41	0.59	0.7	0.84	0.88	0.16	...	0.3
R ₆	0.2	0.07	0.39	0.56	0.71	0.88	0.9	0.2	...	0.34
R ₇	0.17	0.17	0.35	0.53	0.66	0.78	0.87	0.17	...	0.27
R ₈	0.12	0.16	0.37	0.64	0.76	0.87	0.89	0.12	...	0.35
R ₉	0.2	0.3	0.37	0.5	0.64	0.77	0.87	0.2	...	0.34

R₁–R₉ indicate the notations used for US regions: R₁—Northeast; R₂—Northern Rockies and Plains; R₃—Northwest; R₄—Ohio Valley; R₅—South; R₆—Southeast; R₇—Southwest; R₈—Upper Midwest; R₉—West.

Input ← Multivariate Time series T
Output ← Connectivity trend (Small, Moderate, Weak)
Method:
(1) DP ← Data Preparation (T)
(2) S ← Normalize (DP)
(3) CR ← Cross recurrence (S)
(4) RR ← Recurrence rate (CR)
(5) CPR ← Correlation of probability of recurrence (RR)
(6) CT ← CPR Value

ALGORITHM 1: Recurrence based similarity extraction.

Let T_i represent the daily temperature data for year Y_j .

Step 1. It is difficult to analyze daily temperature data for 120 years (43800 days), so we calculate monthly average temperature to ease the analysis process as follows:

$$\text{Average Temperature, } AT_{\text{month}} = \frac{Y_j \left(\sum_{i=1}^{30} T_i \right)}{30}, \quad (10)$$

where month = Jan, Feb, ..., Dec and $j = 1$ to 120.

Table 1 describes the monthly average temperature data for 120 years.

Data normalization is essential to fit all data in one range for efficient organization of the data. We use $Z_{\text{min-max}}$

normalization method to scale data within the range of (0, 1). Normalized results are shown in Table 2.

$$X_{\text{norm}} = \frac{(X_{\text{mn}} - \min)}{(\max - \min)}, \quad (11)$$

where X_{norm} is the result of the normalized value of temperature, X_{mn} is the temperature value to be normalized, max is the upper bound of the temperature value, and min is the lower bound of the temperature value.

Step 2. In this step, we reduce the time span from 1440 points to 120 points because it is difficult to get a clear visualization of temperature data with large window size (120 years * 12 months = 1440) using RPs. Since seasonal calculation represents the extent of seasonal influence for a particular segment of the year and an average for that particular period trend, therefore, to get an accurate analysis of the temperature data and capture their trends, we compute the average in the period of 4 cycles (spring, summer, autumn, and winter) and each cycle involves 3 months.

Season also indicates regular fluctuations which are repeated from year to year with about the same timing and level of intensity. Seasonal effects are usually associated with climatic changes and their variation is frequently tied to yearly cycles. Therefore, the four seasons with 3-year intervals are considered, which results in a reduced window size of 160 (40 years * 4 months). Figure 7 shows the window size

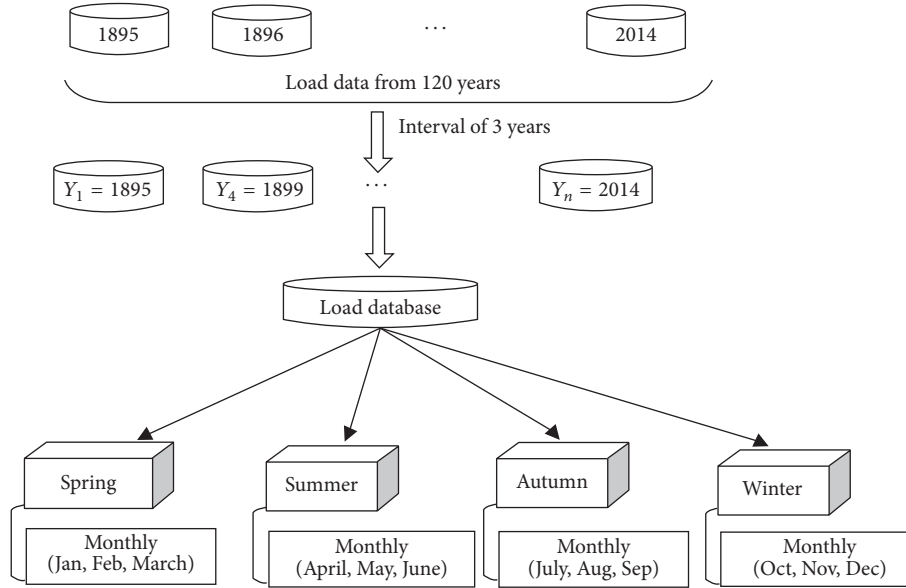


FIGURE 7: Data preprocessing.

reduction process by considering a 3-year time interval and for 4 seasons (spring, summer, autumn, and winter).

4.3. Connectivity Trend Analysis. This connectivity trend analysis enables quantifying a possible similarity and dissimilarity between different regions. It is done by grouping the CPR values into three categories as (a) strongly related ($CT = 1$), (b) moderately related ($CT = 0$), and (c) weakly related ($CT = -1$) using (13). CPR values are calculated using (4) along with the number of pairs for which the CPR value has to be calculated using (12).

The total number of pairs is calculated as follows:

$$\text{number of pairs} = n * \frac{(n-1)}{2}, \quad (12)$$

where n is the number of regions.

Connectivity trend is defined as follows:

$$CT = \begin{cases} 1, & \text{if } |CPR| > \alpha \\ 0, & \text{if } \beta < |CPR| < \alpha \\ -1, & \text{if } |CPR| < \beta, \end{cases} \quad (13)$$

where α and β indicate algorithmic parameters to analyze similarity and dissimilarity. Quantitatively, the similarity between two periodic variations can be computed using CPR.

5. Experimentation

In this section, we perform experiments on both synthetic and real-world datasets to test the performance of the proposed method. All the experiments were conducted on a Windows 7 machine with 2.30 GHz CPU and 4.00 GB RAM. Here, we first describe the dataset, and then the correctness of our approach is shown using heart rate and voice dataset and finally results are calculated on synthetic and climate data.

The algorithmic parameters values are set to $\alpha = 0.8$ and $\beta = 0.5$ for experimentation.

5.1. Dataset. We use our approach on both synthetic and real datasets shown in Table 3. We apply it to data of different kinds but having similar characteristics (i.e., periodic variations) to show the general applicability of the proposed method. To test the applicability of the method, we used datasets such as heart rate and voice where similarity or dissimilarity is known. We compared the outcomes of our method with the known results and found that they are matching with the known results. Although these datasets are unrelated, their characteristics are the same; that is, they have time series data with periodic variations.

Synthetic datasets are generated (named C5Y120, C10Y120, and C15Y120) using *R* fNonlinear package [31]. In this package, to generate different nonlinear time series for 120 points, we used tentSim, logisticSim, and henonSim functions as follows:

- (1) tentSim ($n, n.\text{skip}, \text{parms} = c(a = 2)$): C5Y120
- (2) logisticSim ($n, n.\text{skip}, \text{parms} = c(r = 4)$): C10Y120
- (3) henonSim ($n, n.\text{skip}, \text{parms} = c(a = 1.4, b = 0.3)$): C15Y120

The number of time series points ($n = 120$) is the same for all functions. These functions are used to generate datasets by changing the number of initial values to be skipped from the series ($n.\text{skip}$) and the rest of the parameters are considered by default.

US Climate dataset is obtained from the National Climatic Data Center [32] over the period 1895–2014 for the nine US regions (Ohio Valley, Upper Midwest, Northeast, Northwest, South, Southeast, Southwest, West, and Northern Rockies and Plains).

In China Climate data, the analysis is done on monthly average temperature data to detect abrupt climate changes

TABLE 3: Dataset description.

Dataset	Groups	Number of samples in each group	Remark	Description
<i>Synthetic datasets</i>				
C5Y120	5	120 points	5 (parameters)	Generated using tentSim R fNonlinear package
C10Y120	10	120 points	10 (parameters)	Generated using logisticSim R fNonlinear package
C15Y120	15	120 points	15 (parameters)	Generated using henonSim R fNonlinear package
<i>Real datasets</i>				
US Climate data	9	120 (years)	Samples contain regions' monthly average data	Climate data having monthly average temperature data
China Climate data	8	50 (years)	Samples contain regions' monthly average data	Climate data having monthly average temperature data
Heart rate	4	10 (people)	Samples are grouped based on age	There are a total of forty 120 min ECG recordings for different age groups The duration of these vowel samples was 3 s for healthy voices and 1 s for pathological voices. A 25 or 50 kHz sampling rate was employed to pathological and healthy voices, respectively. All the files were downsampled to 25 kHz and a single 400 ms frame of analysis was considered for each signal
Voice data	6	10 (people)	Samples are grouped based on healthy status and diseases	

in all regions of China for the recent 50 years from 1965 to 2015. China is divided into eight climate regions as follows: (a) South China, (b) the middle and lower reaches of the Yangtze River, (c) North China, (d) Northeast China, (e) the east of Northwest China, (f) the west of Northwest China, (g) Tibet, and (h) Southwest China [32].

In heart rate variability data, the analysis is performed on the PhysioBank [33] dataset for different age groups to analyze the heart rate dynamic properties. There are a total of forty 120 min ECG recordings with 10 people from each group (10–24 years old, 25–40 years old, and 45–67 years old) and 10 elderly people (68–85 years old). The continuous ECG was digitized at 250 Hz.

In voice data, the quantification recurrence measurements are extracted from sustained vowels of speech signals recordings from Disordered Voice Database, Model 4337, developed by Kay Massachusetts Eye and Ear Infirmary (MEEI) Voice and Speech Lab [34]. The database includes samples from patients with a wide variety of voice disorders. We present analysis of speech signals to find the difference between healthy voices and voices affected by vocal diseases (normal, Reinke's edema, nodule and vocal cord paralysis, vocal polyps, laryngitis, and contact ulcers). All samples were collected in a controlled environment with the following features: low-noise level, constant microphone distance, direct digital 16-bit sampling, and robust signal conditioning. The selected cases comprise 50 patients with pathological voices (10 with Reinke's edema, 10 with nodule, 10 with laryngitis, 10 with vocal cord paralysis, and 10 with contact ulcers) and 10 patients with healthy voices.

5.2. Correctness of the Proposed Approach. The correctness of our method is demonstrated by applying it to a variety of applications to cope with different situations like heart rate and voice dataset. These datasets are selected because they follow a recurring pattern and have similar characteristics to time series data.

First, we have demonstrated that there occurs a recurring pattern in heart rate which is indicated by the RPs shown in Figure 8(a). If the RP shows a distinct pattern, then there is periodicity in variations. Figures 8(a)(A) and 8(a)(B) indicate RPs of two persons from the same age group (10–24) and their variations are the same so their RPs are similar, while Figures 8(a)(A) and 8(a)(C) indicate RPs of different age groups and their variations are different so both are showing distinct patterns. The similarity and dissimilarity between variations can also be observed using CRP plots. If variations are similar, then CRP plots will show a periodic pattern as indicated by Figure 8(b)(A) and if variations are different then no such pattern is observed as indicated by Figure 8(b)(B).

In other words, we can say that if people belong to the same dataset, their RP and CRP will both follow a recurring pattern but at the same time it is not necessary that if they are from different datasets they follow a recurring pattern in RPs and their CRP will also follow the same, which indicates that there exists a similarity between people belonging to the same age group and difference between people of different age groups (i.e., heart rates of young and old people). Similarly, we can see the similarities and difference between the voice

of healthy people and that of people who have vocal cord paralysis from Figures 9(a) and 9(b).

We also validated our heart and voice data results by the results of previous researchers [35, 36]. They show that heart rate of different age groups differs by plotting RPs. Similarly, the results were observed for voice data.

Table 5 shows the probabilistic correlation of one group of people with another group. It also validates our CRP results by categorizing CPR into three categories. For example, we got a higher number of connections in the strong category and a smaller one in the weak category for a group of people which indicates that the heart rate of one age group or the voice of healthy people does not differ more within a group but it differs with another group of people.

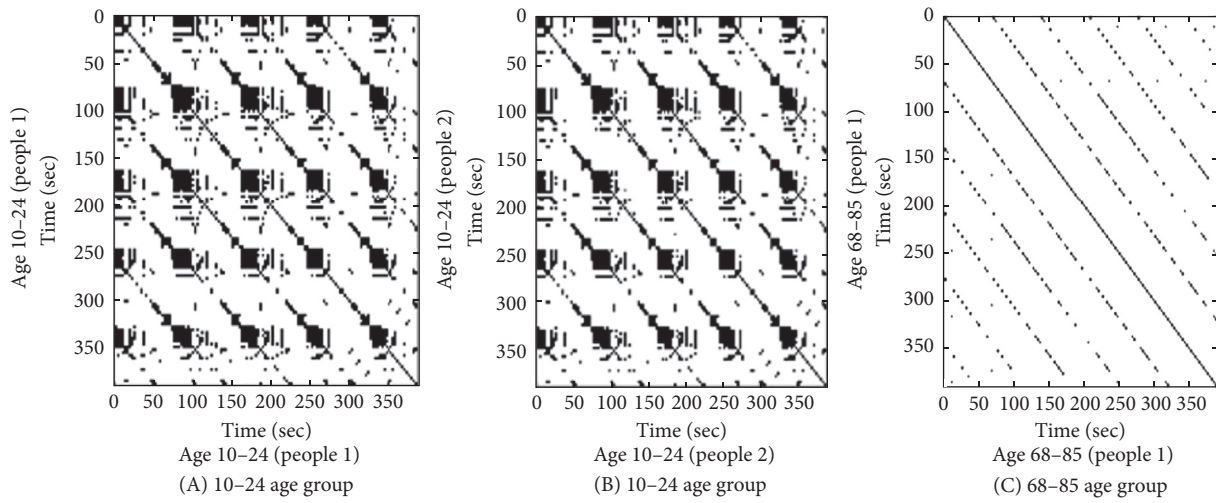
5.3. Climate Data Results. From Figure 10, we can see that RPs of nine US regions have similar periodic variations which indicate that the occurrence of recurrent points along the main diagonal for each region is the same. This means the temperature of one region follows some periodic variation which is different from another region. The recurrence plot for nine regions with 3-year intervals with step size $\tau = 4$ is shown in Figure 10. To show clearer structural changes in the behavior of temperature data and to see the similarities in patterns across the time series, we show the RPs for the first 120 months. RPs for season-wise and 1440 months' data are shown in Appendix 1 (Figures 17 and 18 in the Supplementary Material available online at <https://doi.org/10.1155/2017/7836720>).

Figure 11 shows the CRP between time series of monthly US data for a 10-year time period with lengths of 120 months. We can observe that there is no occurrence of recurrent points along the main diagonal. This means two time series are different and the temperature variation of one region is different from another region.

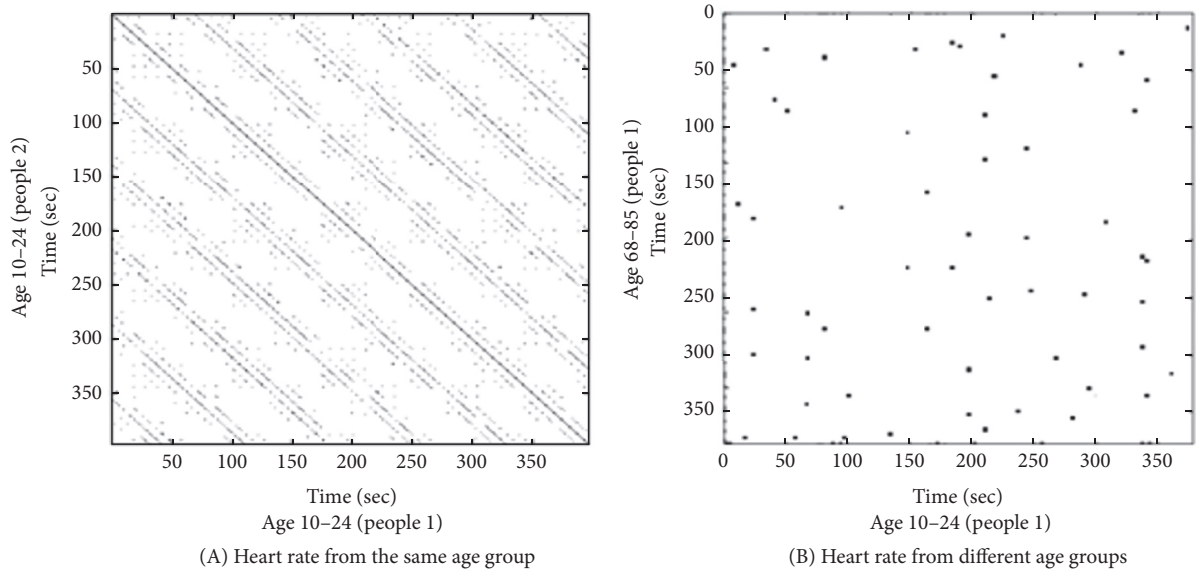
In Figure 11(a), we got more correlated points which show the strong similarity between Northwest and West regions. Similarly, Figures 11(b) and 11(c) show the weak and very weak (less correlated points) connection. Figure 11(d) shows moderate similarity. This relationship can be validated using Figure 1(a). We can also observe that the regions follow similar temperature periodic variations within a region but differ with another region.

These climatic region similarities can also be validated by their longitude and latitude location. For example, in US regions, from Figure 1(a), we can see that Northwest and Southeast regions are situated diagonally, so very low similarity will appear in their temperature. In other words, in the case of Northwest and Southeast regions, sunrays have a direct impact on Northwest and less on Southeast regions, so their temperature differs, which is shown by the smaller number of points in CRP (Figure 11(c)). RPs and CRP for some regions of China are shown in Figures 12 and 13.

Table 4 describes the autocorrelation of US regions for a time period 1895–2014. It is calculated using (2). All region recurrence rate values start from 1 because the probability of recurrence is always 1 at $\tau = 0$. Because of autocorrelation, successive values can be treated as recurrences;



(a) Recurrence plots for heart rate variability data



(b) Cross recurrence plots for heart rate variability data

FIGURE 8

TABLE 4: Probability of recurrence.

US regions	1895/01	1895/03	1895/05	...	1898/01	1898/03	1898/05	...	2014/09	2014/11
R_1	1	0.33	0.67	...	1	0.33	0.66	...	0.57	0.69
R_2	1	0.33	0.68	...	1	0.33	0.73	...	0.71	0.69
R_3	1	0.33	0.68	...	1	0.34	0.69	...	0.71	0.67
R_4	1	0.33	0.69	...	0.99	0.33	0.7	...	0.43	0.66
R_5	1	0.33	0.68	...	1	0.33	0.69	...	0.71	0.7
R_6	1	0.33	0.67	...	1	0.34	0.7	...	0.43	0.7
R_7	1	0.33	0.72	...	0.98	0.33	0.7	...	0.71	0.7
R_8	1	0.33	0.67	...	1	0.33	0.68	...	0.57	0.66
R_9	1	0.34	0.67	...	1	0.35	0.69	...	0.57	0.68

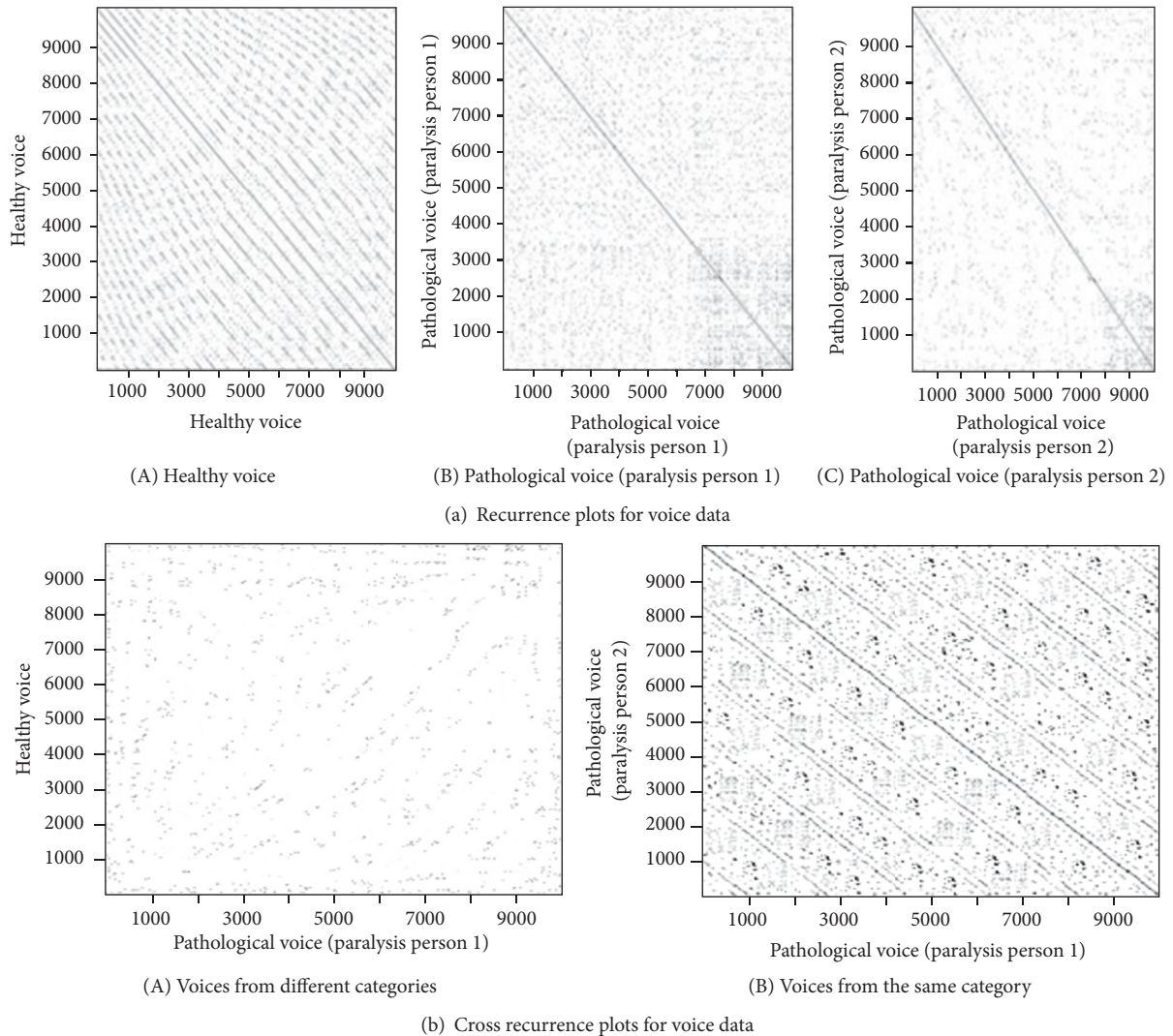


FIGURE 9

thus, a greater recurrence density occurs around the main diagonal.

Figure 14 describes that the spatial distribution of the RR corresponding to the monthly average temperature data of all regions remains unchanged over the 120 months in the US. The figure demonstrates that the monthly average temperature data of each region are similar to the characteristics of the distribution of climate types in the US. This indicates that there exists a slight change in temperature of one region for a particular month (say January) and shows a periodic pattern.

Table 5 describes the number of connections in each bin along time, that is, the results of correlation strength in three categories (i.e., strong, moderate, and weak) calculated using (13). Here, we calculate the CPR (see (4)) for both synthetic and real datasets.

In Table 5, climate region CPR results are shown on monthly data (i.e., correlation between regions). We can interpret that most of the correlation is coming under the weak category for all synthetic, US, and China climate

regions, which indicates that climate change of all regions in the US and China is independent of climate change of other regions. For example, in the US, regions fall under three categories, which are strong (Northwest-West, Ohio Valley-Southeast, and Northeast-Southeast), moderate (Ohio Valley-Upper Midwest, Upper Midwest-South, Northeast-Ohio Valley, Northwest-Southwest, Northwest-South, Northern Rockies and Plains-Southwest, and Northern Rockies and Plains-South), and weak (the rest of the regions) (i.e., the regions having similar temperature variations either latitude- or longitude-wise). Season-wise CPR results for US and China climate regions are shown in Appendix 1 (Table 9).

To show the appropriateness of our climate region results, we represent the correlation connectivity trend enabling quantifying a possible similarity and dissimilarity between US regions for all three categories in Figure 15. From Figure 15(a), we can see that Ohio Valley and Southeast follow an almost similar climate change pattern by moving up and down on the same time periods, which is the indication of

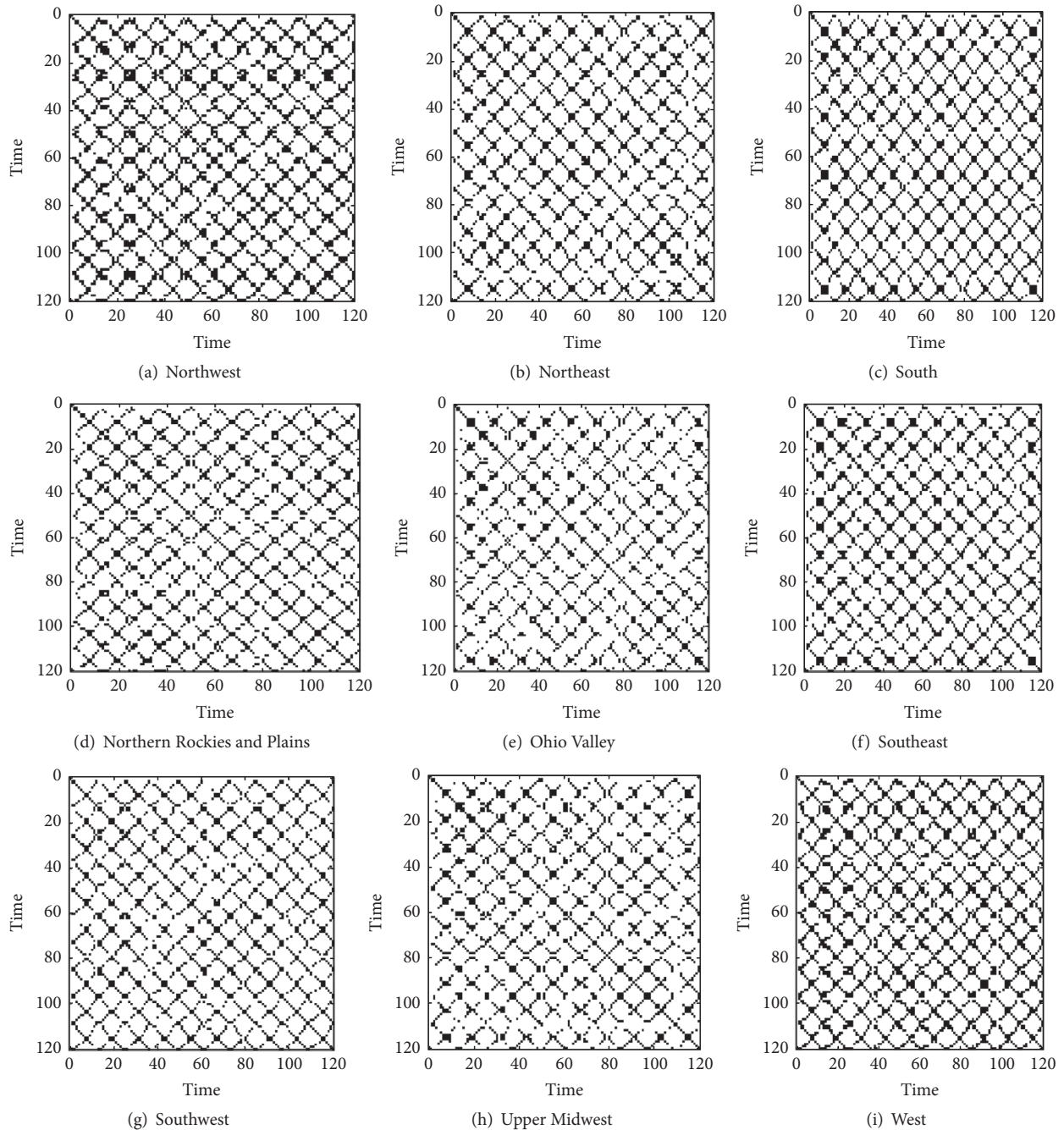


FIGURE 10: Recurrence plots for US regions.

strong connectivity. Similarly, other connectivity trends can be observed.

5.4. Validation Using Significance Testing: ANOVA, Kruskal-Wallis, and z-Test. It is not possible to give an accurate analysis only on the basis of recurrence rate, recurrence plot, and cross recurrence plots on time series. This should be done using a statistical test and an appropriate null hypothesis significance test. So, for the statistical significance of our approach, we are using ANOVA, Kruskal-Wallis, and z-significance test [27, 28] against the analysis obtained

from the recurrence based method on time series data. The statistical methods can be used to analyze similarity between two distinct pieces of data.

Both the Kruskal-Wallis test (often using ordinal data) and one-way ANOVA (typically using interval data) are used to analyze similarity between data series or to determine the statistically significant differences between three or more groups.

If the hypothesis of similarity of means is rejected, this will show that the data does not have a similar pattern and now a query occurs as to which pattern means are distinct.

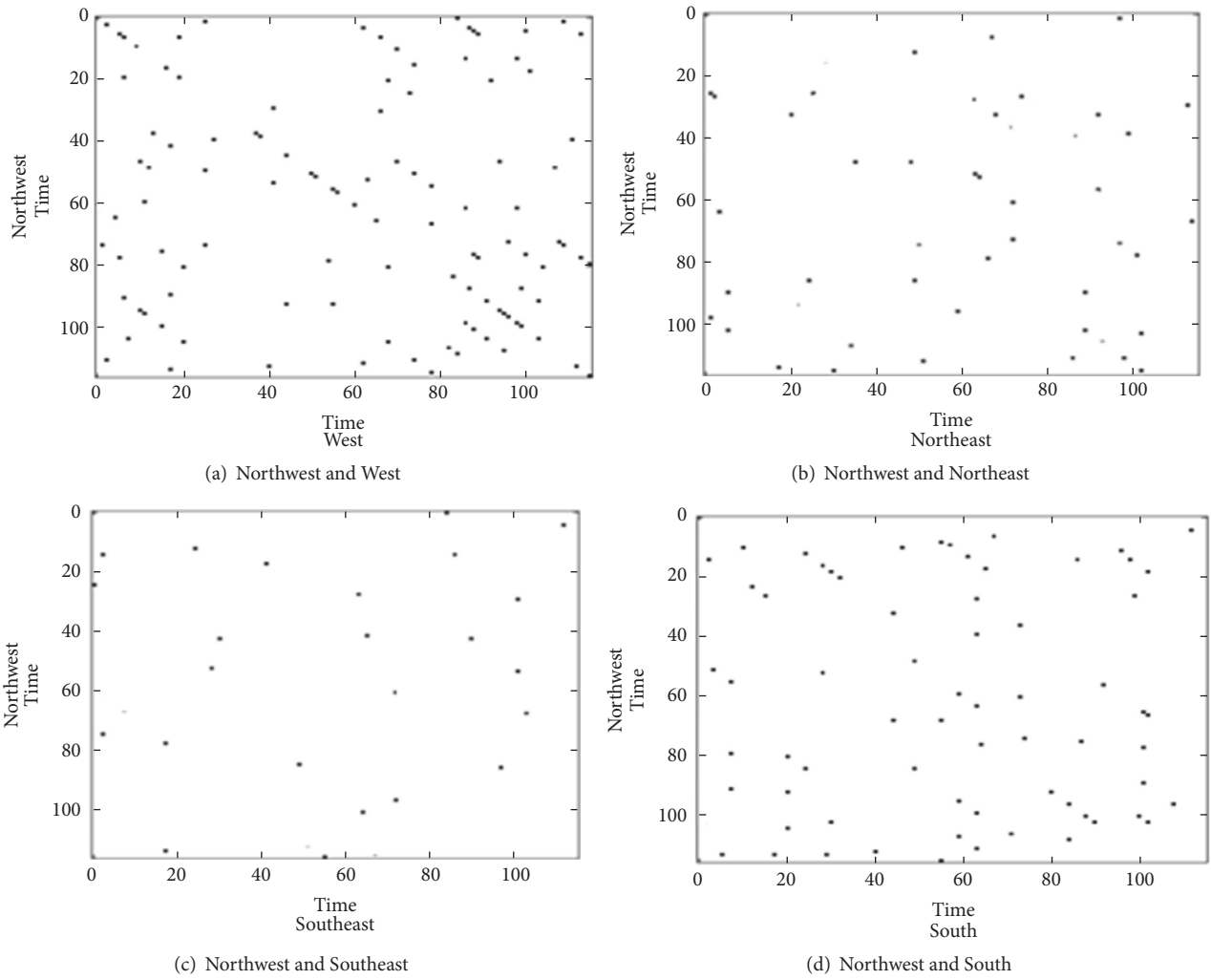


FIGURE 11: CRP for US regions.

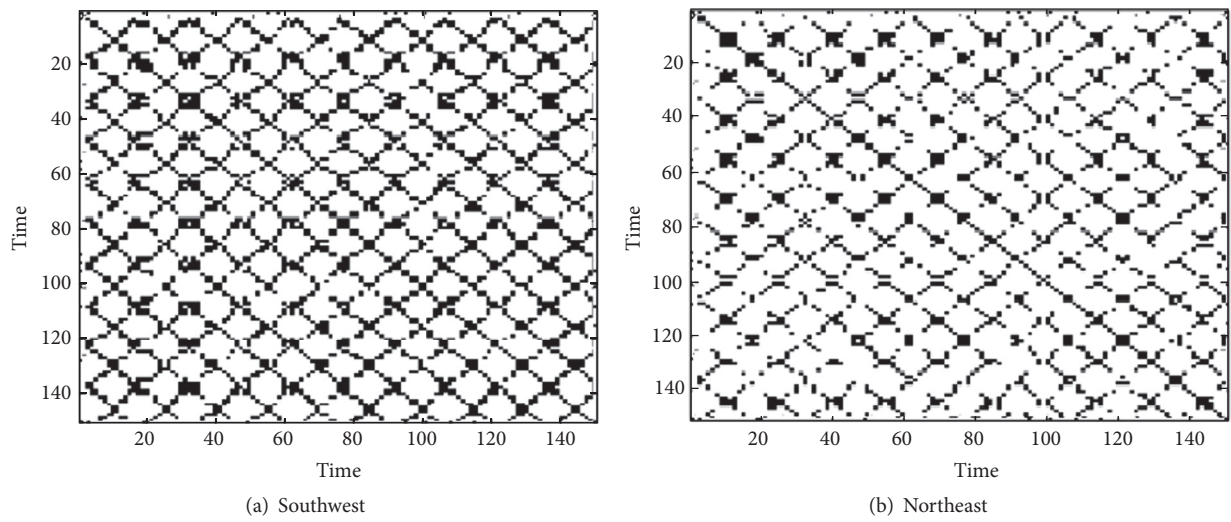


FIGURE 12: Recurrence plots for the regions in China.

TABLE 5: CPR binning table for real and synthetic datasets.

	Strong	Moderate	Weak
<i>Synthetic datasets</i>			
C5Y120	2	1	7
C10Y120	5	4	36
C15Y120	9	11	85
<i>Real datasets</i>			
<i>US Climate data (36 pairs)</i>			
Nine regions	3	7	26
<i>China Climate data (28 pairs)</i>			
Eight regions	4	5	19
<i>Heart rate variability (45 pairs)</i>			
10–24 (age)	36	3	6
25–40	38	5	2
41–67	37	5	3
68–85	32	7	6
<i>Voice data (45 pairs)</i>			
Healthy	38	4	3
Reinke's edema	35	8	2
Nodule	36	5	4
Vocal cord paralysis	40	3	2
Laryngitis	37	5	3
Contact ulcers	33	7	5

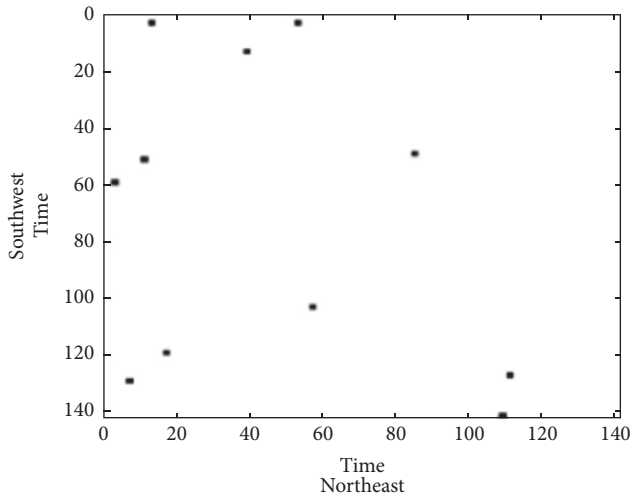


FIGURE 13: CRP for the regions in China: Southwest and Northeast.

The statistical methods used to resolve this query are known as multiple paired comparison procedures. We calculated the hypothesis by using two-tailed significance level estimates (z -test).

The hypothesis is as follows:

$H_0: \mu_1 = \mu_2$, null hypothesis; there are no differences between the groups (9 US regions, 8 climate regions, 6 types of voice, and 4 age groups of heart rate variability).

$H_1: \mu_1 \neq \mu_2$, alternative hypothesis; differences exist.

Validation Using ANOVA Test. Table 6 describes the ANOVA results representing BM (between mean squares of all groups) and WM (within mean square of a group) and their F -statistics value for each dataset.

We observed that the F -test statistic exceeds the significance level of F_{crit} (0.05) in all cases except healthy voice data and heart rate variability data (10–24). For example, for US Climate dataset as seen by the ANOVA test, the calculated F -test statistic (5.10) is greater than F -critical. From this test, it is evident that there are statistically significant differences existing in temperature values between the nine US regions. Similarly, for regions of China, the result indicates that there exists a significant gap between the eight climate regions of China, which demonstrates the effectiveness and reliability of the recurrence based approach in significant climate change recognition in the US and China. In the case of healthy voice data and heart rate variability data (10–24), the calculated F -test statistic is less than F -critical. This F -value indicates similarity within a group (i.e., the same group of people have fewer changes in voice and heart rate).

Validation Using Kruskal–Wallis Test. Table 7 describes the calculated p value of the Kruskal–Wallis test for all datasets, which is less than 0.05 except for healthy voice data and heart rate variability data (10–24). For example, for US Climate dataset, as seen by the Kruskal–Wallis test function, the calculated p value is $2.2e - 16$ which is certainly less than the criterion p value ≤ 0.05 . From this test, it is evident that there are statistically significant differences existing in temperature values between the nine US regions. In the case of healthy voice data and heart rate variability data (10–24), the calculated p value is greater than 0.05, which indicates similarity within a group (i.e., the same group of people have fewer changes in voice and heart rate).

Validation Using z-Test. We calculated the hypothesis at $\alpha = 0.05$ level that there is no difference between all groups versus one group for all datasets. The results are shown in Table 8, which describes the results of testing for similarity of means between all groups for each dataset. Each group is significantly different from the group of all.

From Table 8, we observed that, most of the time, our hypothesis is rejected except for voice data. This indicates that each group has an identity (i.e., there exists less similarity between groups on the basis of temperature). We observed that, for each dataset, there is some exception. For example, in US Climate data, we got only one exception as Southwest, which indicates that there exists less similarity between groups on the basis of temperature. Similarly, we got the exceptions for other datasets. This is a strong indication of each group identity. In case of voice data, most of the time, our hypothesis is accepted which indicates similarity in a group of the same type of people.

5.5. Scalability. To evaluate the scalability of the proposed approach on the CPR value and number of pairs, experiments are done with varying numbers of years. Figure 16(a) represents the correlation of Ohio Valley with Southeast and of

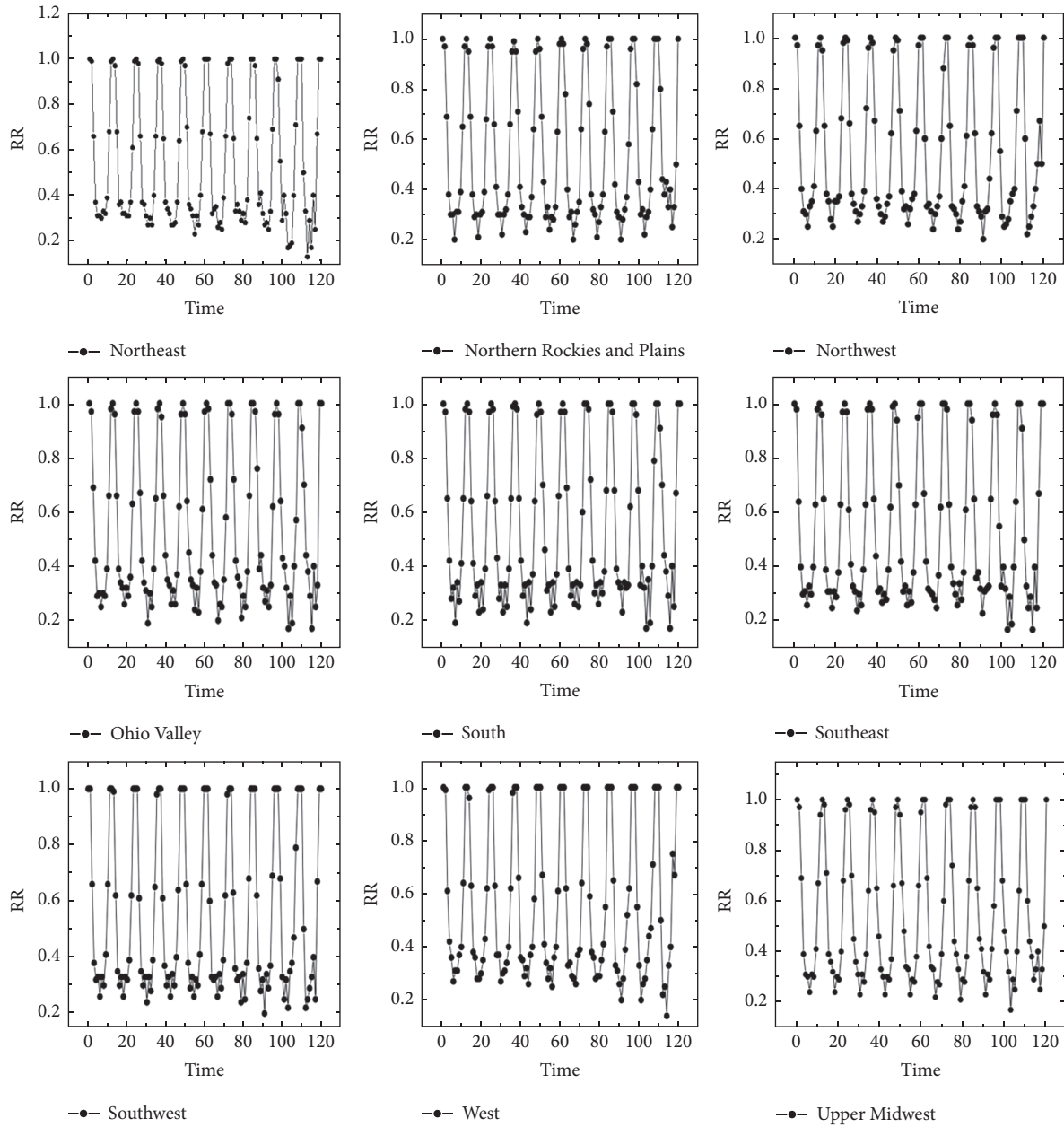


FIGURE 14: Recurrence rate (RR), $p(\tau)$ of each region in the US for 120 months.

TABLE 6: ANOVA test.

Dataset	BM	WM	F -statistics	F -critical
C5Y120	9.45	1.85	5.10	2.13
C10Y120	8.78	3.48	2.52	2.13
C15Y120	6.47	1.18	5.48	2.13
US Climate data	0.32	0.06	5.10	2.13
China Climate data	1.26	0.17	7.41	2.13
Heart rate variability data (age 10–24)	2.45	1.97	1.24	2.13
Heart rate (4 groups)	3.27	1.26	2.59	2.13
Healthy voice data	1.34	0.82	1.63	2.13
Voice data (6 groups)	1.47	0.26	5.65	2.13

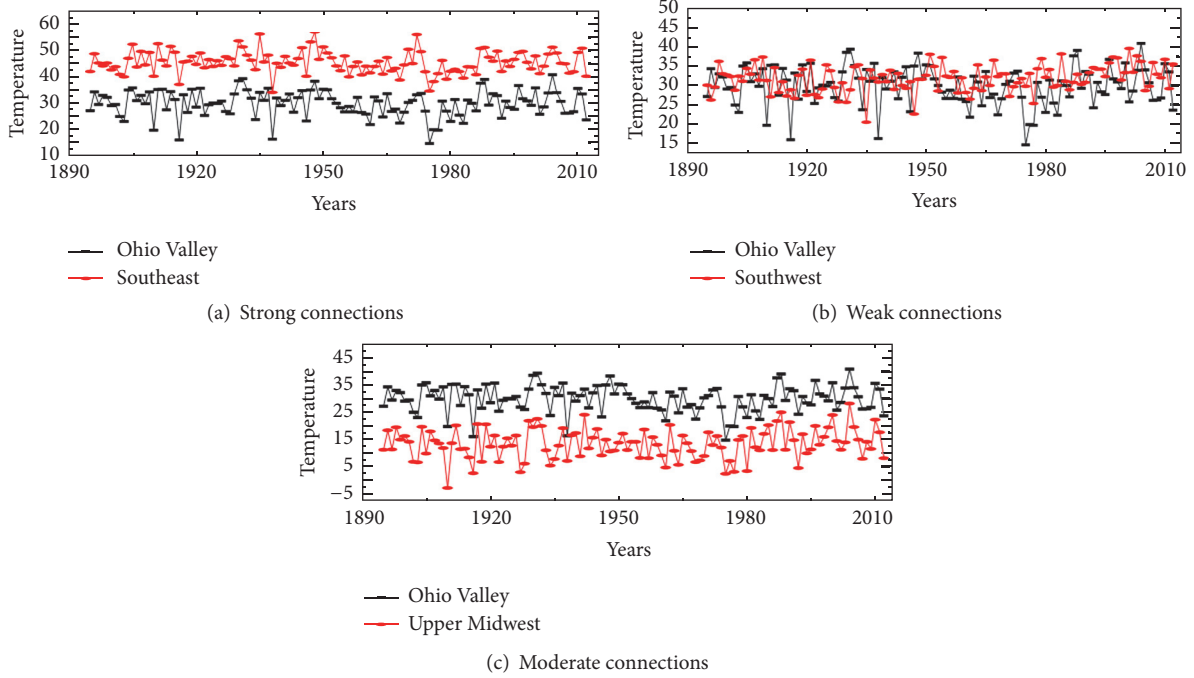


FIGURE 15: Patterns of connectivity.

TABLE 7: Kruskal–Wallis test.

Dataset	p value
C5Y120	$1.4e - 13$
C10Y120	$1.4e - 11$
C15Y120	$1.2e - 11$
US Climate data	$2.2e - 16$
China Climate data	$1.9e - 12$
Heart rate variability data (age 10–24)	1.623
Heart rate (4 groups)	$1.2e - 12$
Healthy voice data	1.412
Voice data (6 groups)	$1.8e - 13$

Southwest and Upper Midwest which indicates that there is a slight change in relationship (i.e., CPR values) throughout the years. In Figure 16(b), it could be seen that the category of relatedness in US regions will be the same with a varying number of years (i.e., extracted pairs belonging to a particular category are not varying much).

6. Conclusion and Discussion

In this paper, we have presented a method to find out similarity or dissimilarity between the two pieces of time series data where each series has periodic variations in the data. Normally, if the variations are periodic, then the two time series may provide the same RP though their nature of variations is different. Analyzing only the RP of the two time series is not sufficient to test whether they have similar periodic variations, so we applied CRP to test the similarity of periodic variations. We have also indicated visual similarity

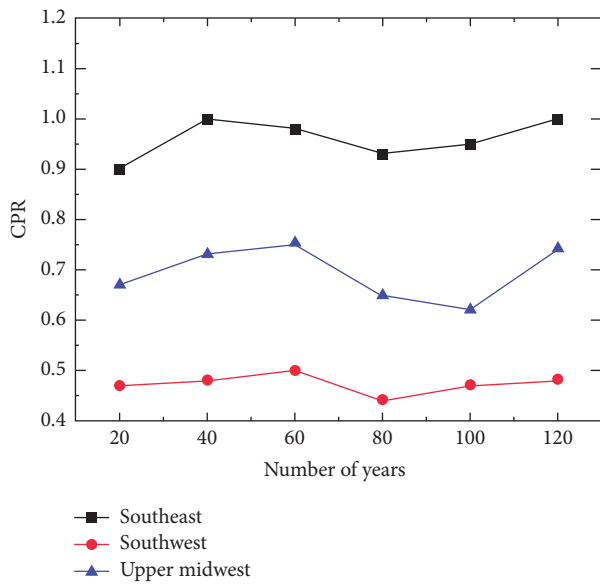
(connectivity) between the two time series using modified CPR.

First, we have tested our approach on the datasets having known similar or dissimilar periodic variations and found that the result of our method matches the already established results and, for that, we have used heart rate dataset, voice dataset, and synthetic datasets generated using the $\sin()$ function. After validating results on the known datasets, we have extended the method for climate data which has similar characteristics (i.e., time series data having periodic variations). We have analyzed data of different climatic regions and inferred that the regions which have similar latitudes and longitudes also have similar variations, while variation patterns change if regions have different latitudes and longitudes which are consistent with the known results. Our outcomes conclude that if the two time series are periodic and have a similar recurrence pattern, this does not mean that the same recurring pattern will emerge in CRP also.

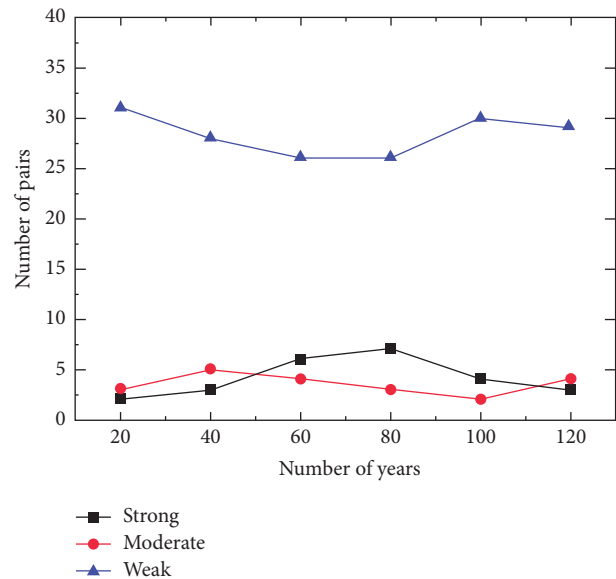
The analysis is done using methods such as quantitative RR, recurrence plots (RPs), cross recurrence plot (CRP), and correlation of probability of recurrence (CPR). First, we have demonstrated the periodicity of temperature variations using the RP plot which is visualized using diagonal lines or square boxes. After that, we have used the modified CPR approach to test similarity (connectivity) of these periodic variations. We have statistically validated our methodology by using ANOVA, Kruskal–Wallis, and z -statistics. This quantitative analysis can effectively recognize the changes of dynamic structure within and between groups. The obtained results suggest that the proposed approach provides a good potential for discrimination between groups of data having periodic variations and can be used to analyze

TABLE 8: Multiple group comparison.

Country 1 versus Country 2	Z-value	Hypothesis results
<i>US, nine regions</i>		
All regions versus Northern Rockies And Plains	-9.13	Hypothesis failed
All regions versus Northwest	-13.47	Hypothesis failed
All regions versus Ohio Valley	-11.33	Hypothesis failed
All regions versus South	2.78	Hypothesis failed
All regions versus Southeast	19.82	Hypothesis failed
All regions versus Southwest	0.85	Hypothesis accepted
All regions versus Upper Midwest	-12.06	Hypothesis failed
All regions versus West	5.79	Hypothesis failed
<i>China, eight regions</i>		
All regions versus South China	-3.009	Hypothesis failed
All regions versus middle and lower reaches of the Yangtze River	-2.263	Hypothesis failed
All regions versus North China	-1.280	Hypothesis accepted
All regions versus Northeast China	2.136	Hypothesis failed
All regions versus east of Northwest China	-1.985	Hypothesis failed
All regions versus west of Northwest China	1.077	Hypothesis accepted
All regions versus Tibet	-2.666	Hypothesis failed
All regions versus Southwest China	1.313	Hypothesis accepted
<i>Voice identification in healthy people</i>		
All persons versus person 1	1.661	Hypothesis accepted
All persons versus person 2	1.302	Hypothesis accepted
All persons versus person 3	1.324	Hypothesis accepted
All persons versus person 4	4.228	Hypothesis failed
All persons versus person 5	0.541	Hypothesis accepted
All persons versus person 6	1.030	Hypothesis accepted
All persons versus person 7	1.44	Hypothesis accepted
All persons versus person 8	1.25	Hypothesis accepted
All persons versus person 9	1.51	Hypothesis accepted
All persons versus person 10	1.293	Hypothesis accepted



(a)



(b)

FIGURE 16: Scalability of the CPR based approach in terms of (a) CPR value. (b) Number of pairs.

the climate data which is provided in the form of time series.

The economic growth of any region or country is different from others on the basis of education, finance, health, environment, business industries, living standard, and agriculture productivity. Somehow, these parameters depend on climate change; the economic time series data shows periodic variations and cycles which may result in differences in economic conditions. Our approach will also help experts to make any climate based policies which affect investment, environment, political stability, technological development, and industrial output such as designing the policies of environmental protection agencies.

In the future, we will try to use recurrence based measures (RQA) with uniform scaling to evaluate recurring patterns with other climate parameters (cloud, weather, pressure, rainfall, etc.) for a better understanding of their interconnection and analyze their effects on economic growth. Furthermore, we can try to parallelize the proposed approach, to reduce the relative time of similarity analysis and memory consumption on extremely large time series datasets.

Conflicts of Interest

The authors declare that they have no conflicts of interest.

Authors' Contributions

Anita Bai conceived the idea, designed and supervised the research, and wrote the article. She analyzed and interpreted the data. Swati Hira was responsible for algorithm and manuscript revision for important intellectual content. Swati Hira and Anita Bai were involved in the system design and implementation and drafted the article. S. Deshpande Parag gave valuable pieces of advice on conducting the study and helped in editing the article. All authors read and approved the final manuscript.

Acknowledgments

The authors would like to thank the Department of Computer Science and Engineering, VNIT, Nagpur, for making the required computing facilities available.

References

- [1] M. L. Parry, O. F. Canziani, P. J. Palutikof, P. J. v. d. Linden, and C. E. Hanson, *Climate Change 2007: Impacts, Adaptation and Vulnerability*, Cambridge University Press, 2007.
- [2] M. K. Linnenluecke, A. Griffiths, and M. I. Winn, "Firm and industry adaptation to climate change: A review of climate adaptation studies in the business and management field," *Wiley Interdisciplinary Reviews: Climate Change*, vol. 4, no. 5, pp. 397–416, 2013.
- [3] S. M. Howden, J.-F. Soussana, F. N. Tubiello, N. Chhetri, M. Dunlop, and H. Meinke, "Adapting agriculture to climate change," *Proceedings of the National Academy of Sciences of the United States of America*, vol. 104, no. 50, pp. 19691–19696, 2007.
- [4] C. Okereke, B. Wittneben, and F. Bowen, "Climate change: Challenging business, transforming politics," *Business and Society*, vol. 51, no. 1, pp. 7–30, 2012.
- [5] W. Wu, P. H. Verburg, and H. Tang, "Climate change and the food production system: Impacts and adaptation in China," *Regional Environmental Change*, vol. 14, no. 1, pp. 1–5, 2014.
- [6] S. J. Vermeulen, B. M. Campbell, and J. S. I. Ingram, "Climate change and food systems," *Annual Review of Environment and Resources*, vol. 37, pp. 195–222, 2012.
- [7] A. J. Haverkort and A. Verhagen, "Climate change and its repercussions for the potato supply chain," *Potato Research*, vol. 51, no. 3–4, pp. 223–237, 2008.
- [8] D. I. Gustafson, J. W. Jones, C. H. Porter et al., "Climate adaptation imperatives: untapped global maize yield opportunities," *International Journal of Agricultural Sustainability*, 2014.
- [9] O. Ovalle-Rivera, P. Läderach, C. Bunn, M. Obersteiner, and G. Schroth, "Projected shifts in Coffea arabica suitability among major global producing regions due to climate change," *PLoS ONE*, vol. 10, no. 4, Article ID e0124155, 2015.
- [10] Z. Liu, P. Yang, H. Tang et al., "Shifts in the extent and location of rice cropping areas match the climate change pattern in China during 1980–2010," *Regional Environmental Change*, vol. 15, no. 5, pp. 919–929, 2015.
- [11] S. E. Park, "A review of climate change impact and adaptation assessments on the Australian sugarcane industry," in *Proceedings of the 2008 Conference of the Australian Society of Sugar Cane Technologists*, Queensland, Australia, April–May 2008.
- [12] A. Fleming, S. E. Park, and N. A. Marshall, "Enhancing adaptation outcomes for transformation: climate change in the Australian wine industry," *Journal of Wine Research*, vol. 26, no. 2, pp. 99–114, 2015.
- [13] C. L. Webber and J. P. Zbilut, "Recurrence quantification analysis of nonlinear dynamical systems," *Tutorials in Contemporary Nonlinear Methods for The Behavioral Sciences*, pp. 26–94, 2005.
- [14] N. Marwan and J. Kurths, "Cross recurrence plots and their applications," *Mathematical Physics Research at The Cutting Edge*, pp. 101–139, 2004.
- [15] M. I. Coco and R. Dale, "Cross-recurrence quantification analysis of categorical and continuous time series: An R package," *Frontiers in Psychology*, vol. 5, article 510, 2014.
- [16] J. Sukharev, C. Wang, K.-L. Ma, and A. T. Wittenberg, "Correlation study of time-varying multivariate climate data sets," in *Proceedings of the IEEE Pacific Visualization Symposium, PacificVis 2009*, pp. 161–168, Beijing, China, April 2009.
- [17] S. Liu, X. Huang, Y. Ni, H. Fu, and G. Yang, "A high performance compression method for climate data," in *Proceedings of the 12th IEEE International Symposium on Parallel and Distributed Processing with Applications, ISPA 2014*, pp. 68–77, Milan, Italy, August 2014.
- [18] M. N. Sap and A. M. Awan, "Finding spatio-temporal patterns in climate data using clustering," in *Proceedings of the International Conference on Cyberworlds (CW'05)*, pp. 155–162, Singapore, Singapore, November 2005.
- [19] W. Hendrix, I. K. Tetteh, A. Agrawal, F. Semazzi, W.-K. Liao, and A. Choudhary, "Community dynamics and analysis of decadal trends in climate data," in *Proceedings of the 11th IEEE International Conference on Data Mining Workshops, (ICDMW '11)*, pp. 9–14, BC, Canada, December 2011.
- [20] N. Marwan, M. Carmen Romano, M. Thiel, and J. Kurths, "Recurrence plots for the analysis of complex systems," *Physics Reports*, vol. 438, no. 5–6, pp. 237–329, 2007.

- [21] C. L. Webber and J. P. Zbilut, "Recurrent structuring of dynamical and spatial systems," in *Proceedings of the International Meeting*, pp. 101–133, 1997.
- [22] J. Belaire-Franch, D. Contreras, and L. Tordera-Lledó, "Assessing nonlinear structures in real exchange rates using recurrence plot strategies," *Physica D: Nonlinear Phenomena*, vol. 171, no. 4, pp. 249–264, 2002.
- [23] F. Strozzi, E. Gutiérrez, C. Noé, T. Rossi, M. Serati, and J. M. Zaldívar, "Measuring volatility in the Nordic spot electricity market using recurrence quantification analysis," *European Physical Journal: Special Topics*, vol. 164, no. 1, pp. 105–115, 2008.
- [24] J. Zbilut, M. Koebbe, H. Loeb, and G. Mayer, "Use of recurrence plots in the analysis of heart beat intervals," *Computers in Cardiology*, pp. 263–266, 1990.
- [25] P. M. Crowley, "Analyzing convergence and synchronicity of business and growth cycles in the euro area using cross recurrence plots," *The European Physical Journal Special Topics*, vol. 164, no. 1, pp. 67–84, 2008.
- [26] D. F. Silva, V. M. A. De Souza, and G. E. A. P. A. Batista, "Time series classification using compression distance of recurrence plots," in *Proceedings of the 13th IEEE International Conference on Data Mining (ICDM '13)*, pp. 687–696, IEEE, Dallas, TX, USA, December 2013.
- [27] S. Hira, A. Bai, and P. S. Deshpande, "Estimating the similarities of G7 countries using economic parameters," *Advances in Intelligent Systems and Computing*, vol. 435, pp. 59–67, 2016.
- [28] R. I. Levin and D. S. Rubin, *Statistics for Management*, Pearson Prentice Hall, University of North Carolina, 1997.
- [29] J. P. Eckmann, S. O. Kamphorst, and D. Ruelle, "Recurrence plots of dynamical systems," *EPL*, vol. 4, no. 9, pp. 973–977, 1987.
- [30] M. C. Romano, M. Thiel, J. Kurths, I. Z. Kiss, and J. L. Hudson, "Detection of synchronization for non-phase-coherent and non-stationary data," *Europhysics Letters*, vol. 71, no. 3, pp. 466–472, 2005.
- [31] "fNonlinear package," 2015, <https://cran.r-project.org/web/packages/fNonlinear/fNonlinear.pdf>.
- [32] "Climate center data link," 1970, <http://www.ncdc.noaa.gov>.
- [33] D. Hoyer, B. Pompe, H. Herzel, and U. Zwiener, "Nonlinear coordination of cardiovascular autonomic control: The fundamentals of nonlinear dynamics," *IEEE Engineering in Medicine and Biology Magazine*, vol. 17, no. 6, pp. 17–21, 1998.
- [34] K. Elemetrics, *Elemetrics Corp. Disordered Voice Database*, Model 4337, 3 edition, 1994.
- [35] H. Ding, S. Crozier, and S. Wilson, "A new heart rate variability analysis method by means of quantifying the variation of nonlinear dynamic patterns," *IEEE Transactions on Biomedical Engineering*, vol. 54, no. 9, pp. 1590–1597, 2007.
- [36] M. A. Little, P. E. McSharry, S. J. Roberts, D. A. E. Costello, and I. M. Moroz, "Exploiting nonlinear recurrence and fractal scaling properties for voice disorder detection," *BioMedical Engineering Online*, vol. 6, article 23, 2007.

Research Article

Research on the Method of Traffic Organization and Optimization Based on Dynamic Traffic Flow Model

Shu-bin Li,¹ Guang-min Wang,² Tao Wang,³ and Hua-ling Ren⁴

¹Department of Traffic Management Engineering, Shandong Police College, Jinan 250014, China

²School of Economics and Management, China University of Geosciences, Wuhan 430074, China

³School of Automation and Electronic Engineering, Qingdao University of Science and Technology, Qingdao 266042, China

⁴School of Traffic and Transportation, Beijing Jiaotong University, Beijing 100044, China

Correspondence should be addressed to Shu-bin Li; li_shu_bin@163.com

Received 23 November 2016; Revised 7 February 2017; Accepted 16 February 2017

Academic Editor: J. R. Torregrosa

Copyright © 2017 Shu-bin Li et al. This is an open access article distributed under the Creative Commons Attribution License, which permits unrestricted use, distribution, and reproduction in any medium, provided the original work is properly cited.

The modern transportation system is becoming sluggish by traffic jams, so much so that it can harm the economic and society in our country. One of the reasons is the surging vehicles day by day. Another reason is the shortage of the traffic supply seriously. But the most important reason is that the traffic organization and optimization hardly met the conditions of modern transport development. In this paper, the practical method of the traffic organization and optimization used in regional area is explored by the dynamic traffic network analysis method. Firstly, the operational states of the regional traffic network are obtained by simulation method based on the self-developed traffic simulation software DynaCHINA, in which the improved traffic flow simulation model was proposed in order to be more suitable for actual domestic urban transport situation. Then the appropriated optimization model and algorithm were proposed according to different optimized content and organization goals, and the traffic simulation processes more suitable to regional optimization were designed exactly. Finally, a regional network in Tai'an city was selected as an example. The simulation results show that the proposed method is effective and feasible. It can provide strong scientific and technological support for the traffic management department.

1. Introduction

In recent years, ITS (Intelligent Transportation System) has developed rapidly since 2011 and will enter into the mature period in China after 2020. But with the increased of vehicles and road construction, the latter is far behind the former, so a series of unavoidable traffic problems were triggered such as traffic congestion, traffic safety, and environment pollution. In order to resolve the contradiction of traffic supply and demand, a viable method is the national policy and the other is to develop intelligent transportation technologies. The latter can optimize transportation resources from all aspects of traffic supply. The traffic organization and optimization are a better way to optimize the existing transportation facilities by using the method of system engineering under the guidance of system science. It can reasonably adjust the relationship between traffic demand and traffic supply so as to

make better use of road resources. Moreover the road can play an important part in traffic system by scientific organization and distribution. Further the traffic flow can be smooth and safety. The traffic congestion can be reduced to a certain degree [1].

The content of traffic organization and optimization varies with different situations. Shi et al. [2] raised the optimization approach of one-way traffic organization in urban micro circulation transportation network by the constraint of road saturation. Long et al. [3] proposed the different model and algorithm for the same problem. Dussutour et al. [4] studied the optimization behavior of ants, whose contribution is published in "Nature." Jia [5] studied the problem of traffic organization optimization on urban main road systematically and realized the two-direction green pass. Xu et al. [6] carried out the traffic organization optimization by using simulation method for road traffic bottlenecks;

its purpose is to reduce traffic congestion. Yao et al. [7] proposed a more practical method of information induced and simulation; in a large flow road the micro circulation method was put forward. Yang et al. [8, 9] proposed the regional traffic organization methods integrated time period; their suggestions and measures were effective. Sun et al. [10, 11] proposed also some valuable suggestions for the urban passenger transport hub by simulation method. Zhengyan [12] addressed some technical method for traffic organization of emergency evacuation.

From the above document analysis, most papers focus on the traffic flow for traffic organization and optimization method. In order to ensure reasonableness and effectiveness of traffic organization, the pros and cons are needed to be considered. In this paper, the dynamic method is proposed in view of the shortcomings of the static method, such as the peak period and flat peak period of traffic flow were considered.

To establish a scientific and effective traffic management and optimization scheme, it is necessary to analyze relationship of the traffic demand and traffic supply. By forecasting interaction of the traffic demand and traffic supply real-time, the response behavior of the drivers can be simulated, and then the traffic control scheme and the traffic guidance strategy were analyzed. The self-developed software system DynaCHINA was used to do some work in this spot.

2. Overview of DynaCHINA

This paper presents a new simulation-based DTA (dynamic traffic assignment) system: DynaCHINA (Dynamic Consistent Hybrid Information Based on Network Assignment). It is the only self-developed software system in China by our team. Although the basic framework of DynaMIT is adopted in its implementation, compared with DynaMIT and DynaSMART, DynaCHINA has four unique features: modeling mixed traffic and special driver behavior; availability of floating car data (FCD) in urban networks; anisotropic mesoscopic supply simulator; availability of true OD flows in freeway networks. Predictive capacity is the core of DynaCHINA. DynaCHINA shows the potential for real-time traffic prediction application according to the laboratory evaluation results with data collected from real activity. It is the first and the only Traffic Estimation and Prediction System (TrEPS) in China.

DynaCHINA integrates the advanced dynamic traffic demand analysis technology, the dynamic traffic assignment technology, many discrete choice models, off-line and online system parameters calibration method, and so forth. The software can provide simulation test, analysis, and evaluation method for the related research and implementation of intelligent transportation system. It has the ability to estimate and forecast the network traffic flow, density, and speed which will provide technical support for the traffic control and traffic guidance system. It makes these systems more effective to ease traffic congestion and improve the efficiency of travel.

DynaCHINA contains many mathematical models, such as dynamic OD estimation model, mesoscopic traffic simulation model, vehicle moving model, speed-density model,

queuing model, and network model. At the same time, in order to achieve the purpose of online application, the efficient algorithms were designed, such as path generation algorithm and simulation steps of the specific design. The developed prototype is basically completed; the source code reached tens of thousands. Some other functions of bus simulation and VIP route guidance for specially vehicles were also proposed.

DynaCHINA targets more realistic approaches to short-term transportation planning such as special events and work zones and addresses the growing importance of real-time applications such as incident management, route guidance, and emergency response. It is capable of providing predictive traffic information (speeds, densities, and queues/flows) based on a rolling-horizon implementation of an assignment-simulation framework. DynaCHINA can be operated in a distributed computation mode in support of real-time operations, including data synchronization, self-calibration of system parameters, and self-correcting of system states. Currently DynaCHINA team is working with some agencies to conduct laboratory experiment and initial field deployments of the prototypes to investigate functionality, prediction accuracy, computational efficiency, and robustness in the field environment at Beijing, Jinan, and Guangzhou. Figure 1 shows how DynaCHINA can be implemented.

3. The Mesoscopic Traffic Simulation Models and Algorithm

There are a lot of modes developed in DynaCHINA such as road network model, the traveler behavior model, the path generation algorithm, and the capacity models. In these models, the mesoscopic traffic simulation model and the dynamic OD estimation model are the most important ones. The proposed simulation process is designed efficiently. The following focuses on the models and algorithm.

3.1. The Mesoscopic Traffic Simulation Models. There are two key models in the mesoscopic simulation process. One is the speed-density relationship model. It needs some information of road flow, speed, or density in order to more accurately reproduce the current road traffic condition. In general, one or more parameters must be calibrated in the following function:

$$v_u = \max \left\{ v_{\min}, v_{\max} \left\{ 1 - \left\{ \frac{k - k_{\max}}{k_{\text{jam}}} \right\}^{\beta} \right\}^{\alpha} \right\}, \quad (1)$$

where v_u is the vehicle speed, k is the density, k_{jam} is the jam density, k_{\max} is the critical density, v_{\min} and v_{\max} are the minimum and maximum speed designed. In this paper, the traffic simulation technology is used more than one time; the minimum speed is designed to avoid the situation of being unable start the simulation system. In order to be more realistic, the problem can be described as that the upstream of a long road has a constant speed and followed the

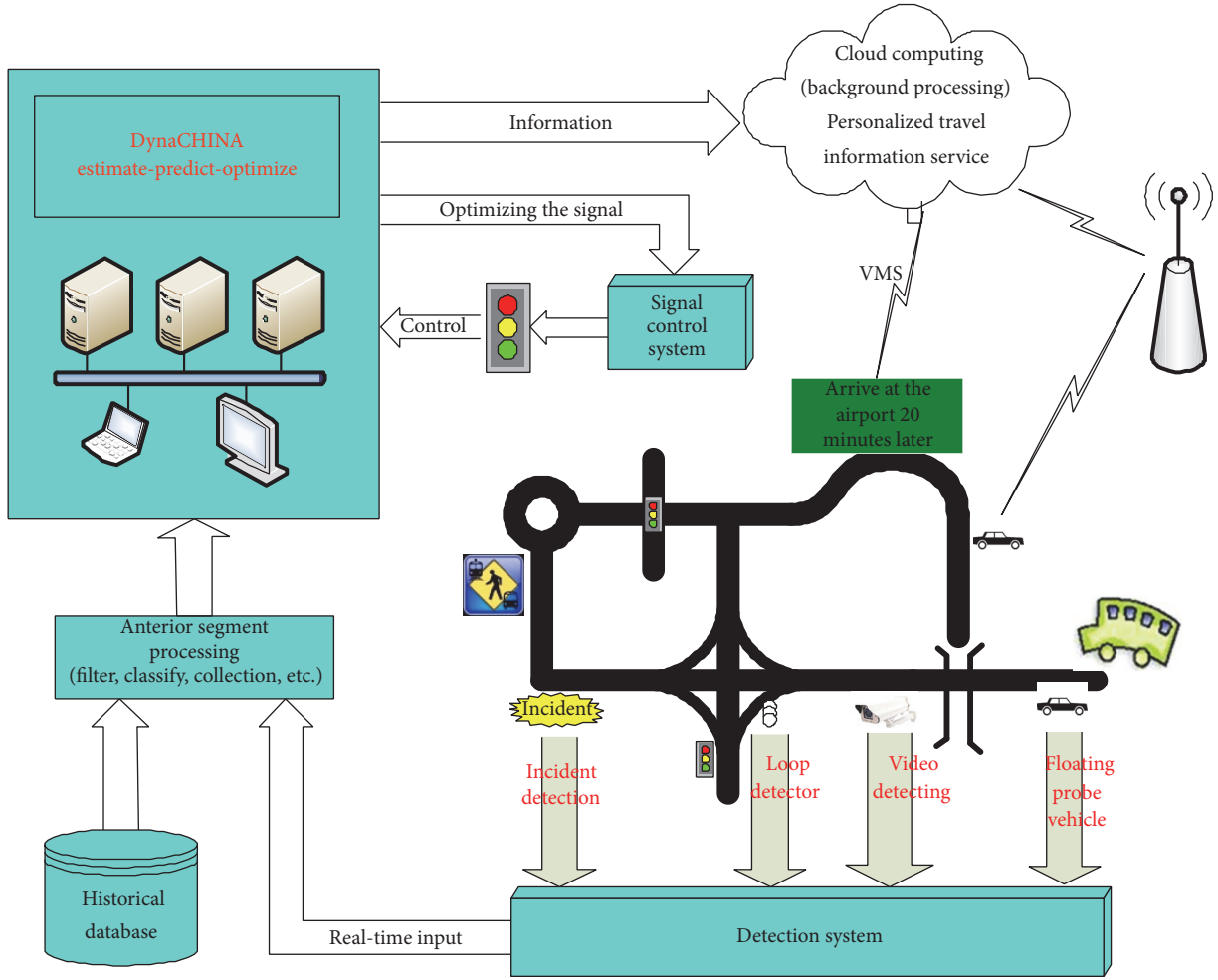


FIGURE 1: DynaCHINA system principle.

speed-density relationship at the downstream. Mathematical description is as follows:

$$v_u = \begin{cases} v_f & k \leq k_{\max} \\ \max \left\{ v_{\min}, v_{\max} \left\{ 1 - \left\{ \frac{k - k_{\max}}{k_{\text{jam}}} \right\}^\beta \right\}^\alpha \right\} & k > k_{\max} \end{cases} \quad (2)$$

where α and β are parameters.

The other is the vehicle movement model. Its function is mainly to put the vehicles at the right position based on the speed of vehicles on the network. This also means the relationship between time and position.

$$t(z) = \begin{cases} \frac{1}{\lambda} \log \frac{\lambda_{z+v_u}}{\lambda_{z_0+v_u}} & \text{if } v_u \neq v_d \\ \frac{z - z_0}{v_u} & \text{if } v_u = v_d, \end{cases} \quad (3)$$

where t is the time and z is the position; when $t = 0$, the position is z_0 . v_d is the downstream vehicle speed; usually parameter λ is consistent with the following formula:

$$\lambda = \frac{v_d - v_u}{L_s}. \quad (4)$$

L_s is the length of the deceleration/acceleration zone of the road.

3.2. The Estimation Method of Dynamic OD Demand. In simulation period, how many vehicles can be loaded on the network? The real-time OD estimation model must be needed. In this section, the generalized least square estimation model is used to resolve the problem.

$$\hat{\mathbf{x}}_h = \arg \min \left[(\mathbf{x}_h - \mathbf{x}_h^a)^T \mathbf{W}_h^{-1} (\mathbf{x}_h - \mathbf{x}_h^a) \right]$$

$$+ \left(\mathbf{y}_h - \sum_{p=h-p'}^{h-1} \mathbf{a}_h^p \widehat{\mathbf{x}}_p - \mathbf{a}_h^h \mathbf{x}_h \right)^T \cdot \mathbf{R}_h^{-1} \left(\mathbf{y}_h - \sum_{p=h-p'}^{h-1} \mathbf{a}_h^p \widehat{\mathbf{x}}_p - \mathbf{a}_h^h \mathbf{x}_h \right) \Bigg], \quad (5)$$

where $\widehat{\mathbf{x}}_h$ is the estimated OD matrix; \mathbf{x}_h^a is the historical OD matrix which refers to a priori values of \mathbf{x}_h in the time period h ; n_l is the section number with monitoring equipment; $\mathbf{y}_h \in R^{n_l}$ is the monitored value on section n_l in time period h ; \mathbf{a}_h^p ($p = h, h-1, \dots, h-p'$) is the dynamic traffic assignment matrix which defined a mapping between the OD vector \mathbf{x}_p in p and the traffic volume vector in h ; if there is not any a priori information, \mathbf{W}_h and \mathbf{R}_h can be defined as a unit matrix [13].

Another dynamic OD demand estimation model is Kalman filtering model. It includes state and space model. The basic idea is proposed by Ashok and Ben-Akiva [14] in 1933. Unlike other approaches in the literatures, the approach is based on deviations from historical values. Considering a network with n_{OD} OD pairs and n_l link counts, let us assume the following notation:

\mathbf{x}_{h+1} is the matrix representing the number of vehicles between each OD pair departing their origins during time interval h and \mathbf{x}_h^H is the corresponding historical estimated matrix. The transition equation can be expressed as

$$\delta \mathbf{x}_{h+1} = \sum_{p=h+1-q'}^h \mathbf{f}_{h+1}^p \delta \mathbf{x}_p + \mathbf{w}_{h+1}, \quad (6)$$

where \mathbf{f}_h^p is a $n_{OD} \times n_{OD}$ matrix mapping from $(x_p - x_p^H)$ to $(x_{h+1} - x_{h+1}^H)$, \mathbf{w}_{h+1} is a $(n_{OD} \times 1)$ vector of random errors, and q' is the degree of the autoregressive process.

The error is assumed as follows:

$$\begin{aligned} E(\mathbf{w}_{h+1}) &= 0, \\ E(\mathbf{w}_h \mathbf{w}_h^T) &= \mathbf{Q}_h \delta_{hl}, \end{aligned} \quad (7)$$

\mathbf{Q}_h is covariance matrix, $\delta_{hl} = \begin{cases} 1, & h = l \\ 0, & h \neq l. \end{cases}$

The measurement equation which relates unknown OD flows to the observed link counts can be stated mathematically as follows:

$$\delta \mathbf{y}_h = \sum_{p=h-p'}^h \mathbf{a}_h^p \delta \mathbf{x}_p + \mathbf{v}_h, \quad (8)$$

where \mathbf{a}_h^p is an assignment matrix of contributions from \mathbf{x}_p to \mathbf{y}_h ; $\delta \mathbf{y}_h = \mathbf{y}_h - \mathbf{y}_h^H = \mathbf{y}_h - \sum_{p=h-p'}^h \mathbf{a}_h^p \mathbf{x}_p^H$, \mathbf{y}_h^H are the link flows obtained by assigning the historical OD flows, \mathbf{y}_h is the detection value of the traffic volume of the road section in the h time, p' is the number of time intervals corresponding to the longest trip; \mathbf{v}_h is the Gauss white noise which is

independent of the system noise and satisfies $E(v_h) = 0$, and $E(v_h v_l^T) = \mathbf{R}_h \delta_{hl}$. Equations (6) and (8) constitute the state and space model of the dynamic OD matrix estimation.

3.3. Simulation Process. The designed simulation process is very important to the simulation accuracy. The simulation time is divided into a number of equal lengths of Update phase. One Update phase is divided into several equal lengths of the Advance interval. In Advance phases, the vehicles can be moved to their new positions. The Update phase is used for updating the traffic dynamics parameters (e.g., densities, speeds, and flow) used in the simulation during each simulation cycle. If the simulation horizon is T , without loss of generality, we assume that the time horizon starts at time $t = 0$ and finishes at time $t = T$. Update phase is Δt_{update} ; Advance phase is $\Delta t_{\text{advance}}$. So,

$$T = k_u \Delta t_{\text{update}}, \quad (9)$$

$$\Delta t_{\text{update}} = k_A \Delta t_{\text{advance}}. \quad (10)$$

k_u and k_A are the positive integers; the specific simulation process is as follows.

Step 1 (initialization, input the following information). The network description, the simulation horizon, and the description of all vehicles at the beginning of the interval include their position on the network, their destination, and their current path. All vehicles present in the network at time $t = 0$ and the loaded positions [15].

Step 2 (sort the nodes of the traffic network). Set up the network node, section, and other parameters; execute the following program.

Step 2.1. Every segment definition is updated according to the incident description. The output capacities of all segments are updated. Initialize the output counter of the output capacity and initialize the input counter of the acceptance capacity.

Step 2.2. For each segment, compute the upstream-speed and the density. For each direction of the segment, compute the downstream-speed.

Step 2.3. Calculate the speed of the downstream segment, and update the acceptance and output capability of the next segment.

Step 2.4. For a vehicle execute Advance phase; call formulas (9) and (10); load the updated vehicles to their new position of the network.

Step 2.5. $i = 0$.

Step 3 (stopping criteria). The algorithm is stopped when all Advance phase intervals have been processed; that is, $i = k_A$.

The detailed process is illustrated in Figure 2.

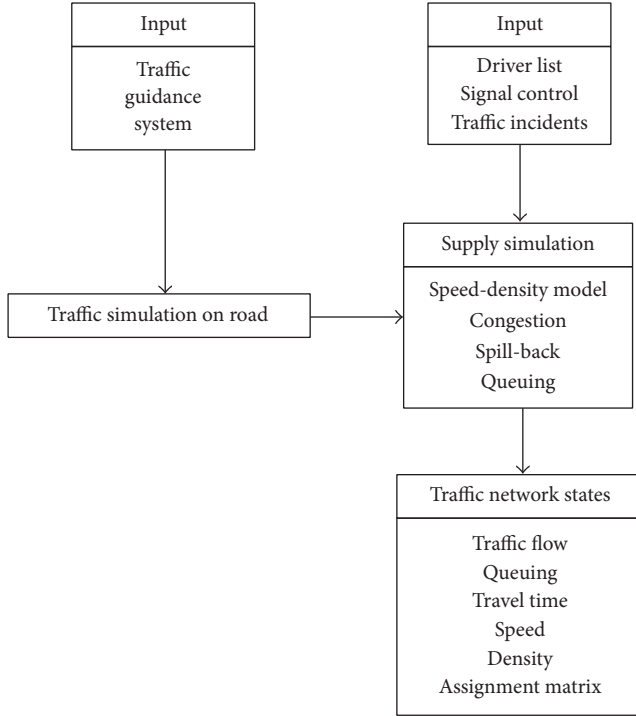


FIGURE 2: General process of simulation.

4. The Optimization Model and Algorithm of Traffic Organization

The static traffic organization mainly refers to traffic signs, traffic markings, boot device and parking management, and so forth. There are all the static characteristic. That means it will not change in a long time once the organization method is determined. In contrast, the dynamic method is more flexible and will be changed with time under different traffic network conditions, such as signal control and information. But in any kind of traffic organization, the purpose is to alleviate the traffic pressure of the road network. It comes to it by balancing traffic flow on the network in time and space.

In this paper, the traffic optimization and organization are carried out by using the combination of the static channelized intersection and the signal optimization. Firstly, the division of the road is implemented on intersection level by the way of road channelization. And then, the signal control scheme is set up by using the method of regional signal optimization and by means of simulation to realize it.

The proposed signal optimization model is as follows:

$$\begin{aligned}
 \min \quad & L(\cdot) \\
 = \quad & \frac{1}{2} (\mathbf{D}(h))^2 + \frac{1}{2} \sum_{h=1} (\mathbf{D}(h))^2 - \sum_h (q + f) \\
 & + \sum_h s.
 \end{aligned} \quad (11)$$

Constraint conditions is as follows:

$$\begin{aligned}
 T_{\min} &\leq T_h \leq T_{\max}, \\
 g_{\min} &\leq g_h \leq g_{\max}, \\
 C &= \sum g, \\
 C_{\min} &\leq C \leq C_{\max}.
 \end{aligned} \quad (12)$$

C is the total cycle length; C_{\max} , C_{\min} are the maximum and minimum cycle length;

$d = \{d_h\}$: d_h is the column vectors for all vehicle delays in the h time period.

g is the effective green time; g_{\max} , g_{\min} are the maximum and minimum effective green time.

$q = \{q_h\}$ is the total queue length of the network in simulation period; q_h is the average queue length of the h period of time all sections of the column vector.

$f = \{f_h\}$ is the sum of all intersection crossing traffic in simulation period; f_h is the flow vector of all the inlet channels of h time period.

$T = \{T_h\}$: timing parameters of all signal controllers in the network.

$T_h = \{t_{ih}\}$: timing parameter vector of all signal intersections in h time period.

$t_{ah} = [t_{a0h}^g, t_{a1h}^g, \dots, t_{ah}^g]^T$ or $[C_{\kappa} s_{a0h}^g, C_{\kappa} s_{a1h}^g, \dots, C_{\kappa} s_{a0h}^g]^T$ is the green time of each phase of the a intersection in h or phase difference of initial phase, C_{κ} is the phase number of a signal intersection, and s_{abh}^g is the green-time-rate in h , the a intersection, and the b phase.

T_{\max} , T_{\min} : the upper and lower bound constraint vector of signal timing parameters.

$L(\cdot)$ is the objective function.

The SPSSA (Simultaneous Perturbation Stochastic Approximation) algorithm is used to solve the problem and also implemented in the simulation system [16]. The SPSSA approximates the gradient of the objective function through finite differences. Critically, the approach infers the components of the gradient vector from two function evaluations, after perturbing all components of the parameter vector simultaneously. The computational savings are thus significant when compared to traditional stochastic approximation methods, though many replications may be required in order to obtain a more stable gradient through smoothing.

The SPSSA algorithm requires calculation only twice for the objective function independent of the number of parameters n . Generally speaking, the SPSSA algorithm will produce a series of parameter estimators; that is, the gradient of objective function gradually tends to 0. Among them, the i iteration of the parameters is updated by

$$\theta^{i+1} = \theta^i - a_i \hat{g}(\theta^i), \quad (13)$$

where θ^i is parameter vector when the i iteration starts, $\hat{g}(\theta^i)$ is the current estimator of the vector, and a_i is gain for the step length.

The SPSA algorithm is only through two evaluations of the function, the gradient approximation can be got, and the calculation formula is as follows:

$$\hat{g}(\theta^i) = \frac{z(\theta^i + c^i \Delta_i) - z(\theta^i - c^i \Delta_i)}{2c^i} \begin{bmatrix} \Delta_{i1}^{-1} \\ \Delta_{i2}^{-1} \\ \vdots \\ \Delta_{ik}^{-1} \end{bmatrix}, \quad (14)$$

where Δ_i is a K -dimensional stochastic perturbation vector; as the numerator for all $k = 1, 2, \dots, K$ are the same, so each iteration has the static calculation (nothing to do with the vector dimension K), which is the most prominent advantages of the algorithm. Of course, the algorithm is required to achieve convergence that must have enough rational number of iterations and then have a good application value. The SPSA algorithm is described below in detail by the steps:

- (1) Initialization and coefficient selection: set counter index: $k = 0$, $i = 0$, and $\theta^i = \theta^0$ are initial value of K -dimensional optimization vector and pick initial guess nonnegative coefficients a , A , c , α , and γ in the SPSA.
- (2) Set iteration number of calculated gradient vectors in each step: grad_rep; that is, in each iteration step, by many times, take the average gradient estimator.
- (3) The iteration counter plus 1; calculate the step length: $ai = a/(A + i)\alpha$; $ci = c/i$.
- (4) Generate a K -dimensional perturbation stochastic vector of independent Δ_i ; each of its elements Δ_{ik} , $k = 1, 2, \dots, K$ is received by a probability distribution. The probability distribution density function is symmetry by the vertical axis (0 axis); $|\Delta_{ik}|$ and $E|\Delta_{ik}^{-1}|$ have upper bound. Reference [16] showed that Bernoulli distribution has these characteristics, and uniform distribution and normal conditions are not met.
- (5) Make use of the mesoscopic traffic flow model or other traffic simulation systems accessed the values of the objective function by $\theta^{i+} = \theta^i + c^i \Delta_i$ and $\theta^{i-} = \theta^i - c^i \Delta_i$, and each point is required to meet the upper and lower limits constraints in the optimization problem.
- (6) According to (9) calculate the K -dimensional gradient vector of the stochastic approximation, in which one component of the gradient vector of the K has the same elements, which make the SPSA algorithm different from the traditional finite difference method (FD).
- (7) Repeat (4)–(6) steps grad_rep times; each time has an independent sample of Δ_i , and then finally acquire average gradient vector at θ^i .

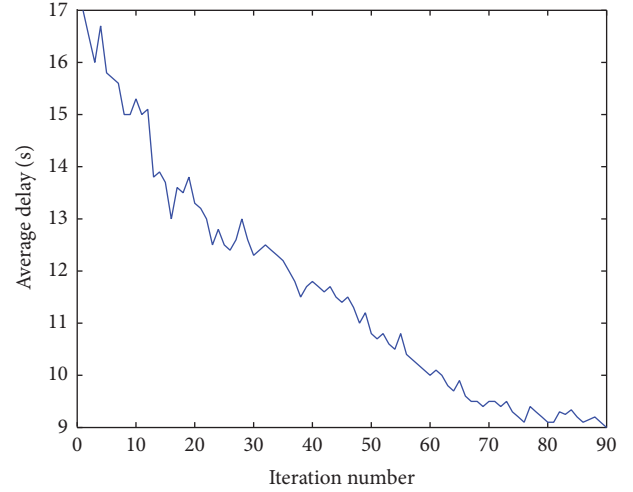


FIGURE 3: Convergence performance of SPSA algorithm.

- (8) A new solution point θ^{i+1} is got from (8), and in accordance with the parameter vector of the upper and lower bound adjust the solution point.
- (9) Go back to step (3), continue to iterate until convergence. When the number of iterations to reach the maximum allowable number of iterations or function value $z(\theta^i)$ corresponding to θ^i is little change in several successive iterates, terminate the algorithm.

The SPSA method outlined in this paper immediately illustrates the potential computational savings for large-scale optimization. Figure 3 is the convergence performance of the SPSA algorithm.

5. Case Study

In this paper, the real regional network of Tai'an city is used to the case study. Daizong street of Tai'an city in Shandong province in China located in the north of the city and next to famous mountain of Tai. It is about 1.68 kilometers long with 7 signal intersections. The major intersections have a large traffic pressure in rush hour, especially in the morning rush from 7:30 am to 8:30 am. In another time, the traffic flow is the relatively smaller one. In peak hour, the vehicles speed is about 10~15 km/h. By survey, the main problem is the badly traffic optimization and organization. There are not reasonable. The capacity of the street decreased sharply by the multitraffic flow from different directions. The marking is not so ideal also. The traffic signal lacks rationality settings which cause serious traffic congestion.

After an investigation in 2016, the hour traffic flow of some day is shown in Figure 4.

Based on the mentioned reasons, the idea of traffic organization in this area is as follows:

- (1) Rechanneling intersection: set traffic signs and marking, vehicles organization, and nonmotor vehicles and pedestrian traffic organization.
- (2) Calculating signal timings of intersections: set the signal timings according to the traffic flow of the

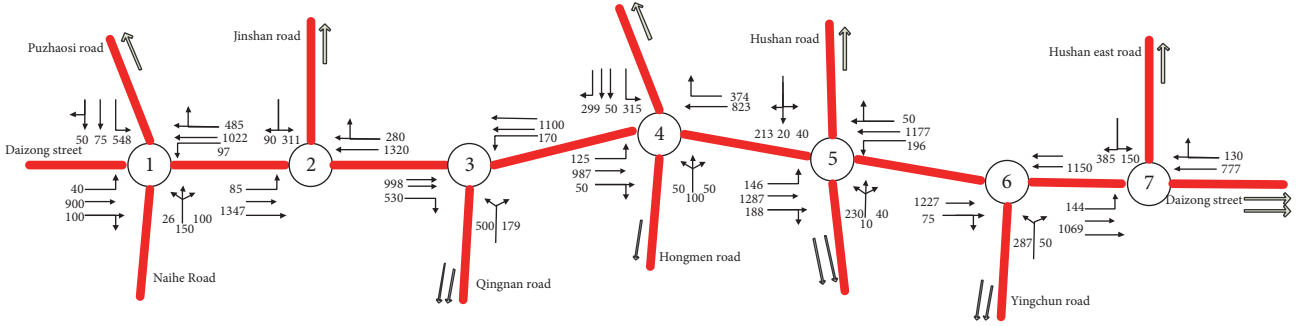


FIGURE 4: Traffic flow of Daizong street.

intersection. In peak hour, execute green pass scheme on main road of the street in order to maximize the through flow. At the same time, control the input traffic flow of intersections on the street.

- (3) Executing the proposed method of signal optimization in this paper.

Figure 5 is the comparison of the distribution of traffic flow and the detected flow by the parameter calibration method in this paper. The calculation method of the error estimation of RMSN is as follows:

$$RMSN = \sqrt{\frac{\sum_h \sum_i (y_{hi} - \hat{y}_{hi})^2}{\sum_h \sum_i \hat{y}_{hi}^2}}, \quad (15)$$

where y_{hi} and \hat{y}_{hi} are the actual measured value and the estimated ones in the h period by the i detector, respectively. As can be seen from Figure 5, the proposed method can estimate the traffic condition of the network accurately. At this point, the simulated road network is equivalent to the actual road network, so the simulation results of the signal control parameters can be as effective as the actual road network.

Figure 3 is the performance index (PI) of iterative optimization of SPSA curve; PI is the average delay by all vehicles on the network. The SPSA algorithm optimized signal timing scheme compared to the Synchro software-based one; the average travel delay of vehicles decreased by 46.67%.

The surveyed data were input into the simulation system. The results show that the traffic flow estimation error was less than 10% which means the system was reliable. The averaged traffic flow, density, and speed of segments can be contrasted by the traffic organization method. Moreover the designed simulation system can be executed online for implementing the dynamic traffic organization scheme.

The simulation time was two hours. The simulation interval was fifteen minutes, so there were eight intervals. The loaded data was cycled double times survey data. The parameters of the traffic simulation model were the same as [16].

If there were not any the traffic organization optimization measures, the averaged density, speed, and flow can be obtained; see Figures 6–8. From the whole simulation time, the maximum averaged density of each segment is 0.2442

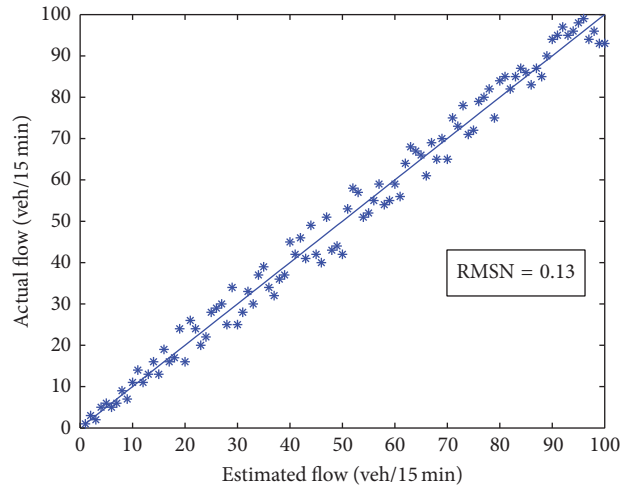


FIGURE 5: Comparison between surveillance flows and estimation flows.

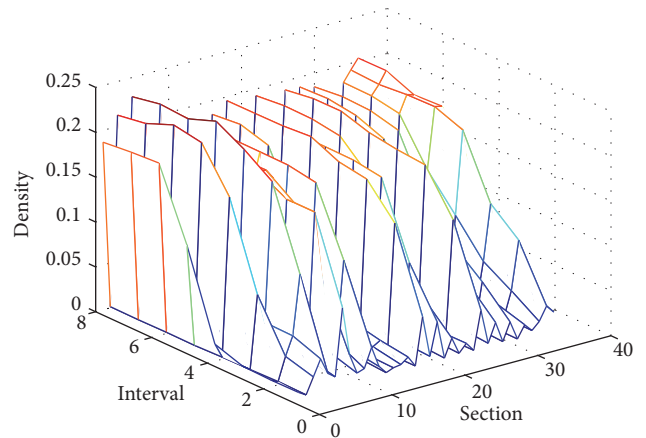


FIGURE 6: Averaged density before optimization.

which existed on the fifth segment in the fifth interval. It was the most crowded at this time. The averaged density and sum density of the network in the whole simulation time were 0.0777 and 22.3873, respectively. Use the same method to analysis the averaged flow and speed. The total flow was 38915. The averaged flow of the network was 135.1215. The

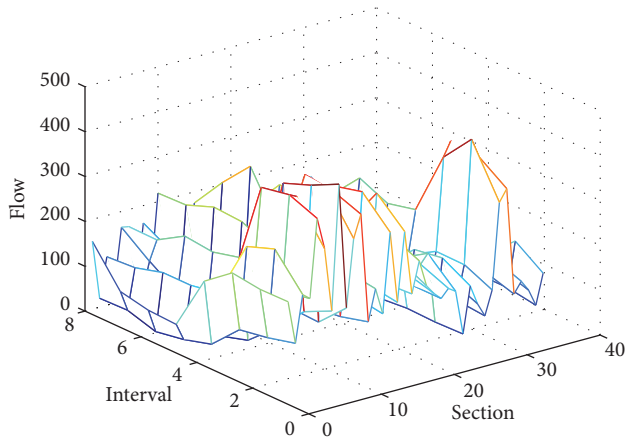


FIGURE 7: Averaged flow before optimization.

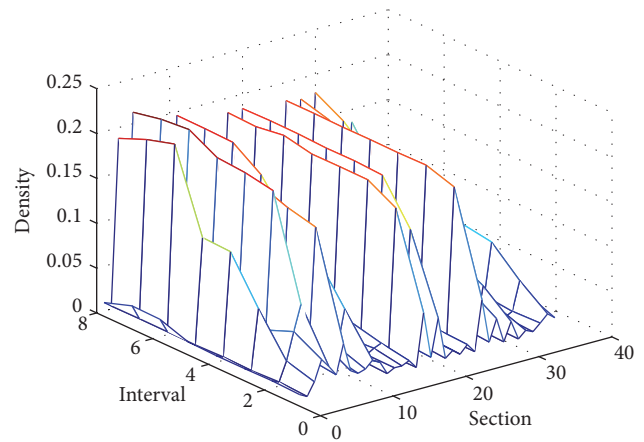


FIGURE 9: Averaged density after optimization.

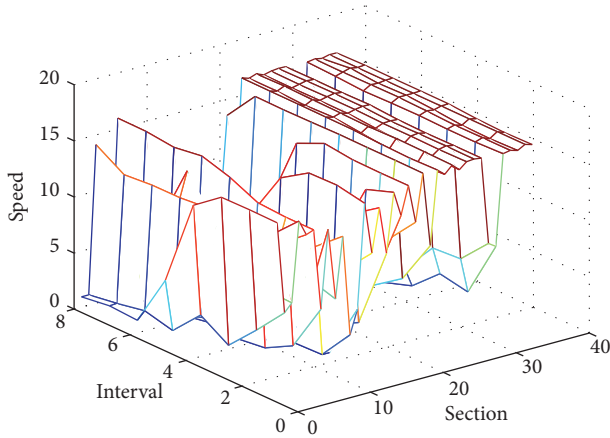


FIGURE 8: Averaged speed before optimization.

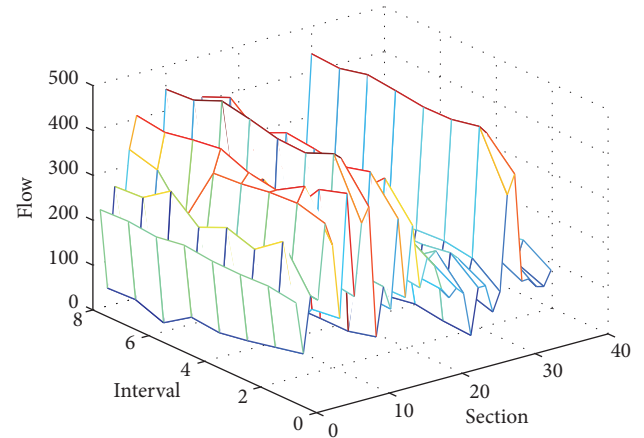


FIGURE 10: Averaged flow after optimization.

maximum flow was 448 on the eighth segment in the first interval. It shows that the segment has the largest traffic demand. Then the averaged speed was analyzed; the total speed of the whole simulation time was $2.7669e + 003$. The averaged vehicle speed was 9.6072 and the maximum average was 16.6600. It appeared on the thirty-fourth segment in the seventh interval. It shows that the segment of the road was relatively smooth, and the vehicles have a higher speed.

When the proposed traffic organization optimization measures were implemented, the mentioned indexes were analyzed in the same way. The total density was 14.9110 in the whole simulation time. The averaged density is 0.0518. The maximum averaged density is 0.2220 which was in the sixth interval on the fifth segment. They all have a little decline. It means that the proposed traffic organization method can balance the density on the network. The network density has been controlled; the congestion on the road has been greatly reduced. The total flow was 59982. The averaged flow was 208.2708. The maximum averaged flow was 479, which appeared on the tenth segment of the sixth interval. It means that the capacity of the network has been greatly improved. The proposed traffic organization method was effective obviously. Moreover the averaged density and total

density were 7.8074 and $2.2485e + 003$, respectively. The maximum speed is 16.5300 appearing in the 25th, 7th, and 6th intervals on 1st, 25th, and 28th segments. This means that the speed was smoothed on some segments which balanced the traffic flow. It was just the purpose of the traffic organization method.

The averaged density, speed, and flow on each segment of every interval were drawn out in Figures 6–11 before and after the traffic organization optimization measures were implemented.

6. Conclusions

In this paper, we overviewed the dynamic traffic simulation software DynaCHINA firstly which is one and only one self-developed software system in China by ours team. The improved traffic simulation model and algorithm were described in detail. The mesoscopic traffic simulation process was designed for suitable dynamic traffic analysis. An optimization method of regional traffic organization was proposed based on dynamic traffic analysis. The method was divided into two steps. First, the researched area was carefully channelized in the intersection level. Then, the traffic signal

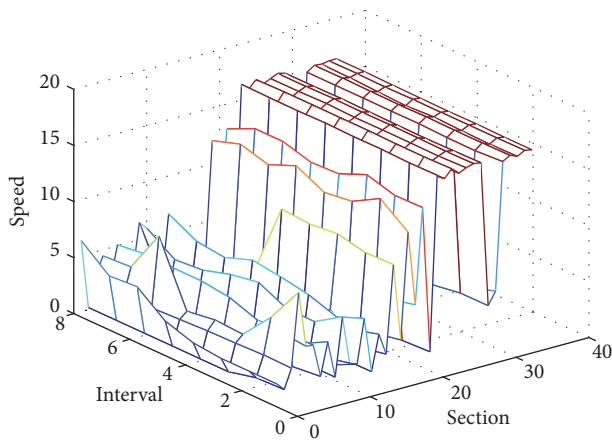


FIGURE 11: Averaged speed after optimization.

timings were optimized. The signal optimal control model was designed accordingly. Finally, the Daizong street of Tai'an city in Shandong province was used as a case study. The averaged density, averaged flow, and averaged speed on segments were selected as analytical index. The simulation results show that the proposed model and method were effective and feasible. The proposed method has been implemented to this area and has a good effect. The followed research will be the collaborative research on the road channelization and the traffic information optimization and the study of the real-time traffic simulation system. The optimization method will be extended to the traffic guidance information.

Conflicts of Interest

The authors declare that there are no conflicts of interest regarding the publication of this paper.

Acknowledgments

This work is supported by the National Natural Science Foundation of China (Grant nos. 71471104, 71371026, 71571109, and 71471167); the University Science and Technology Program Funding Projects of Shandong Province (Grant no. J14LI02); the Project of Public Security Department of Shandong Province (Grant no. GATH2015-236); the Major Social and Livelihood Special Project of Jinan (Grant no. 20150905).

References

- [1] Z. Zhai, *Road Traffic Organization Optimization*, China Communication Press, Beijing, China, 2004.
- [2] F. Shi, E.-H. Huang, Q. Chen, and Y.-Z. Wang, "Optimization of one-way traffic organization for urban micro-circulation transportation network," *Journal of Transportation Systems Engineering and Information Technology*, vol. 9, no. 4, pp. 30–35, 2009.
- [3] D.-F. Long, F. Shi, and Y.-Z. Wang, "One-way traffic organization based on traffic load and road equity," *Journal of Transportation Systems Engineering and Information Technology*, vol. 10, no. 6, pp. 109–114, 2010.

- [4] A. Dussutour, V. Fourcassié, D. Heibing, and J.-L. Deneubourg, "Optimal traffic organization in ants under crowded conditions," *Nature*, vol. 428, no. 6978, pp. 70–73, 2004.
- [5] B. Jia, *The study on traffic organization and optimization of urban arterial road [M.S. thesis]*, Chang'an University, Chang'an, China, 2010.
- [6] H. Xu, Z. Tan, K. Long, and Z. Zhong, "Operational optimization method and simulation of bottleneck section based on urban arterial road," *Computer and Communications*, supplement 1, pp. 4–8, 2009.
- [7] G.-Z. Yao, K.-Q. Wu, and H.-J. Wu, "Empirical analysis of the traffic Micro-circulation organization in heavy traffic networks," *Journal of Transportation Systems Engineering and Information Technology*, vol. 11, no. 1, pp. 160–166, 2011.
- [8] Y.-Z. Yang, B.-H. Mao, X.-J. Zhang, R. Huang, and X.-J. Feng, "Study on traffic micro-circulation organization in heavy traffic networks based on route guidance," *Journal of System Simulation*, vol. 22, no. 7, pp. 1580–1584, 2010.
- [9] B. H. Mao, Z. Z. Sun, S. P. Jia et al., *Regional Traffic Organizational Optimization with Practice*, China Communications Press, Beijing, China, 2007.
- [10] L. Sun and F. Ren, "Optimize of the transfer organization in urban transportation terminal," *Road Traffic and Safety*, vol. 7, no. 3, pp. 18–21, 2007 (Chinese).
- [11] L.-S. Sun, L.-Y. Yao, B.-H. Liu, Y.-Y. Wu, and J. Rong, "Traffic optimization of transportation terminal based on dynamic simulation technology," *Journal of Beijing University of Technology*, vol. 38, no. 4, pp. 570–574, 2012.
- [12] W. Zhengyan, *Study on the methods of traffic organization optimization for emergency evacuation [Ph.D. thesis]*, University of Jilin, 2011.
- [13] Y. Lin and Y. Huang, "GLS model based dynamic OD origin-destination matrix estimation for traffic systems," *System Engineering—Theory & Practice*, vol. 1, pp. 136–144, 2004.
- [14] K. Ashok and M. Ben-Akiva, "Dynamic origin-destination matrix estimation and prediction for real-time traffic management systems," in *Proceedings of the 12th International Symposium on Transportation and Traffic Theory*, pp. 465–484, Elsevier Science, Amsterdam, The Netherlands, 1993.
- [15] Y. Lin, S.-B. Li, and Z. Jiang, "Parameter estimation for vehicle departure time distribution in process of dynamic OD flow loading," *Journal of Beijing Institute of Technology (English Edition)*, vol. 21, no. 2, pp. 252–256, 2012.
- [16] S. Li, *Research on the run State evaluation of urban transportation system and control strategies [Ph.D. thesis]*, Beijing Jiaotong University, Beijing, China, 2012.

Research Article

A Perspective of Evolution for Carbon Emissions Trading Market: The Dilemma between Market Scale and Government Regulation

Qi Zhu

The College of Finance and Statistics, Hunan University, Changsha, China

Correspondence should be addressed to Qi Zhu; zhuqi@hnu.edu.cn

Received 4 November 2016; Revised 20 December 2016; Accepted 4 January 2017; Published 1 February 2017

Academic Editor: Fazlollah Soleymani

Copyright © 2017 Qi Zhu. This is an open access article distributed under the Creative Commons Attribution License, which permits unrestricted use, distribution, and reproduction in any medium, provided the original work is properly cited.

Which means are more effective for reducing carbon emission? Our paper argues the effect of the government regulation and the market trading on the carbon emission. Based on our model, we obtain three conclusions as follows. First, government strengthened regulation can encourage firms to participate in the trading market for carbon emission. Second, there is the negative relation of supervision cost to trading price. Third, there is an alternative relationship between the scale economy level of the supervisory authority and that of the carbon emissions market. Meanwhile, our numerical simulations also confirm our results for our model analyses.

1. Introduction

Developed countries and developing countries are debating the rights and responsibilities for carbon emissions management, making the already difficult global greenhouse gas management more difficult. However, carbon emission management has become a major concern for human development. Developed countries which have established a relatively complete system, such as the United States, Europe, and Japan, have tried to manage carbon emissions by administrative means and market instruments. China, as a developing country, is not compulsively obligated to carbon emission reduction; however, based on Chinese domestic and international environment, it is imperative to take the initiative to assume responsibility for carbon reduction. First, as a responsible big power, China must face the challenge of preventing global warming with international communities; second, China is faced with the task of restructuring the economic structure and optimizing the quality of economic growth. Therefore, establishing a binding carbon emission management mechanism has become a necessity for Chinese development.

The market transaction for carbon emission right is a principal mean for the international carbon emissions

management cooperation. Carbon emission right trading is a method countries utilize to meet their obligations specified by the *Kyoto Protocol*, as signatory nations are committed to achieve a certain carbon emission reduction targets in a certain period of time and then assign it to different domestic enterprises; when one country cannot meet its target on schedule, it can purchase a certain amount of quotas or emission permits from the countries that have the quota or emission permit (mainly developing countries) to meet their own emission reduction targets. Similarly, within a country, companies can also do the trading to meet their own targets. According to the *Kyoto Protocol*, the international greenhouse gas emissions trading system consists of three flexible emission reduction mechanisms (CDM, IET, and JI).

The study of carbon emissions trading can be traced back to scholars' research on emission rights, which is essentially the externality discussion for public goods usage. As public goods, atmospheric pollution is not counted or included in private costs, which suggests that social marginal cost is not consistent with private marginal cost, which leads to market malfunction. In other words, it is difficult for the market to define the property rights of the atmospheric environment, and it loses the function of resource allocation adjustment. In this case, there are two coping strategies in the academic

research: Pigou Tax (Pigou, 1952) and Coase's Property rights (Coase, 1960).

The practice of emission rights is to use Coase's externality bargaining mechanism (Coase, 1960). Crocker [1] and Dales (1968), respectively, put forward the idea of allocating pollution burdens among market players with tradable permits. Montgomery [2] demonstrated in theory that a tradable permitting system provides an effective public economic policy tool for constraining pollution. After that, scholars began to conduct detailed studies in emissions trading transactions.

In the literatures, both the government and the market are viewed as the important roles of carbon emissions trading market. Government regulation, in the carbon emission management, is essentially compulsory third-party contract enforcement. Barzel [3] argues that one believes that when the value of the investment will be negative, it is less likely that the agreement will be self-enforcing and more parties can benefit from third-party enforcement. At the same time, Barzel (2003), while studying the behavioral game of coercing third party and supervised parties, points out that when the right to cohesive mechanisms of collective action is scaled up and exceeds that of coercive third party of the power, it can also effectively suppress the rights of mandatory third parties. As for the result analysis of government control, Stigler [4] and Peltzman (1976) believe that government regulation only results in the redistribution of resources, rather than the overall output and price. About government control on environment issues, Bettney and Stevens (2003) point out that how to choose a supervisory strategy for the implementation status of environmental standards (i.e., how much economic penalties can be relied upon to restrain violations and the relative advantages and disadvantages of civil liability and criminal penalty) is the difficulty in actual implementation.

Proponents of market-based approaches, however, believe that government control of pollution is aimed at forcing each firm to assume the same share of the burden of pollution control. Regardless of the corresponding cost differentials, although it can effectively control corporate emissions, they also force companies to take unduly expensive pollution control measures, which brings huge costs in the process, while the control also tends to hinder the progress of emission reduction technology (Stavins, 2003; [5]). Downing and White [6], Malueg [7], Milliman and Prince (1989), and Jung et al. [8], respectively, did theoretical analysis on dynamic incentive of sewage behavior under different policy conditions and concluded that market-based policy management tools with subject of emissions trading are able to motivate polluters to obtain benefits through technological innovation or using more advanced pollutant emission technologies, compared with regulatory actions. Hahn and Noll [9], by analyzing the operating conditions of the emission permit system to reflect on the effect of government regulation, think that the government's penalties for violating the permit system must exceed the cost of purchasing permits in order to encourage producers to adhere to market rules.

More governments have accepted treaties which regulate carbon emission [10]. The cap-and-trade system is one of the most important regulations for carbon emission, and

Li et al. [11] indicate that this system is the most effective method of regulating carbon emission. Under the cap-and-trade system, firms' carbon emissions must meet their rights, and they could also sell or buy carbon rights to meet their emissions. Because purchase and selling of carbon emission rights can affect the production cost, accounting standard setters argue that firms should disclose and report their carbon liabilities [12]. Besides, capital investment in manufacture or production industry is affected by carbon emission costs [13]. It is acknowledged that compliance with any emission regulation would probably increase firms' costs [10]. And Clarkson et al. (2015) asserted that value of firms whose carbon emissions exceed their rights is abated while value of firms which comply with all the regulations would not be affected by the cap-and-trade system. However, their empirical result also suggested that firms' latent carbon liabilities could be alleviated by their ability of future shifting of costs on carbon emission. Cap-and-trade system also affects other industries; for instance, Li et al. (2015) examined the effect of cap-and-trade system on truck routing, and found that transportation firms try to pursue an equilibrium on which economic cost and carbon emission are balanced under this system. To be more specific, firms try to get a minimum economic cost when carbon is relatively cheap, while trying to get a minimum carbon emission when carbon is extremely expensive. Moreover, other regulations, such as pollution taxes, on carbon emission can make sense. If the elasticity of demand of a certain good is very small, carbon tax could bring a higher return to capital [14].

At the same time, the transaction cost is also an important variable for the decision-making of the government and market actors in the carbon emission trading market. The lawmakers believe that creating a set of rules and regulatory bodies is much less expensive than creating a market or selling sewerage permits (Burgess, 1995). However, the government's ability to monitor carbon emissions is also constrained by the level of capacity, and Barzel (2003) argues that the ability to impose costs limits the scope of third-party enforcement. However, with the improvement of the market system, transaction costs will decline, because intermediary organs can reduce financial transaction costs, through the establishment of trading systems to reduce the transaction information asymmetry (Da, 2007). Chen [15] believes that market can get the real value for pollution right because of value discovery of trading.

In the carbon emission trading market, government regulation and scale economy of market transactions are indispensable factors in the study of functioning of the carbon trading market; specialization has long been known as the basic factor for the formation of scale economy (William and Joanna, 1997). Lin (2002) considers that there are four forms of scale economy, which from a dynamic point of view, through mass production transactions, making the division of labor more specialized, resulting in scale of income. Gu (1999) divides scale economy into three levels, in which the first one is the decrease of unit product cost through the expansion of production scale, till the lowest point of average cost. In terms of the scale income of government regulation,

Barzel (2003) believes that third-party enforcement allows for specialization in the accumulation of enforcement rights.

Based on the perspective of scale economy and transaction costs, our paper uses stochastic dynamic model to analyze the influence of government regulation and market trading on carbon emission. The second section provides a stochastic dynamic model. The third section analyzes the effect of government regulation and trading market on the carbon emission based on stochastic dynamic model. The fourth section provides numerical simulations of our propositions. At last, our paper shows main conclusions and contributions.

2. Model Setup

Suppose that the utility of the carbon market is maximized over time, as there are different preferences at each stage of development; assuming there is a subjective discount rate ρ , where $\rho > 0$, with that, the future welfare can be discounted to the current period. In the planning period $[0, +\infty]$, the welfare function V can be expressed as

$$V(S, t) = \max \int_t^{+\infty} e^{-\rho m} U(S(m), \eta(m)) dm. \quad (1)$$

Among it, S shows the stock of new carbon emissions in current society, $U(S)$ represents the effect of the carbon stock of new emissions on the utility of mankind. The discount rate ρ reflects the contemporary assessment of the future environment, which is influenced by many factors, including people's expectation of technological development, expectation of economic development level, and people's tolerance to greenhouse gas pollution.

Due to the inconsistency of microcosmic expectation, people choose different carbon emission behaviors at different stages, which lead to the random fluctuation of carbon emission increment S ; thus, suppose that the changing path of S obeys Brownian motion:

$$dS = (S_p - \eta S_r) dt + \sigma dz, \quad 0 < \eta < 1. \quad (2)$$

S_p represents the current demand of social carbon emissions; S_r represents the supply of social carbon emissions in the current period; η represents the transaction rate of carbon emissions; σ is the degree of risk in the carbon emission system and is assumed to be constant in this paper; dz is a Wiener process defined in a certain probability space, which is called white noise.

The supply of carbon emission rights is mainly composed of two parts, the carbon emission rights sold by carbon emission authority (government) and carbon emissions trading on the market. In a society with strict carbon regulation, the efficiency of carbon emissions trading is often affected by the two forces, namely, the pressure on carbon emissions enterprises under government regulation and legal punishment and the rationalization of carbon emissions trading prices promoted by the expansion of market transactions scale. Suppose the government's regulation probability to a carbon trading firm is h , which can also be described as

the willingness of individual firms to participate in carbon emissions; then $q = 1 - h$ reflects the probability that government regulation authorities ignore individual carbon-emitting firms; in other words, it is the probability that an enterprise avoids buying the emission permit. N shows the number of participants in the potential carbon trading market as defined by law, that is, the size of potential market transactions. Assuming that an individual firm's violation of the carbon trading rule is an independent event, the probability of the whole firm violating the carbon emissions trading rule is $(1 - h)^N$. Therefore, this paper assumes that the efficiency of carbon emissions trading market is

$$\eta = 1 - (1 - h)^N, \quad (3)$$

in which h represents the efficiency of carbon emissions regulation and N shows the number of participants in carbon emissions trading market, that is, carbon emissions trading scale.

Assuming that the cost of society as a whole is 1, let τ_μ denote the cost of inspection and τ_w the cost of the carbon emissions trading market. Then, the relationship between τ_μ and h and τ_w and N can be expressed as

$$\begin{aligned} \tau_\mu^{\varphi_1} &= \mu h \\ \tau_w^{\varphi_2} &= \omega N, \end{aligned} \quad (4)$$

where μ and ω , respectively, represent regulatory fees and carbon emissions market transaction costs. φ_1 and φ_2 denote the level of government-regulated and market-oriented economies of scale, respectively.

For the stochastic control model of the carbon emission management system, it essentially controls the change of transaction efficiency η in the dimension of time t in order to maximize the social utility. Therefore, it is possible to rewrite (1) as follows:

$$V(S, t) = \max_\eta E_t \int_t^{+\infty} e^{-\rho m} U(S(m), \eta(m)) dm. \quad (5)$$

Equation (5) can also be defined as

$$\begin{aligned} V(S_0, t_0) &= \max_\eta E \int_{t_0}^{+\infty} e^{-\rho m} U(S(m), \eta(m)) dm \\ &= \max_\eta E \left[\int_{t_0}^{t_0 + \Delta t} e^{-\rho m} U(S(m), \eta(m)) dm \right. \\ &\quad \left. + \int_{t_0 + \Delta t}^{+\infty} e^{-\rho m} U(S(m), \eta(m)) dm \right] = \max_\eta E \\ &\quad \cdot [e^{-\rho m} U(S, \eta) \Delta t + V(t_0 + \Delta t, S_0 + \Delta S)]. \end{aligned} \quad (6)$$

We can use Ito's lemma for Taylor expansion applied to $V(t_0 + \Delta t, S_0 + \Delta S)$ at any (t_0, S_0) and get

$$\begin{aligned} V(t_0 + \Delta t, S_0 + \Delta S) &= V(t_0, S_0) + V_t(t_0, S_0) \Delta t \\ &\quad + V_s(t_0, S_0) \Delta S + \frac{1}{2} \sigma V_{ss} \Delta S^2. \end{aligned} \quad (7)$$

Substituting (7) into (6), we can get

$$0 = \max_{\eta} \left[e^{-\rho t} U(S, \eta) \Delta t + V_t(t_0, S_0) \Delta t + V_s(t_0, S_0) \Delta S + \frac{1}{2} \sigma V_{ss} \Delta S^2 \right]. \quad (8)$$

Substituting (2), we can get

$$0 = \max_{\eta} \left\{ \left[e^{-\rho t} U(S, \eta) + V_t(t_0, S_0) + V_s(t_0, S_0) (S_d - \eta S_r) + \frac{1}{2} \sigma V_{ss} \right] \Delta t + V_s \sigma \Delta z \right\}. \quad (9)$$

HJB equation is thereby obtained:

$$0 = \max_{\eta} \left[e^{-\rho t} U(S, \eta) + V_t(t, S) + V_s(t, S) (S_d - \eta S_r) + \frac{1}{2} \sigma V_{ss} \right]. \quad (10)$$

That is,

$$-V_t(t, S) = \max_{\eta} \left[e^{-\rho t} U(S, \eta) + V_s(t, S) (S_d - \eta S_r) + \frac{1}{2} \sigma V_{ss} \right]. \quad (11)$$

The boundary conditions are as follows:

$$\begin{aligned} V_t(t, S) &= \max(S(T) - u, 0) \\ V_t(t, 0) &= 0, \quad \forall 0 \leq t \leq T \\ V_t(t, S) &= w, \quad \text{let } S \rightarrow +\infty \\ V_t(0, S) &= u. \end{aligned} \quad (12)$$

3. Main Results

Based on the optimal carbon emissions trading efficiency η^0 , with comparative static analysis on the variables in the carbon emissions trading system, the mutual influence relationship between the carbon emissions trading system variables is studied, and the following propositions are obtained.

Proposition 1. *With the expansion of the carbon trading market, the probability for supervision increases, but the regulation is marginally diminishing.*

From HJB equation, we can get

$$\begin{aligned} -V\eta &= e^{-\rho t} U\eta - V_s S_r \\ \eta_h &= N(1-h)^{N-1} \end{aligned} \quad (13)$$

$$\eta_N = -(1-h)^N \ln(1-h)$$

$$\frac{\partial N}{\partial h} = -\frac{N}{(1-h) \ln(1-h)} > 0 \quad (14)$$

$$\frac{\partial^2 N}{\partial h \partial h} = N \frac{1 + \ln(1-h)}{(1-h)^2 \ln^2(1-h)}. \quad (15)$$

Thus, from (15), we can see that when $h > 1 - 1/e$, $\partial^2 N / \partial h \partial h < 0$, and when $h < 1 - 1/e$, $\partial^2 N / \partial h \partial h > 0$.

Equation (14) shows that h , the inspection strength of carbon emissions regulation authorities, and N , carbon emissions trading market size, vary in the same direction. As N , carbon emissions trading market size, expands, the rent-seeking income of the supervisory organs has increased, making supervisory authority increase their inspection efforts to obtain inspection proceeds. However, from (15), we can see that there is a critical value of $1 - 1/e$; when $h < 1 - 1/e$, h is accelerated to increase along with the expansion of market scale (N), and when $h > 1 - 1/e$, h is slowed down to increase along with the expansion of market scale (N). This indicates that the regulation cost will gradually restrict the behavior of the supervisory organ, with the expansion of the carbon emissions market to a certain degree; the regulation intention will therefore decline.

Proposition 2. *There is the negative relation of supervision cost to trading price. However, increase of regulation cost is faster than trading price for carbon emission right.*

From (4), we can get

$$h_{\mu} = -\frac{1}{\mu^2} \tau_{\mu}^{\varphi_1} < 0 \quad (16)$$

$$N_{\omega} = -\frac{1}{\omega^2} \tau_{\omega}^{\varphi_2} < 0. \quad (17)$$

From HJB equation, we can get

$$\frac{\partial V}{\partial \mu} = -\left(e^{-\rho t} U_{\eta} - V_s S_r \right) N (1-h)^{N-1} \frac{1}{\mu^2} \tau_{\mu}^{\varphi_1} \quad (18)$$

$$\frac{\partial V}{\partial \mu} = -\left(e^{-\rho t} U_{\eta} - V_s S_r \right) (1-h)^N \ln(1-h).$$

Then

$$\frac{\partial \omega}{\partial \mu} = -\frac{N(1/\mu^2) \tau_{\mu}^{\varphi_1}}{(1-h) \ln(1-h)} > 0 \quad (19)$$

$$\frac{\partial^2 \omega}{\partial \mu \partial \mu} = \frac{2N(1/\mu^3) \tau_{\mu}^{\varphi_1}}{(1-h) \ln(1-h)} < 0.$$

Equation (16) indicates that, with the enlargement of carbon trading market, the number of competitors in the market increases, the market is gradually approaching a competitive market, emission reduction technology and emission reduction quota are gradually standardized, and the transaction cost of the market decreases. From (17) we can see that the increase in carbon inspection costs will increase the regulation cost, decreasing the regulation intention.

From (19) we can see that the cost of carbon emission inspection and transaction costs change in the same direction; however, the transaction costs change faster. It indicates that there is no competition in regulation market of carbon emissions. With monopoly of government regulation, the inspection costs are rigid, less sensitive, and slower in

adjustment. But in the carbon emissions market, changes in transaction costs will promptly stimulate market players to adjust carbon emissions (through the market to complete the task of carbon emission reduction, or use their own technology or to cut production or even avoid regulation to complete the task of emission reduction), affecting carbon emissions trading market participation, which will further affect the carbon emissions trading market costs.

Proposition 3. *There is an alternative relationship between the scale economy level of the supervisory authority and that of the carbon emissions market, and there is a phenomenon of accelerated substitution.*

$$\eta_{\varphi_1} = N(1-h)^N h \ln \tau_\omega$$

$$\eta_{\varphi_2} = N(1-h)^N h \ln \tau_\mu$$

$$\frac{\partial V}{\partial \varphi_1} = (e^{-\rho t} U \eta - V_S S_r) N(1-h)^N h \ln \tau_\omega \quad (20)$$

$$\frac{\partial V}{\partial \varphi_2} = (e^{-\rho t} U \eta - V_S S_r) N(1-h)^N \ln(1-h) \ln \tau_\mu$$

$$\frac{\partial \varphi_2}{\partial \varphi_1} = \frac{h}{\ln(1-h)} \frac{\ln \tau_\omega}{\ln \tau_\mu} < 0 \quad (21)$$

$$\frac{\partial^2 \varphi_2}{\partial \varphi_1 \partial \varphi_1} = \left[\frac{1}{\ln(1-h)} - h(1-h) \right] h \ln \tau_\omega > 0. \quad (22)$$

Equation (21) shows that the scale economy of carbon emissions regulation is negatively related to that of the carbon emissions trading market; that is, when scale economy increases in the carbon emissions trading market, the scale economy of the supervisory authority declines and vice versa. This indicates that the expansion of the carbon emission trading market will reduce the transaction costs and attract the enterprises to complete the emission reduction task through the transaction, reducing the motive of enterprises to evade regulation or take illegal actions; thus the scale economy of the supervisory organs will be reduced.

From (22), we can see that the increase of scale economy of carbon emission trading market will lead to the accelerated decrease of scale economy of regulation organs. As mentioned above, there is an alternative relationship between the scale economy of the supervisory authority and that of the trading market; meanwhile, specialization also encourages the trading for carbon emissions, so that the scale economy for carbon emissions market is enhanced; if above setting, the cost for transaction will be reduced; the welfare of carbon emissions demand and supply enterprises is therefore increased, encouraging more companies to fulfill legal obligations through carbon trading rather than by evading the regulation, which tends to gradually reduce the effect of regulation authority and accelerate the decline of its scale economy.

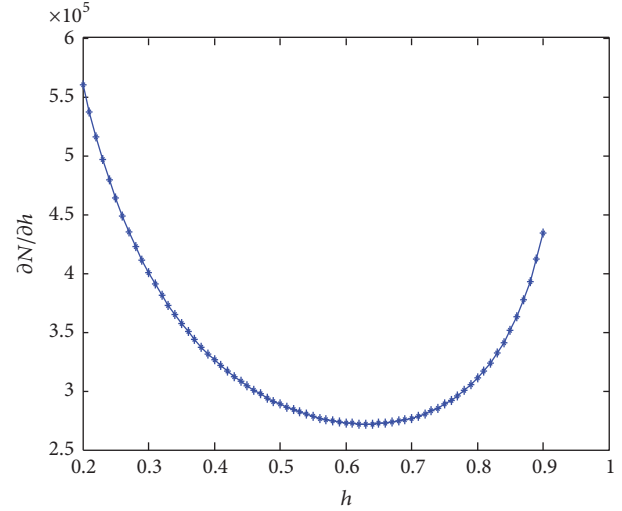


FIGURE 1: The relation between market size and supervision probability with $N = 100000$; $h = (0.2, 0.9)$.

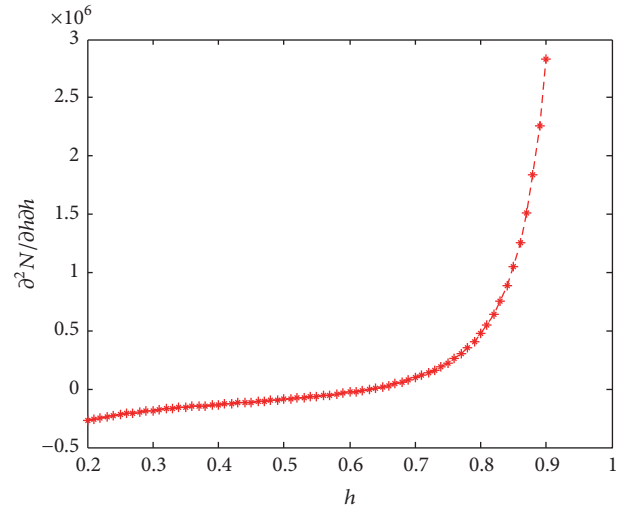


FIGURE 2: The change rate for the relation between market size and supervision probability with $N = 100000$, $h = (0.2, 0.9)$.

4. Numerical Simulation

In our paper, our models are stochastic and our propositions are embodied by function which still are not intuitional. In this section, based on the MATLAB software, we furtherly use simulation to illustrate the relation between carbon emissions trading market and government regulation.

In Figure 1, we present numerical simulation for the relation between the market size and supervision strength. There is the positive effect of supervision strength on the market size, suggesting that as government strengthens the supervision for carbon emission, firms have incentive to meet regulation condition by the trading market of carbon emission. Meanwhile when $h = 1 - 1/e$, the incentive for firms to trade carbon emission right is stronger. The above results are confirmed by Figure 2.

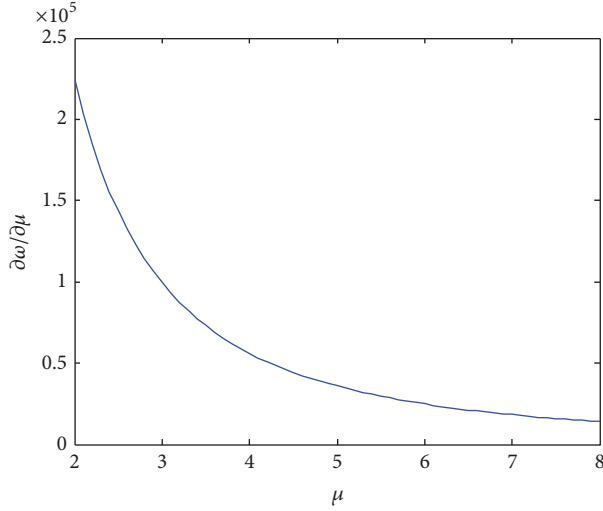


FIGURE 3: The relation between supervision cost and the price for carbon emission right with $N = 100000$; $h = 0.7$; $\tau_\mu = 5$; $\varphi_1 = 0.5$; $u = (2, 8)$.

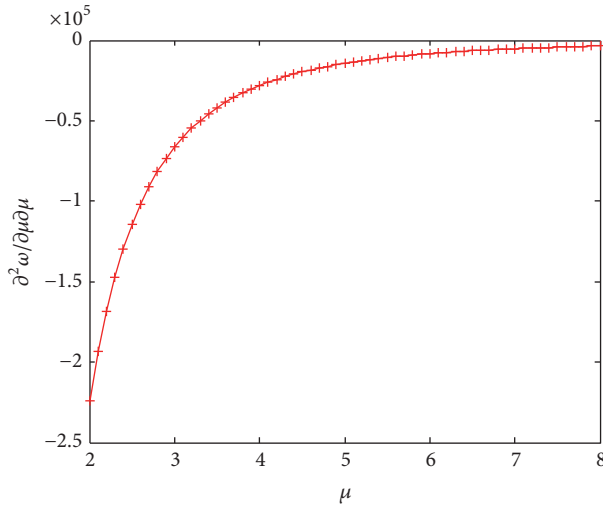


FIGURE 4: The change rate for the relation between supervision cost and the price for carbon emission right with $N = 100000$; $h = 0.7$; $\tau_\mu = 5$; $\varphi_1 = 0.5$; $u = (2, 8)$.

Figure 3 reports the results for the numerical simulation about the relation between supervision cost and trading price for carbon emission right. There is the negative relation of supervision cost to trading price. These results suggest that, with low supervision cost, government has potential incentive to raise the probability for regulation. Thus, firms are more eager to trade the carbon emission right, so that trading price for carbon emission right rises. However, the increase of regulation cost is faster than trading price for carbon emission right, as in Figure 4. Therefore, firms have potential incentive to participate in the trading market of carbon emission right.

Figure 5 reports that the relation of scale economy for regulation and trading market. In accordance with results

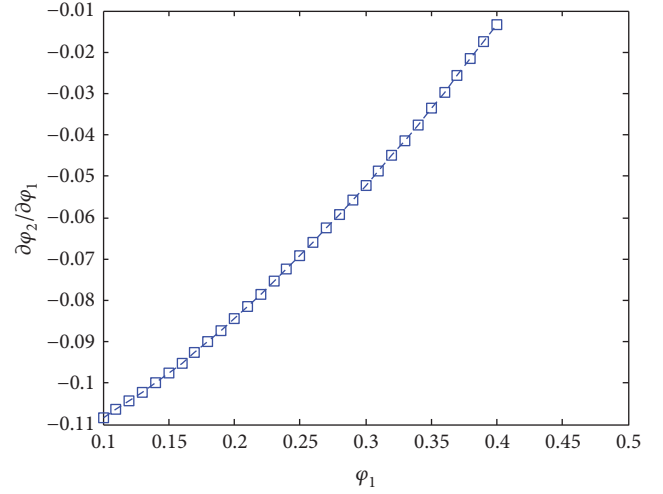


FIGURE 5: The relation of scale economy for regulation and trading market with $u = 5$; $\tau_\mu = 5$; $\tau_w = 3$; $\varphi_1 = (0.1, 0.4)$.

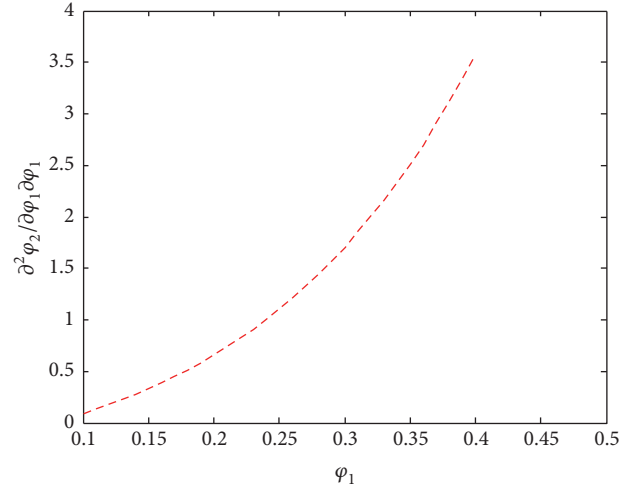


FIGURE 6: The change rate for the relation of scale economy for regulation and trading market with $u = 5$; $\tau_\mu = 5$; $\tau_w = 3$; $\varphi_1 = (0.1, 0.4)$.

of the numerical simulation, there is the negative relation between the scale economy of regulation and the scale economy of trading market. Meanwhile, in accordance with Figure 6, the scale economy of regulation is restrained when the market of carbon emission right is growing. These results suggest that if the market of carbon emission right is growing, firms are likely to make use of market to reduce the carbon emission.

5. Conclusion

Our paper argues the relation between regulation and trading market for carbon emission. our model and the numerical simulation obtain three conclusions as follows. First, government strengthened regulation can encourage firms to participate in the trading market for carbon emission.

Second, there is the negative relation of supervision cost to trading price. However, increase of regulation cost is faster than trading price for carbon emission right. Third, there is an alternative relationship between the scale economy level of the supervisory authority and that of the carbon emissions market, and there is a phenomenon of accelerated substitution.

Our findings extend the understanding of the market for carbon emission right. Though the regulation and trading market are two parts of reducing carbon emission, they play different role of development for carbon emissions trading market. At initial development stage, the regulation plays more important role in reducing carbon emission. However, if government expects reducing carbon emission by low cost, the development of carbon emissions trading market maybe the only option.

Competing Interests

The author declares that there is no conflict of interests regarding the publication of this paper.

References

- [1] T. D. Crocker, "The structuring of atmospheric pollution control systems," *Economics of Air Pollution*, vol. 29, no. 2, p. 288, 1966.
- [2] W. D. Montgomery, "Markets in licenses and efficient pollution control programs," *Journal of Economic Theory*, vol. 5, no. 3, pp. 395–418, 1972.
- [3] Y. Barzel, *Property Rights and the Evolution of the State. Conflict and Governance*, Springer, Berlin, Germany, 2003.
- [4] G. J. Stigler, "The theory of economic regulation," *The Bell Journal of Economics and Management Science*, vol. 2, no. 1, pp. 3–21, 1971.
- [5] G. E. Helfand, "Erratum: standards versus standards: the effects of different pollution restrictions," *American Economic Review*, vol. 81, no. 3, pp. 622–634, 1991.
- [6] P. B. Downing and L. J. White, "Innovation in pollution control," *Journal of Environmental Economics and Management*, vol. 13, no. 1, pp. 18–29, 1986.
- [7] D. A. Malueg, "Emission credit trading and the incentive to adopt new pollution abatement technology," *Journal of Environmental Economics and Management*, vol. 16, no. 1, pp. 52–57, 1989.
- [8] C. Jung, K. Krutilla, and R. Boyd, "Incentives for advanced pollution abatement technology at the industry level: an evaluation of policy alternatives," *Journal of Environmental Economics & Management*, vol. 30, no. 1, pp. 95–111, 1996.
- [9] R. W. Hahn and R. G. Noll, "Environmental markets in the year 2000," *Journal of Risk & Uncertainty*, vol. 3, no. 4, pp. 351–367, 1990.
- [10] P. M. Clarkson, Y. Li, M. Pinnuck, and G. D. Richardson, "The valuation relevance of greenhouse gas emissions under the European Union carbon emissions trading scheme," *European Accounting Review*, vol. 24, no. 3, pp. 551–580, 2015.
- [11] J. Li, Q. Lu, and P. Fu, "Carbon footprint management of road freight transport under the carbon emission trading mechanism," *Mathematical Problems in Engineering*, vol. 2015, Article ID 814527, 13 pages, 2015.
- [12] Y. Ertimur, J. Francis, A. Gonzales et al., "Credibility, commitment and voluntary environmental disclosures," Working Paper, Duke University, 2010.
- [13] B. Sarkar, S. Saren, D. Sinha, and S. Hur, "Effect of unequal lot sizes, variable setup cost, and carbon emission cost in a supply chain model," *Mathematical Problems in Engineering*, vol. 2015, Article ID 469486, 13 pages, 2015.
- [14] D. Fullerton and G. Heutel, "The general equilibrium incidence of environmental taxes," *Journal of Public Economics*, vol. 91, no. 3–4, pp. 571–591, 2007.
- [15] C.-Y. Chen, "Discussion on the orientation of Chinese property right exchange market," *Journal of Property Rights*, no. 3, 2007.